Cryogenic Liquids for Energy Storage and Carbon Capture

By

Sidra Rama

Main Supervisor: Dr Yongliang Li

Secondary Supervisor: Professor Yulong Ding

A thesis submitted to the University of Birmingham for the degree of

DOCTOR OF PHILOSOPHY

Energy Storage Group

School of Chemical Engineering

College of Engineering and Physical Sciences

The University of Birmingham

November 2019

Abstract

Carbon capture is widely recognised as an essential strategy to meet global goals for climate protection. Although various CO_2 capture technologies including absorption, adsorption and membrane exist, they are not yet mature for post-combustion power plants mainly due to the high energy penalty. Hence researchers are concentrating on developing non-aqueous solvents like ionic liquids, CO_2-binding organic liquids, nanoparticle hybrid materials and microencapsulated sorbents to minimise the energy consumption for carbon capture.

This research aims to develop a novel and efficient approach by encapsulating sorbents to capture CO_2 in a cold environment. The conventional emulsion technique is selected for the microcapsule formulation by using 2-amino-2-methyl-1-propanol (AMP), monoethanolamine (MEA) and triethanolamine (TEA) as the core sorbents and silicon dioxide (SiO_2) as the shell. The microcapsule formulation parameters like core-shell ratio and emulsifiers are studied to formulate good microcapsules. Additionally, the microcapsules are characterised in terms of physio-chemical properties and structural properties. Furthermore, the sorption dynamics and effect of temperature on the CO_2 loading capacity of the microcapsules using a self-developed pressure decay method and a continuous reactor are investigated. The results have shown that the following parameters formulated the best microcapsules: AMP core, 1 wt% Span85, 6:4 core-shell ratio, 400 rpm mechanical stirrer speed and 1200 rpm homogeniser speed. However, samples formulated with 0.5 wt% PGPR emulsifier (AMP core, 6:4 core-shell ratio, 400 rpm mechanical stirrer speed and no homogeniser) showed better surface properties with a larger surface area (92 m^2/g) (SA) and pore size (43 Å) compared to the samples produced with the other two emulsifiers. Similarly, this

sample showed both the best absorption capacity as well as absorption kinetics at both room temperature (0.0505 g/g) and low temperature with the highest absorption seen at -60 °C (0.0993 g/g). The encapsulation of CO_2 sorbents showed promising result though further research is needed to replace the conventional sorbents.

Dedication

To Allah (the most gracious and compassionate), my parents and family.

Acknowledgements

First, I would like to thank my supervisors Dr Yongliang Li and Professor Yulong Ding for their continued, excellent supervision, advice, encouragement and contributions during the duration of this PhD. I would also like to express my thank you to the members of Birmingham Centre for Energy Storage (BCES) group for their experience and help. The group was always ready to help in any way they could.

A special thanks also goes to Dr Tiejun Lu for not only his technical support but also his help in setting up the pressure rig and continuous reactor. The experimental set-up without him would have been tedious and more difficult. I am very grateful to Dr Cyprian Negoescu for his continuous encouragement and discussions that often lead to new ideas; I would also like to send my special thanks to Dr Helena Navarro for her technical support on using the instruments and equipment; I also acknowledged Dr Yan Zhan for his insightful and technical discussions. I would also convey my biggest thanks to the staff members in the Chemical Engineering Department: Dr Mark Tylor, David Boylin and Lynn Draper, and for their help with instruments, equipment, trainings and administrative support.

I would also like to gratefully acknowledge the financial support of the Engineering and Physical Science Research Council (EPSRC) of the United Kingdom under the grants EP/N000714/1 and EP/N021142/1.

Lastly, my heartfelt thanks go to my family for their patience, support and understanding. I would also like to thank all the friends I made in the University of Birmingham who were always there to support me whether with my work or the emotional struggles. Thanks to them I had an unforgettable time during my PhD.

Table of Contents

List of Illustrations

List of Tables

List of Abbreviations

-OH	Hydroxyl group
AMP	2-amino-2 methyl-1-propanol
ATR	Attenuated total reflectance
BCCES	Birmingham Centre for Cryogenic Energy Storage
BCES	Birmingham Centre for Energy Storage
BET	Brunauer-Emmet-Teller
BJH	Barret, Joyner and Halenda
CC	Carbon capture
CCC	Cryogenic carbon capture
CCCS	Cryogenic carbon capture and storage
CES	Cryogenic energy storage
CH_4	Methane
CO_2	Carbon dioxide
CO_2BOLs	CO2-binding organic liquids
DEA	Diethanolamine
DSC	Differential scanning calorimetry
EE	Encapsulation efficacy
EOR	Enhanced oil recovery
EtOH	Ethanol
FTIR	Fourier Transform Infrared Spectroscopy
Hg	Mercury
HPVA	High Pressure Volumetric Analyzer
IFP	Interfacial Polymerisation

IGCC	Integrated gasification combined cycle
IL	Ionic liquids
IPCC	Intergovernmental Panel on Climate Change
MCES	Microencapsulated carbon sorbents
MDEA	Methyldiethanolamine
MEA	Monoethanolamine
MOF	Metal-organic frameworks
MSDS	Material Safety Data Sheet
N_2	Nitrogen
NAOH	Sodium hydroxide
NO	Nitrogen oxide
NPWIP	Nobel Prize-winning Intergovernmental Panel
O_2	Oxygen
OH-	Deprotonated hydroxyls
PCC	Pulverised coal combustion
PGPR	Polyglycerol polyricinoleate
PID	Piping and instrumentation diagram
PR	Pressure rig
PREoS	Peng Robinson Equation of State
PSD	Pore size distribution
PV	Pore Volume
PZ	Piperazine
RI	Refractive index
SA	Surface area

SE	Secondary electrons
SEM	Scanning Electron Microscope
Si-O	Silicon dioxide
SiO2	Silicon dioxide
SLS	Static light scattering
TEA	Triethanolamine
TEOS	Tetraethyl orthosilicate
TG	Thermogravimetry
TGA	Thermogravimetry analysis
XRD	X-ray powder diffraction
ZIF	Zeolitic imidazolate frameworks

List of Symbols

$F_{N_2,in/out}$	Nitrogen fraction from flow at inlet/ outlet
$F_{CO_2,out}$	CO_2 flow out
$F_{Gas,in}$	Flowrate of gas mixture at inlet (0.5 L/min)
$F_{gas\ mixture,out}$	Gas mixture flow at outlet (L/min)
F_{out}	Gas mixture flow out
fN_2	Volume fraction of nitrogen
P_C	critical pressure
P_E	Pressure at the end of experiment
P_I	Initial pressure
P_{abs}	Absorbed pressure
P_r	Reduced pressure
R_0	Drop radius of the curvature of the drop apex
T_C	Critical temperature
T_r	Reduced temperature
V_{abs}	Absorbed CO_2 volume (L)
$f_{CO_2}(out)$	CO_2 volume fraction at outlet
$f_{N_2}(out)$	Nitrogen fraction out
m_I	Initial weight of sample
m_{CO_2}	Absorbed CO_2 mass
m_S	Weight of shell after core evaporation process
ρ_{CO_2}	Density of CO_2
$\emptyset$	Payload (wt%)

$\Delta\delta$	Density difference between the two fluids
R	Universal gas constant ($Jmol^{-1}K^{-1}$)
V	Volume at experimental temperature
a	CO_2 volume out (%)
f	CO_2 Vol fraction out
g	Gravitational constant
m	Absorbed mass
$\alpha,\ b$	Critical properties
β	Shape defined by Young-Laplace equation
γ_1	CO_2 absorbed
γ_2	Surface tension
ρ	Density of CO_2
ω	Acentric factor

Papers and Conferences

From the work presented in this thesis the following paper was accepted:

- Rama S, Zhang Y, Tchuenbou-Magaia F, Ding Y, Li Y. Encapsulation of 2-amino-2-methyl-1-propanol with tetraethyl orthosilicate for CO_2 capture. Front. Chem. Sci. Eng. Accepted

During the PhD period, the experimental work was also presented at conferences:

- Rama S, Zhang Y, Tchuenbou-Magaia F, Ding Y, Li Y. Encapsulation of 2-amino-2-methyl-1-propanol with tetraethyl orthosilicate for CO_2 capture. Chemical Science and Technology in the UK and Society of Chemical Industry's Chinese UK Reginal Group (CSCST-SCI). 2018. Oral Presentation
- Rama S, Zhang Y, Tchuenbou-Magaia F, Ding Y, Li Y. Emulsion polymerisation for encapsulation of 2-amino-2-methyl-1-propanol with tetraethyl orthosilicate for CO2 capture. UKES. 2018. Oral Presentation
- Rama S, Zhang Y, Tchuenbou-Magaia F, Ding Y, Li Y. Cryogenic CO2 Capture with Microencapsulated Sorbent Suspensions. UK Particle Technology Forum. 2017. 2nd Prize Poster Award.

Chapter 1 Introduction

1.1 Background

The world's environmental organisations declared in 2013 that the critical level of 400 ppm for carbon dioxide (CO_2) has been reached which forced all countries to try to reduce CO_2 emission into the environment. The global industrialisation and growing population keep increasing the yearly energy consumption (1) where the leading sources of global primary energy demand are fossil fuels which are most likely to remain the primary energy source for the unforeseen future. The estimated global energy-related emission increase is predicted to be 3.7Gt of CO_2 by 2030 (1). The increase of CO_2 emission into the environment has contributed to global warming as well as climate change which is a primary concern today (2) that necessitates carbon capture (CC) to reduce CO_2 emission while still making use of fossil fuels to mitigate global climate change. Hence the need to research CC technologies to reduce cost and improve efficiency of CO_2 capture. Two of the main CO_2 emission sources are transport and energy electricity generation that account for 25% and 25% of the total emission respectively. Thus, the necessity to reduce CO_2 emission form mobile and fixed sources in the upcoming future. Even though addressing both sources is equally important, the mobile sources have shown to be a greater challenge (3). Consequently, the importance of sustainable energy sources cannot be highlighted enough since the greenhouse effect has led to a yearly increase in the earth's surface temperature. Even the Nobel Prize-winning Intergovernmental Panel (NPWIP) have concerns and advise that a cut of 50-80% is required by 2050 to avoid the most harmful effects of climate change (4). The greenhouse effect is instigated by carbon dioxide (CO_2), methane (CH_4), nitrogen oxide (NO) and water vapor, also known as greenhouse gases, emission into the environment with CO_2 being the predominant gas (3).

To minimise the greenhouse gas emissions more energy efficient, fossil fuel power plants need to be further improved. The combustion of fossil fuels can be reduced by: (i) decrease the burning of fossil fuels; (ii) increase the efficiency coal fired plants; (iii) CO_2 capture and storage; (iv) improve the CO_2 partial pressure in exhaust gas. To decrease the burning fossil fuels is quite challenging as it would require a decrease in electricity production and alternatively find replacements for fossil fuels (3). Additionally, trying to increase the coal fired plants efficiency is also not a feasible option to reach the target of nearly zero CO_2 emission. Thus, the carbon capture and storage (CCS) has shown to be more promising method for continuous and permanent reduction in CO_2 emission that are related to fossil fuel combustion. This would also give more time to develop alternatives to fossil fuels. In contrast, the improvement of CO_2 partial pressure in the exhaust gas would only improve the electrical energy efficiency (3).

To reduce CO_2 emission into the environment, countries have considered different approaches that include:

- improve energy-efficient use and better promotion of energy conservation
- recommend higher usage of low carbon fuels, natural gas, nuclear and hydrogen power
- utilise renewable energy like wind, solar, bioenergy and hydropower more
- deploy geoengineering approaches with afforestation or reforestation
- invest and research more in CO_2 capture and storage (CCS)

These different approaches have distinct applications that have their own advantages and limitations which are displayed in Table 1-1. A few of these approaches are focused on carbon emission reduction like the use of clean fuels, whereas others are

more directed towards demand-side management such as energy conservation. The advantages and disadvantages of each approach determines its applicability. However, it is not likely to meet the Intergovernmental Panel on Climate Change (IPCC) goal of CO_2 reduction by adopting only one approach. Hence why there is a rising need for better CO_2 emission reduction strategies (5). Currently a wide range of CO_2 capture technologies are available that emphasises on the CO_2 separation from flue gases in biomass or fossil fuel which can occur through different means and might involve several steps. Assuming the flue system contains large quantities of carbon dioxide, oxygen and air as an input, then a concentrated CO_2 stream can be separated via different pathways (Figure 1-1) (6):

- Post-combustion: The CO_2 is separated from the flue gas after combustion of a fuel (coal, oil, biomass or natural gas) from the product stream which often contains O_2 (oxygen), N_2 (nitrogen), CO_2 and water. The capture can take place anywhere between the product processing and before the emission into the atmosphere.
- Pre-combustion: The separation occurs by converting fuel into CO_2 and hydrogen by gasification with oxygen or air. The CO_2 is captured from a high-concentration stream of hydrogen and carbon dioxide, whereas hydrogen is used on other energy utilities.
- Oxy-fuel combustion: This separation concentrates on producing an N_2-free oxidiser stream where the stream only contains CO_2 (higher concentrations than post-combustion stream) by separation O_2 from the nitrogen in the air (6).

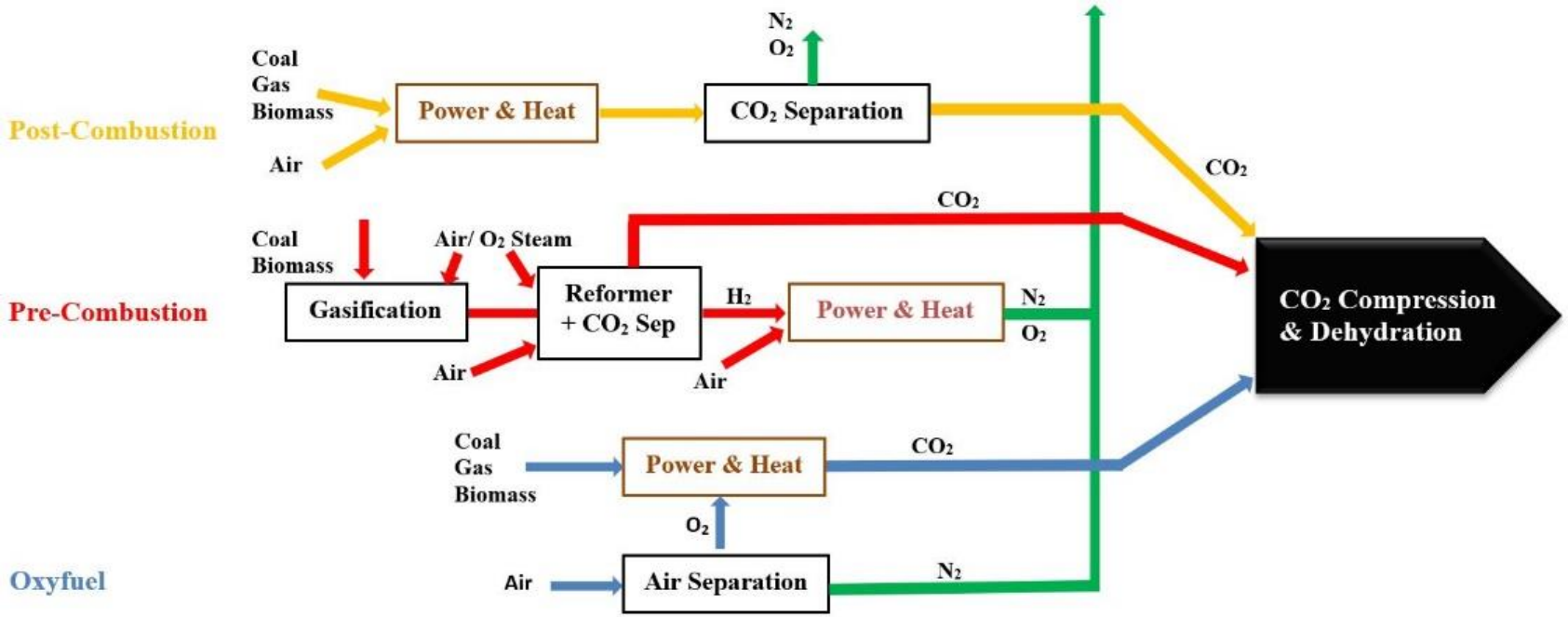

Figure 1-1 Illustration of the different pathways for CO_2, N_2 and O_2 separation (Adapted from (6)).

Table 1-1 The different approaches to reduce CO_2 emission and their application sector, advantages and limitations (Adopted from (3)).

Approach	Application sector	Advantage	Limitation
EE & EC	Commercial & industrial building	Easy 10-20% energy saving	Potential high capital investment for energy-saving technology installation
High clean fuel usage	Substitute coal with natural gas in power generation	Natural gas has a 40-50% lower CO_2 emission compared to coal because of higher ignition/ combustion efficiency & lower carbon content; Cleaner exhaust gas due to lower sulphur dioxide (SiO_2) and particulates concentration	Higher cost of fuel which is comparable to shale gas
Adoption of clean coal technology	Replacement of conventional combustion, e.g. integrated gasification combined cycle (IGCC)	Lower air pollutant emission with coal use	Extensive investment required to adopt technology on a large scale
Higher renewable energy use	Highly developed renewable energy source (wind, solar, hydro and biofuels)	Local natural resources are used; Low to none greenhouse gas emission	Depended on local resources availability and cost; In most cases cost more than conventional energy sources; intermittent source that is not fully mature, e.g. wind and solar power
Nuclear power development	Nuclear fission adopted in few countries like Japan and US; Technology still in development and research phase	No greenhouse gas, i.e. CO_2 or air pollutant emission	Controversial; Hindered development due to Fukushima Nuclear Accident (2011)
Afforestation & reforestation	Can be applied to any country	Simple approach for natural & sustainable CO_2 capture	Land use gets restricted/ not available for other applications
CCS	Applicable to high CO_2 emission sources	>80% CO_2 capture efficiency	CCS technology not developed yet for commercial scale

1.2 Aims

The Cryogenic Carbon Capture and Storage (CCCS) has a high energy output due to it's cooling process to liquify the captured CO_2, thus the aim of this thesis is to reduce the energy consumption of the CCCS process through the encapsulation of CO_2 sorbents. The formulated microcapsules will absorb CO_2 while being exposed to low temperatures. The concept is that these capsules who have CO_2 absorbed would further cool down the CCC system.

Thus the thesis aims to encapsulate CO_2 sorbents and thus use these formulated microcapsules in low absorption temperature process to reduce energy consumption of existing post-combustion carbon capture technologies. These microcapsules will undergo several experimental tests to:

- Identify formulation parameters that lead to successful encapsulation of the CO_2 sorbents and optimise the following conditions for maximise absorption: emulsifiers, emulsifiers concentrations, core materials, core-shell ratio, mechanical stirrer speeds and homogeniser speeds
- Characterise the formulated microcapsules for physio-chemical and structural properties
- Study the absorption capacity of the formulated sample under high pressure using a manometric method
- To observe the effect of low temperature inside a continuous reactor on: size, core material and emulsifiers

The novelty of this thesis' work is to combine the advantages of both CO_2 solvents and microcapsules in order to provide an alternative CO_2 absorption method for post-

combustion process. Current research is concentrated on CO_2 absorption in high temperatures.

1.3 Thesis Outline

There are eight chapters in this thesis where chapter one background concentrates on the information for the need of CO_2 capture as well shows the current CCS status.

Chapter two encompasses a critical literature review on the different CO_2 capturing methods. This chapter also outlines the different microencapsulation methods available along with potential core and shell materials for CO_2 capture.

Chapter three describes the experimental methodology used during this work in detail.

Chapter four analyses the formulation method for encapsulating amine cores with silica shell for CO_2 absorption where each of the parameter affecting the formulation as well as morphology is studied such as different core material 2-amino-2-methyl-1-propanol (AMP), monoethanolamine (MEA), triethanolamine (TEA)), different emulsifiers and their concentrations, different stirring and homogenisation speeds.

In chapter five the formulated microcapsules from chapter four are characterised in terms of physio-chemical, structural and initial absorption properties. The formulated samples are also examined in terms of quality to identify good formulating parameters for the encapsulation of an amine core with tetraethyl orthosilicate for CO_2 capture.

Afterwards the formulated microcapsules are tested regarding the CO_2 loading capacity in chapter six. For this purpose, a pressure rig was set-up to study the effect of pressure on the different microcapsule. Hence the loading capacity of the different microcapsules are related back to their properties like size and core material.

Chapter seven examines the effect of low temperature on the absorption capacity and absorption kinetics of a range of microcapsules. For this purpose, a continuous reactor is set-up which was used to identify the effect of low temperature on different size, core material and emulsifiers.

In the last chapter (chapter eight) the conclusions of the thesis are provided along with suggestions for future work.

Chapter 2 Literature Review

2.1 Introduction

The capture and storage of CO_2 is a process that contains several steps: 1) separation of CO_2 from energy-related or industrial sources; 2) transport to a storage location; 3) long-term isolation from atmosphere. The CO_2 capture allows the process to be applied to large point sources. Moreover, the compressed gas can be stored rather easily and there are different storage places available, such as in the ocean (e.g. deep under the seafloor), in mineral carbonates (fixation of CO_2 with inorganic carbonates) or in geological storage (oil and gas fields). Furthermore, the stored CO_2 can also be used for industrial processes like fossil fuel, biomass energy, synthetic fuel plants and natural gas production (7). The capture and storage of carbon has been widely acknowledged for a long time as an economical and efficient technique to regulate emissions. There is a considerable amount of carbon capture storage (CCS) plants already in use; however, the main challenge of capturing CO_2 with low energy cost in an efficient way has still to be overcome (8). The CCS requires a lot of energy that leads to the reduction of the overall efficiency of the system, which in turn increases the fuel supply, solid waste and the environmental impact compared to a plant without the CCS. Hence why minimising the energy requirement for carbon capture combined with improving the energy conversion is a high priority for future CCS development to reduce the overall cost and environmental impact. Additionally, an energy plant with CCS system is considered to be able to capture 85-90 % of the processed plant CO_2, but this process requires 10-40 % more energy than a plant without the CSS system. Most of the extra energy is required for the storage and compression of the carbon (7). Though, there are several existent technologies that can separate CO_2 from a stream with the required concentration.

To apply the CCS system to a large scale of industries, the CO_2 emission sources need to be predicted. Despite being able to determine the emission sources like the CO_2 concentration and geographical location for past years like year 2000 with acceptable accuracy for most of the industrial sectors, the challenge arises to try to predict the future location of CO_2 emissions. Even though all projections so far have indicated to an increase in CO_2 emission, the actual locations of potential new plants cannot be predicted as they are a subjective business. Additionally, a detailed storage capacity description is required for the world's sedimentary basins. Though estimates are available they do not show the full resource assessment. This information is important to be acquired for identifying storing opportunities for CO_2 emission at large point sources (9).

In this chapter, the previous literature on carbon dioxide (CO_2) capture technologies, cryogenic liquids for energy storage, microencapsulation techniques and carbon absorbent materials are reviewed. The literature review is divided into various sections. The first section provides a general introduction to the different existing carbon capture methods. This will then be followed by a brief introduction of cryogenic liquids for carbon capture and energy storage (CCCS/CES). In the third section, the existing encapsulation methods will be reviewed subsequently the encapsulated liquid sorbents for CO_2 capture literature will be studied. The forth section will revise the polymerisation methods and the encapsulation parameters like emulsifiers.

2.2 Current status of CO_2 capture technologies

A wide range of different methods exist to capture CO_2 however each method relies on different materials and technology. The most commonly used methods will be discussed in this section.

2.2.1 Separation with Solvents/Sorbents

Depending on the solvent used, the absorption, adsorption and chemisorption method and the condition for CO_2 separation during the capturing process will differ greatly from each other.

2.2.1.1 Chemical Solvents

Chemical solvents such as amines are used to capture low CO_2 concentrations through the absorption process from a gas stream (7). This technology is most commonly used nowadays in the oil and chemical industries, even though it has limitations regarding efficiency, scale and stability due to the need of high-volume gas streams, high investment cost and energy consumption (materials used during process require changes in conditions). Moreover, over time the process produces corrosive products that might require hazardous handling procedures (10).

An example of CO_2 capture with amines from a flue gas stream is the Warrior Run coal-fired power station, which captures 150 t/d of CO_2. The most commonly used amine is mono-ethanolamine (MEA), which gives a 98% recovery rate and 99% product purity for CO_2 capture (10). The energy requirement for this process could be reduced by 40% with improved solvents. Recently there has been an interest in

sterically-hindered amines like AMP, which are thought to have better absorption and desorption features compared to MEA (10).

2.2.1.2 Physical Absorption

Absorbents are used as an alternative to solvents to allow gas permeation or desorption into a solid or liquid under specific conditions. For this method the temperature and pressure control the rate of desorption or absorption and therefore, eliminates the production of hazardous products. Moreover, the smaller the difference in conditions are, the less energy is required with an increase in absorbent for CO_2 capture at an equivalent rate. For physical absorption either physical solvents or mixed chemical-physical solvents are used. The most common physical solvent Selexol® can release CO_2 through depressurisation, leading to a decrease in heat consumption compared to chemical solvents (7,10).

2.2.1.3 Physical Adsorption

This process relies on carbon dioxide's affinity to material surfaces under certain conditions without forming a chemical bond. Adsorbents separate CO_2 from a stream by attracting the gas to a materials' surface under high pressure due to Van der Waals forces (7).

2.2.1.4 Chemisorption

Gas molecules can bond chemically to some material surfaces. If the whole molecule bonds to a material surface, the process is called associative, and if a molecule breaks up to form a bond, it is called dissociative. Chemisorbents often have an active surface

layer which is supported by an inert substrate. Most often small particles are used as substrates to increase the surface area. Examples of chemisorption are metal oxide air separation method or dry chemical absorbents (7).

2.2.1.5 Chemical Bonding

Materials that can create stable, thermodynamically favourable, chemical bonds with a gas in a solution or mixture are either endothermically regenerable or form a stable, waste materials for storage. Most often this technique depends on O_2 mineralisation for CO_2 separation from a gas stream with the use of reactant minerals like limestone (7).

2.2.2 Separation with Membranes

Membrane separation is a combination between absorption and desorption with selective permeability of certain gases, i.e. one component of the gas stream is allowed to pass the thin barrier faster than the others (7,10). The most commonly used membranes for gas separation are palladium, porous inorganic, zeolites, polymeric membranes. Different membranes have diverse characteristics, and sometimes several membranes might be required to produce a high purity CO_2 stream, e.g. polymeric membranes like polysulfone are used to separate CO_2 from nitrogen, though they have a relatively low selectivity compared to other membranes. (10).

Most membranes are not able to achieve high degrees of separation due to the difference in gas transport rate and therefore require several stages and/or recycling of the stream. This leads to an increase in energy consumption, cost, complexity. But

a potentially high surface area for membranes might be able to reduce the potential chemical difference (7,10).

2.2.3 Separation with Cryogenics

Separation with cryogenics is also known as phase separation, which works by cooling down gas molecules below their boiling points where they begin to move very slowly due to lower kinetic energy, and have weak intermolecular forces (7). Within gas mixtures, each gas has a different boiling point and therefore are separated by continuous cooling the gas mixture until different phases are created at the specific gas boiling points. This cryogenic process is used to separate gases into a pure stream (10). Similarly, CO_2 separation from a gas mixture is achieved by cooling and condensation and is used for streams with high CO_2 (>90%) concentrations. Though the major disadvantage of cryogenic separation is the high amount of energy required for the refrigeration of the process. Moreover, other substances like water need to be removed before the CO_2 stream can be cooled down to avoid blockage (10).

2.2.3.1 Cryogenic liquids

Gases which are kept in their liquefied state at very low temperatures are known as cryogenic liquids. All cryogenic liquids are extremely cold and have boiling points under -150°C. CO_2 and NO (nitrogen oxide) are included within cryogenic liquids even though their boiling points are slightly higher than -150°C. Cryogenic liquids are in a gaseous state at room temperature and pressure. Cryogens need to be cooled down below room temperature before they can be liquefied through increasing the pressure. Different cryogens have different conditions for pressure and temperature for

liquefaction (Table 2-1); however, they all have two common properties: being extremely cold and small liquid volume expanding into large gas volume. The gases and vapours which are released from cryogenic liquids remain very cold and create highly visible fogs due to the condensation of the moisture in air (11,12).

Table 2-1 The most common cryogenic liquids and their physical properties (Adapted from (11)).

Cryogen	Boiling Point (1 atm; °C)	Critical Pressure (psig)	Liquid Density (g/L)	Gas Density (27°C, g/L)	Liquid-to-Gas Expansion ratio
Ar	-186	710	1402	1.63	860
He	-269	34	125	0.16	780
H_2	-253	188	71	0.082	865
N_2	-196	492	808	2.25	710
O_2	-183	736	1410	1.4	875
CH_4	-161	673	425	0.72	650
CO_2	-78	739	1256	1.98	845

2.3 Cryogenic Liquids for Energy Storage

The use of cryogenic liquids for energy storage has many advantages and industrial application as it can serve as an intermittent renewable energy source and allow large electricity generation with flexibility in terms of location due to no ‘wrong time’ electricity generation, which means neither too much nor too little energy is generated but just the correct amount required. Furthermore, it provides an optimised return on investment (ROI) for renewable plants and reduces the investment cost for asset base and fuel costs. The better flexibility with cryogenic liquids energy stores lowers the cost for network investment and reduces the risk of interconnection and SMART grid (13).

2.3.1 Cryogenics Energy Storage (CES)

Cryogenic Energy Storage (CES) uses off-peak energy, e.g. when the wind is blowing, and there is low demand, to cool down the air to -196 °C for it to become a cryogenic liquid or ‘liquid air’ or in case of nitrogen (gas) being cooled down it becomes liquid

nitrogen. This allows the cryogenic liquid to be stored easily in very large quantities until energy is needed at peak-times, e.g. wind stopped blowing. The liquid air is then pumped out of their container and warms up at room temperature or by the use of heat from a nearby source which allows fast expansion of liquid into a gas with a 1:700 liquid to volume ratio, producing enough energy to turn a turbine for electricity generation (Figure 2-1) (14).

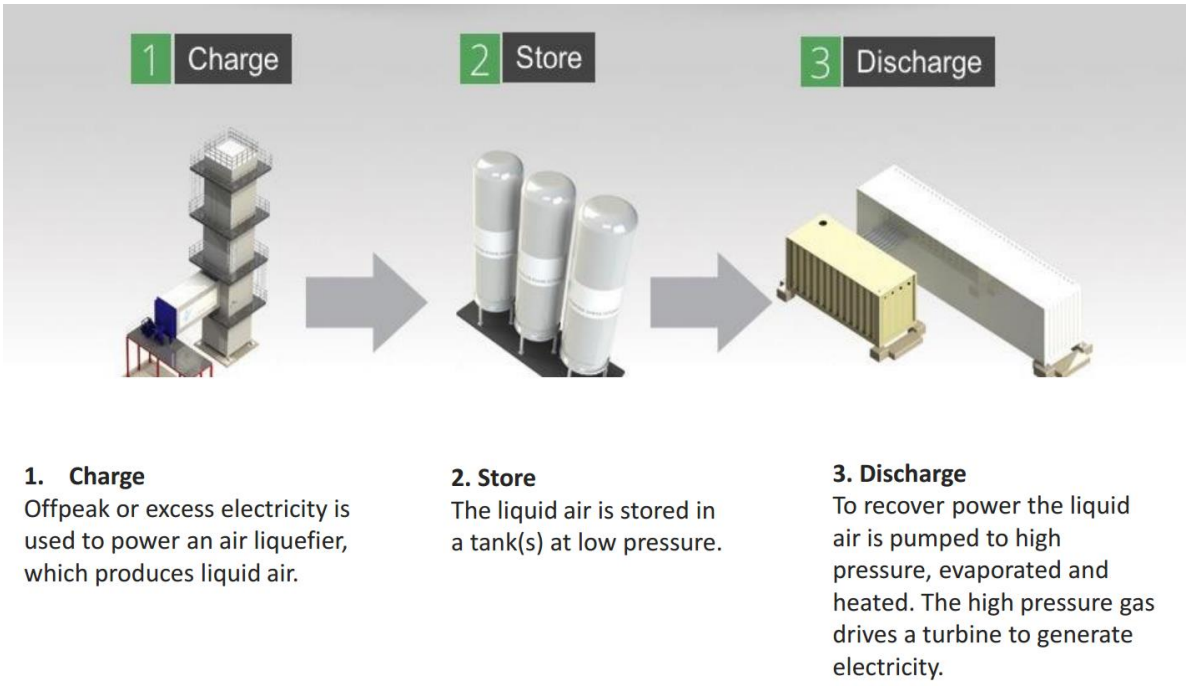

Figure 2-1 The three different steps involved in the CES process: 1) charge; 2) store; 3) storage (14).

The CES system has a low efficiency of around 25%, however there are ways to significantly improve the performance by storing the cold which is released during air expansion at the end of CES process and use it to help in cooling down the air at the start of CES. This cold recycling allows CES efficiency to increase to ~70%. This method addresses the intermittent energy generation problems. The only by-product of the process is cold air; hence no toxic substances or materials are required, and the CES familiarity of parts and technology reduce any risk involved with the technology.

Furthermore, the CES is suitable for electricity capture from renewables due to them being able to easily scale according to the electricity consumption by adjusting: the size of the liquefaction unit, total amount of energy captured that can be stored in large or small containers, the delivered power by the size of the installed turbine. Furthermore, the system also does not have any geographical or geological constraints, e.g. no hydro or compressed air energy storage is required, which allows it to be placed near demand or generation centres. Due to its favourable economics, process and operational advantages, CES is able to dominate the energy market, example Birmingham Centre for Cryogenic Energy Storage (BCCES) (15).

2.3.2 Cryogenic Carbon Capture and Storage (CCCS)

The cryogenic carbon capture (CCC) was developed and designed to separate an almost pure CO_2 stream from a power plant flue gas. The CCC system is used for post-combustion and is suitable for fitting already existing power plants (16). CCC is based on phase change (Figure 2-2) to separate CO_2 and other gases from exhaust or process gas. The system works by cooling down CO_2 to low temperatures like -140 °C to desublimate or change the gas to a solid. The solid CO_2 is then separated, pressurised, melted and delivered or stored at pipeline pressure from the residual gases. Pollutants are removed from the remaining gas after CO_2 separation, giving a nearly pure nitrogen product that can be safely released into the atmosphere, whereas the captured CO_2 can be used for various application like biofuel production and enhanced oil recovery (EOR) (17).

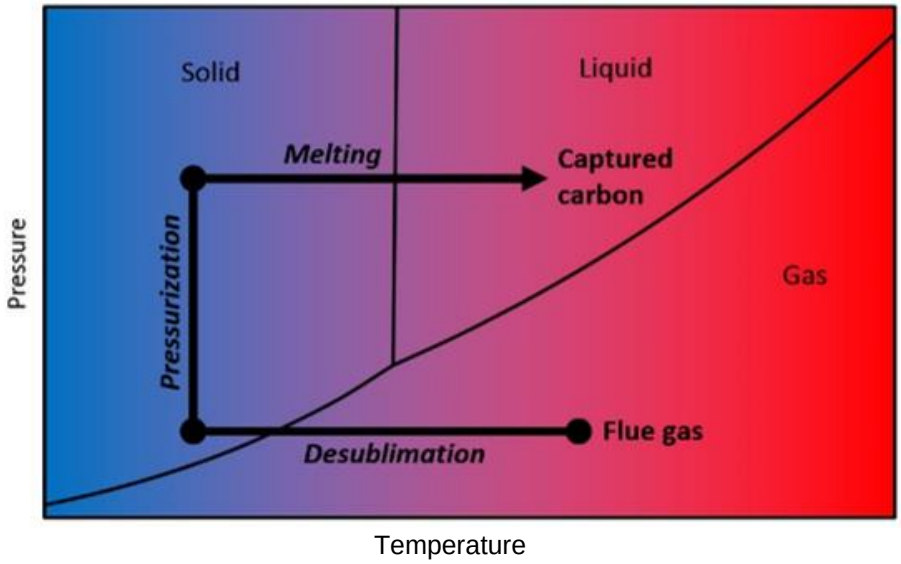

Figure 2-2 Graph showing the different phases that are found in the CCC and their functionality. A flue gas changes into a solid when the temperature is decreased sufficiently due to the desublimation of the gas. In contrast, an increase in pressure followed by a melting allows the solid CO_2 to change into a liquid which is easily captured (18).

In the CCCS system, the flue gas stream is dried and cooled down, and then modestly compressed to further cool down the gas to slightly above the freezing point of CO_2 (Figure 2-3). The solid CO_2 is then separated from the flue gas, and the pure CO_2 is pressurised, whereas the cooled down N_2 and CO_2 streams are used for cooling down the new incoming flue gas in a heat exchanger. The result of the process is a liquid CO_2 and gaseous N_2 stream. As mentioned many technologies exist for CO_2 capture but CCC shows the most potential due to its many advantages (16).

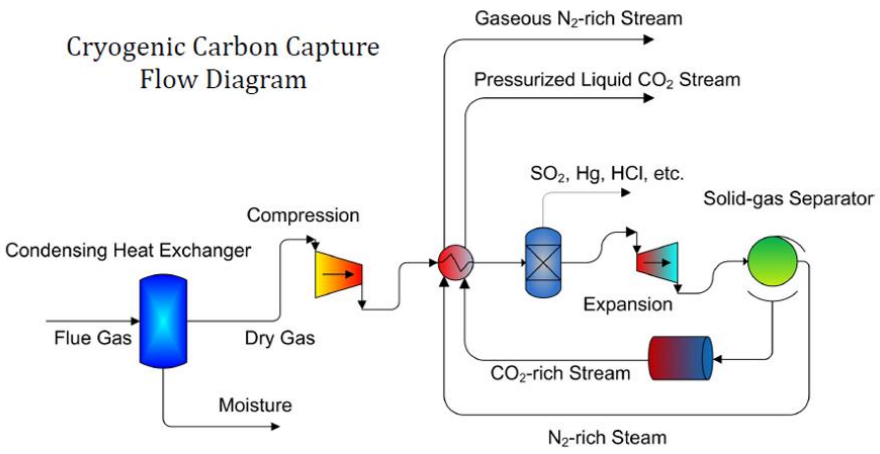

Figure 2-3 Schematic illustration of a cryogenic carbon capture and storage (CCCS) process (19).

2.3.2.1 Pollutant Capture

Not only is the CCC system able to capture up to 95-99% CO_2 from a flue system, but the system also captures other pollutants such as mercury (Hg), NO_x and SO_x (Table 2-2). These pollutants are captured similarly to CO_2 through desublimation where the captured concentration is reliant on the low temperature (18).

Table 2-2 The temperatures required to capture the different pollutants gases (11).

Temperature (°C)	Captured Pollutants
-48	up to 100% mercury from coal
-77	the above & 99% of the mercury from the atmosphere
-117	the above & 90% of the CO_2 from coal; SO_2 EPA standard met
-132	the above & 99% of the CO_2 from coal
-143	the above & 100% of the CO_2 from coal; exhaust exiting the plant is cleaner than the surrounding air
-150	the above & 80% of the CO_2 from the atmosphere
-162	the above & 99.5% of the CO_2 from the atmosphere

2.3.2.2 Steam Cycle Integration

Another advantage of the CCC is its ability to integrate into the steam cycle by allowing the warm exhaust entering the system to heat the feed water to the boiler in a Greenfield installation. This enhances the power input and steam cycle efficiency of the plant (18).

2.3.2.3 Energy and Economics

The main advantage of CCC is the overall lower cost and energy requirement to capture CO_2 compared to the other existing CO_2 capture methods. The cost is further lowered upon considering the benefits of a steam cycle integration and/or pollutant capture with the CO_2 capture (Figure 2-4). Currently, the amine absorption process for CO_2 capture costs around $69 per tonne, whereas the CO_2 capture with CCC system is considered to be around $35 per tonne which is half of the previous method. The

cost can further be lowered to $14 per tonne by combining the CCC with steam cycle integration or pollutant capture. Furthermore, the CCCS requires only half of the energy than the amine absorption process for post-combustion processes (18).

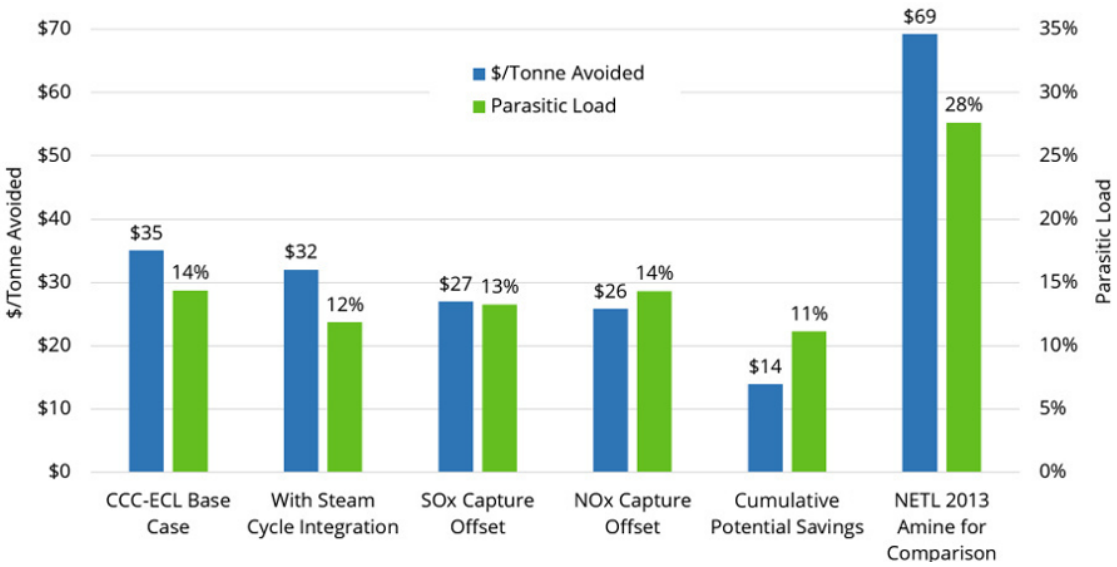

Figure 2-4 Comparison of cost between the different carbon-capturing technologies during the first year of system implantation (18).

2.4 Microencapsulation of adsorbents for CO_2 capture

Although various CO_2 capture technologies exist, post-combustion CO_2 capture is the most mature technique including absorption, adsorption and membranes (20–24). However, these technologies are not mature enough to be used in power plants due to the mass transfer limitation in the sorption processes that occur with high flue gas quantity as well as high energy demand during the regeneration process, high capital and high chemical cost. Hence researchers are concentrating on developing non-aqueous solvents like ionic liquids, CO_2-binding organic liquids, nanoparticle hybrid materials and microencapsulated sorbents due to their potential of being more energy-saving and environmentally friendly (25).

The most established CO_2 absorption technique during post-combustion is the contact of an aqueous amine with flue gas to form carbamates as the amine reacts with CO_2. The commonly used amine is monoethanolamine (MEA), which has a high absorption rate and loading capacity. However, drawbacks such as high corrosiveness, toxic degrading side-products and high amount of energy required for CO_2 removal during the sorbent regeneration prevent its widespread use. Thus, new sorbents are proposed to overcome these limitations by combining the liquid sorbents (core) with solid ones (shell) by forming microcapsules. The liquid solvent would provide high loading capacity, selectivity as well as water tolerance, whereas the solid sorbents would provide a high surface and in turn, higher absorption capacity as well as low volatility (26). Moreover, microencapsulation can lower the cost of CO_2 capture by containing precipitates and isolate the solvent from reactor equipment (27).

However, these microcapsules are dependent on the chemical absorption process, which is by far the most commercially viable and mature technology. The most common materials used for chemical absorption are Monoethanolamine (MEA), Methyldiethanolamine (MDEA), 2-Amino-2-Methyl-1-Propanol (AMP) and Piperazine (PZ), which are selective CO_2 solvents. Amines absorb CO_2 through a multi-step reaction creating a carbamate salt through the formation of zwitterionic intermediate product (Equation 2-1/3) (28):

$$CO_2 + RNH_2 \leftrightarrow RNHCOO^- + H^+$$

Equation 2-1: Zwitterionic Intermediate produced by AMP during CO_2 Capture (28).

$$RNHCOO^- + H_2O \leftrightarrow RNH_2 + HCO_3^-$$

Equation 2-2: Hydrolysis of Carbamate to form Bicarbonate Ions, releasing free Amine. Free Amine reacts with another CO_2 Molecule, resulting in the theoretical loading capacity of 1 mol CO_2 per mol Amine (28).

$$RNH_2{}^+COO^- + RNH_3{}^+ \leftrightarrow RNHCOO^-$$

Equation 2-3: Carbamate Formation by Deprotonation of Zwitterion (28).

2.4.1 CO_2 adsorbents and Microencapsulated Carbon Sorbents (MCES)

MEA is the most common solvent used within PCC power plants (24) due to their fast CO_2 absorption kinetics, cheapness, and being a proven technology (29). However, amines, especially MEA, degrade easily in the presence of flue gas impurities, resulting in the release of harmful volatiles and corrosion of equipment (30). In comparison, MDEA and AMP possess higher CO_2 absorption capacity. Both are sterical, amine groups surrounded by a crowded, steric environment, hindered amines allowing them to bind 1 mole of CO_2 for every 1 mole of amine, whereas for every 1 mol of MEA 0.5 mole of CO_2 is bound. This reluctance of loading beyond 0.5 mol of CO_2/mol of amine is attributed to stable carbamate formation (Equation 2-1). The maximum loading can only be increased by high pressures where hydrolysis of solvents creates free amines to react with additional CO_2, thus exceeding the 0.5 loading. The tertiary or sterically hindered amines show a different limiting behaviour as they form bicarbonate ions (Equation 2-2) and carbamates are the intermediates. While the higher CO_2 loading makes tertiary amines more attractive in practice, the lower CO_2 absorption rates might limit their use (31).

To overcome the limitations of MEA, new sorbents are required. In recent years a new class of sorbent materials has been established, called liquid sorbents that combine the advantages of solid sorbents (such as their low volatility and high surface area) and liquid solvents (like their water tolerance, high capacity and selectivity). These liquid sorbents can be microencapsulated to form a highly permeable, microencapsulated carbon sorbents (MECS). These MECS are made up of CO_2

absorbing liquid solvents which are contained in a solid polymer shell and are carbon dioxide permeable (32).

Absorption in the MECS happens by CO_2 diffusion through the thin capsule shell, which then dissolves and reacts with the liquid solvent to form the desired product. This reaction can be reversed by heating to release high purity CO_2 which subsequently can be utilised or stored; this process is known as regeneration (33).

The microcapsule system requires certain features, where selectivity and permeability are competing parameters:

- Spherical and highly uniform in size
- Sorbent cores with controlled geometry and composition must be encapsulated
- Sufficient permeability of polymeric shells or membranes for CO_2 to allow the absorption rate to dominate the encapsulated sorbent system
- Sorbent system must be strong enough to withstand multiple CO_2 absorption-desorption cycles without failure (regeneration)
- The retained mechanical integrity of microcapsule during repeated cycling

It is imperative to choose the materials for the liquid sorbent and capsule shell very carefully, as they have to fulfil the mentioned criteria. Furthermore, the liquid sorbent and capsule shell need to be compatible with each other for the microcapsule to be able to capture carbon and release it upon heating when required for further utilisation or capture (32,33).

2.4.2 Potential Core Materials

To select a suitable core for the microcapsule formation, certain criteria must be met: 1) adsorption capacity; 2) selectivity of CO_2; 3) adsorption/desorption kinetics; 4) mechanical strength of sorbent; 5) chemical stability/tolerance to impurities; 6) regeneration of sorbents; 7) cost and availability of sorbent (34).

Microencapsulation allows certain criteria to be neglected due to the presence of a selective shell wall. Solvents were previously discounted due to their slow kinetics and susceptibility to degradation through the presence of high oxygen content or the presence of SO_x or NO_x within the flue gas. Now they can be investigated through the process of microencapsulation as it exponentially increases the surface area for solvents (35).

For new sorbents to be competitive with the current MEA solvents on the market, they need to meet a minimum CO_2 capacity of 3-6 $mmol^{-1}g^{-1}$ solvent (35). One research showed that through encapsulation of **carbonates,** a 10-fold increase in absorption rate could be achieved as well as the containment of precipitates thus mitigating the typical issues found with encapsulation of carbonates. Furthermore, encapsulated carbonates save energy by 26% compared to MEA (aqueous) (33). Carbonates like K_2CO_3 and Na_2CO_3 precipitate into a solid by reacting with CO_2, which presents an issue in a two-phase system, but containment of the solid is offered through the presence of a shell. However, these microcapsules need to be tested for multiple cyclic loading (36).

In comparison, organic or polymers that contain the NH_x group bind acidic CO_2 chemically at low reaction temperatures, thus making it attractive for CO_2 capture. Most **amines** like MEA or diethanolamine (DEA) react with CO_2 to form carbamates which

are more stable than the bicarbonate ions produced during the CO_2 capture by carbonates (37). However, amine-based solvents are still not in widespread use due to their high corrosiveness, fouling of equipment, producing toxic degrading products and high energy requirement for CO_2 removal during sorbent recovery. But these drawbacks of the material could be overcome by encapsulating the solvent. Vericella et al. (2015) used Optical Adhesives (NOA 61) for the shell to encapsulate MEA, however, during microcapsule characterisation the shell material showed inhabitation of small molecule diffusion like CO_2 into the microcapsules. In contrast, Stolaroff J.K. (2016) tried to use Semicosil for the microencapsulation of MEA, but the shell material failed to cure during the encapsulation process (36). Since many advanced solvents contain amine groups, shell materials for them must be chosen carefully with amine-compatible curing mechanism.

There are many other solvents like **Ionic liquids** (IL) and **Piperazine** (PZ) for CO_2 capture. ILs, also known as low-temperature molten salts, are attractive for CO_2 capture because of their low vapour pressure, high chemical diversity, high thermal stability, negligible volatility and CO_2 capacity of 1 mol CO_2/mol IL (similar to Amines) (37). Several researches have shown that IL has a high CO_2 solubility, better performance and low energy requirement during the regeneration cycle compared to other commercial solvents. However, the main challenge for the use of IL in carbon capture is their high viscosity and poor mass transfer. Currently, research is being undertaken to encapsulate IL to improve the mass transfer to make them competitive with amine-based solvents (38).

Each of the core solvents has its advantages and disadvantages, hence why the core material must be chosen carefully while deciding which material property to prioritise and the end application.

2.4.3 Potential Shell Materials

The primary selection criteria for the shell material is the high permeability to CO_2 to ensure the limiting factor to CO_2 mass transfer is the solbent, not the shell (34). The shell should also provide excellent mechanical and thermal stability to handle the robust nature of the carbon capture process and resist degradation during the regeneration cycle. At last, the shell should be chemically compatible with the solvent (36).

For the microfluidic device, UV curable polymers with precursors that are liquid at room temperature are particularly suitable. Silicone has the highest CO_2 permeability compared to common polymers with typical values of 3000 Barrer (Table 2-3). In previous research, a commercial silicone, Semicosil 949-UV (Wacker Chemie AG), has been reported to meet the criterion mentioned earlier and encapsulation of sodium and potassium carbonate into capsules was successful (36). But the Semicosil 949-UV failed to encapsulate MEA due to the inhibition of the platinum catalyst by the amine group. Even though silicone shells have one of the highest CO_2 permeability, they are not compatible with a dominant solvent group. There are also other polymers with high CO_2 permeability like Thiol-ene, Tetraethyl Orthosilicate (TEOS) and Tego Rad (Table 2-3). TEOS forms a polymer network through hydrolyses and condensation reactions to form siloxane bonds (Si-O-Si) (39,40).

To successfully encapsulate a solvent, a clear interface between solvent and shell must be formed while maintaining two distinct liquid phases. The shell must be curable in the solvents presence unlike Semicosil 949-UV/MEA combination, and lastly, the cured shell material should be stable in the solvent (39).

Table 2-3 Potential shell materials for MCES with their different properties (36).

Industrial Name	Material	Permeability (barrer)	Amine Compatibility	Properties	Curing Time
Semicosil 949	Silicone	3100	No	Strong; Elastic; Tacky	30 min
Thiol-ene	Silicone	2700	No	Strong; Elastic; Tacky	30 sec
SiTRIS	3-[Tris(trimethylsiloxy)silyl]propyl methacrylate	400	Yes after curing	Strong; Stiff; Untacky	10 sec
Tego Rad 2650	Silicone	3200	Yes after curing	Friable; Elastic; Untacky	10 sec

2.4.4 Microencapsulation

Microencapsulation is defined by either enveloping or surrounding one substance within a different substance at a small scale to yield micro-sized capsules. The microencapsulated material has limitless applications such as pharmaceuticals, cosmetics, textiles, agriculture, foods, paints, coatings and fragrances (41). The microcapsule can vary in shape from spheres with a core surrounded by a continuous wall to asymmetrical with various shapes containing embedded droplets of core material throughout the capsules. This provides more comfortable handling of liquid and gas material as solids, allowing a measure of protection against hazardous material handling. In the case of carbon capture, the microcapsules can offer the potential of combining chemical absorption of CO_2 with physical adsorption. Chemical absorption creates chemical bonding between the chemical solvent and the captured CO_2, whereas the physical adsorption allows gas permeation or desorption into solid/

liquid under specific conditions. Temperature and pressure control the rate of desorption or absorption and therefore, eliminate the need for the production of hazardous products (7,42).

2.4.4.1 Microencapsulation example

In recent years, a microfluidic device was designed to produce microcapsules with liquid carbonate core and silicon shells (26). The idea was to link the liquid sorbents selectivity and capacity with the high surface area of the capsules for fast and controlled CO_2 absorption and desorption over multiple cycles. The study reported a lower mass transport across the capsule shell compared to conventional liquid sorbents. However, the enhanced surface area gained through encapsulation delivers an increase in CO_2 absorption rate for the given sorbent mass (26). In another study by the same research group, water-lean solvents were developed for better CO_2 capture efficiency (36). In this study, ionic liquids (IL), as well as CO_2-binding organic liquids (CO_2BOLs), were chosen as the solvents. However, these materials are highly viscous and change phase, but MECS can encase these solvents with a CO_2 permeable polymer shell; thus, these challenges can be overcome with encapsulation (36).

2.5 Formulation

Currently, there are two main fabrication techniques available to encapsulate solvents, bulk emulsion and double emulsion with a microfluidic device.

2.5.1 Bulk Emulsion

In bulk emulsion, interfacial polymerisation occurs when two reactants from the polycondensate meet at an interface. As a result, a condensed polymer wall is formed on the surface of the shell-core interface (43). This technique involves dispersing an immiscible solvent within a carrier liquid, most often oil. The subsequent phase separation caused by the solvent and oil creates an interface for the shell material to react upon and thus encapsulating the core. Mechanical stirring during the process results in collision of the capsules, forming microcapsules and preventing their coagulation as well as depositing at the bottom. As a result, the bulk emulsion method gives a wide range of microcapsule size (44).

This method is mainly used in industries for drug delivery and food production and has been well established since 1964 (45,46).

2.5.2 Double Emulsion – Microfluidic device

This technique is more accurate for producing microcapsules than bulk emulsion (Figure 2-5). The set-up, a microfluidic device for a double emulsion two glass capillaries, is inserted into a glass tube while lying end-to-end. The inner fluid, solvent, is pumped through the tapered end of the injection tube to the collection tube. A middle fluid, shell, moves in the same direction as the inner fluid on the outside of the injection tube, whereas the carrier fluid flows in the opposite direction. All three fluids meet at

the collection, thus forming a double emulsion. The set-up of the double emulsion with a microfluidic device allows control over shape, size and composition of the microcapsules (44).

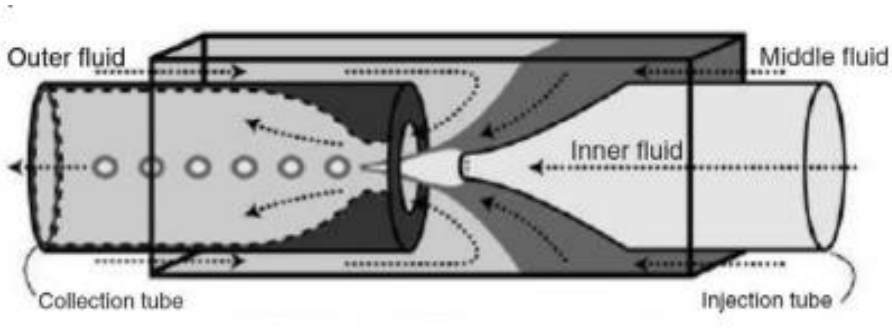

Figure 2-5 Fabrication of double emulsions in microfluidic devices Schematic of a capillary microfluidic device that combines co-flow and flow focusing (42).

2.5.3 Microencapsulation – Chemical Method

2.5.3.1 Solvent Evaporation

This is a technique that has been used in producing microcapsule in liquid manufacturing vehicles by companies like NCR Company and Fuji Photo Film Co. This method works by dissolving the microcapsule coating in a volatile solvent which is immiscible to the liquid phase (47). The core material that is to be encapsulated is dissolved in a polymer solution through agitation to obtain the appropriately sized capsules. This mixture is then heated for the polymer-solvent evaporation. The dispersion of the core material into the polymer leads to shrinkage of the polymer around the core material. However, if the core material is dissolved in a coating polymer solution, microcapsule with a matrix structure are produced rather than a core-shell type capsule. After the solvent evaporation, the temperature is cooled down to ambient throughout continuous agitation. At the end of the process, the microcapsules

can be isolated as a powder, used in suspension from or even coated onto substrates (47).

This solvent evaporation technique can be applied to a wide variety of solid and liquid core materials that are either water-soluble/insoluble materials (47).

2.5.3.2 Interfacial Polymerisation (IFP)

This process occurs when two reactants come in contact at an or on the interface of the droplet and react to form a capsule shell. The generally used materials are multifunctional monomers that include isocyanates and acid chlorides either in combination or individually. Interfacial polymerisation occurs when a multifunctional monomer is dissolved into a liquid core. This solution is then dispersed into an aqueous phase that contains a dispersing agent. Additionally, a multifunctional amine is added for rapid interfacial polymerisation leading to the formation of a capsule shell material. The fundamental reaction can be described by the Schotten Baumann reaction of an acid with a molecule that contains active hydrogen like alcohols, amines and polyurea. A thin flexible film is formed when the two reactants meet that the interface under the correct conditions. An example of an interfacial polymerisation is the emulsification of a pesticide and diacid chloride mixture in an amine and isocyanate solution (47). The base is added to neutralise the acid formation during the polymerisation. Polymer walls are formed rapidly at the emulsion droplet interface (47,48). Another successful example of interfacial polymerisation is the encapsulation of di-ammonium hydrogen phosphate (DAHP) by a polyurethane-urea membrane which gave a yield synthesis of 22% with a 62 wt% fill content. The produced microcapsules had a mean size of 13.35 mm where 95% of the capsules had a lower diameter than 30.1 mm (48).

2.5.3.3 In Situ-Polymerisation

In situ-polymerisation similarly to IFP occurs due to polymerisation of the monomer using an encapsulation reactor. However, during this process, no reactive agents need to be added to the core material as the polymerisation occurs primarily at the continuous phase. At the start of the process, a pre-polymer with a low molecular weight is formed, which grows in size over time, and then deposits on the surface of the dispersed core droplets, leading to the formation of a solid capsule over time (48). An example of in-situ polymerisation would be the encapsulation of cellulose fibres with polyethylene in the presence of dry toluene. Thus, giving a deposition rate of 0.5 µm/min with a thickness of 0.2 – 75 µm. This method is more useful for a uniform coating of material (47).

2.5.3.4 Matrix Polymer

By embedding a core material in a polymer matrix during the formulation leads to the formation of a matrix material. The most common and simplest matrix polymerisation method is spray-drying, where the capsules are formed when the solvent is evaporated form the matrix material. However, a chemical change of the material can also lead to the matrix solidification. This phenomenon has been used to prepare microcapsule with protein solutions through the incorporation of the desired protein in an aqueous amine phase. Thus, allowing enzymes to be encapsulated that were able to convert blood urea into ammonia when used in a shunt system. Furthermore, this technique has also been utilised by different companies for microencapsulation like Eurand America (47).

2.5.4 Emulsion and Emulsifiers

Forming an emulsion with the proper conditions is important to the encapsulation success. An emulsion is formed when one liquid is dispersed into another liquid due to their immiscibility, creating two phases where water is one phase, and the other is an organic liquid, most common an oil.

A core material dispersed into a bulk phase, i.e. the emulsion, forms an unstable phase due to the immiscibility of the two phases because of the repulsion between the emulsion and core material which leads to the need to stabilise the emulsion with emulsifiers. Emulsifiers are made up of hydrophilic and hydrophobic sections which contains fatty acids (lipophilic moiety) and polar molecules respectively. The size and type of hydrophilic and lipophilic moieties regulate the emulsion system, where the relationship between the two can be either estimated through the calculation or experimental determination of HLB value (hydrophilic to lipophilic balance). A low HLB value is favoured for water-in-oil (w/o) emulsions, whereas a high HLB value is able to stabilise an oil-in-water (o/w) emulsion better (49).

2.6 Summary

This chapter reviewed the most common CO_2 capturing methods like CES, Cryogenics, membranes, sorbents and MCES. It also covered the different formulation processes available for potential encapsulation of an CO_2 adsorbent. Additionally, a range of potential core and shell materials are studied.

The most common method for CO_2 absorption is the use of chemical solvent like MEA that have a high absorption capacity however, over time corrosive side-products are formed (10). In recent years physical absorption has become more widespread due to

no hazardous side-products forming as well as lower energy requirement for CO_2 capture. In contrast membranes have not been able to show a similar degree of separation due to the difference in gas transport rate which requires several recycling steps of the stream, hence increasing cost and energy consumption of the process (7,10). CCC is a relatively new CO_2 capturing method that uses cryogenics for CO_2 separation from a gas mixture through cooling and condensation, however, this method requires high energy for the cooling process, though a 90% CO_2 concentration can be reached with the method (18). The better flexibility through using cryogenic liquids for energy storage leads to a decrease in network investment cost (13).

Although these various CO_2 capture technologies exist (Figure 2-6), these technologies are not mature enough to be used in power plants due to the mass transfer limitation in the sorption processes that occur with high flue gas quantity as well as high energy demand during the regeneration process, high capital and high chemical cost. Hence the need to develop new methods to capture CO_2 and thus microencapsulated carbon sorbents (MCES) have been proposed as microencapsulation as it would combine the advantages of microcapsules and solvents. This allowed solvent to be used that have previously been not considered due to their slow kinetics and susceptibility to degradation (35). These microcapsules can offer the potential of combining chemical absorption of CO_2 with physical adsorption. Chemical absorption creates chemical bonding between the chemical solvent and the captured CO_2, whereas the physical adsorption allows gas permeation or desorption into solid or liquid under specific conditions (7,42).

Furthermore, the two main formulation technique to encapsulate solvents were discussed in this chapter, emulsion and microfluidic device. The emulsion method is

easy to set-up but produces microcapsules in a wide size range (44), whereas the microfluidic device allows the shape, size and composition of a microcapsules to be controlled (44). However, for successful encapsulation the use of emulsifiers is important as they are responsible for stabilising the oil phase to allow the encapsulation of the solvent with a shell material (49).

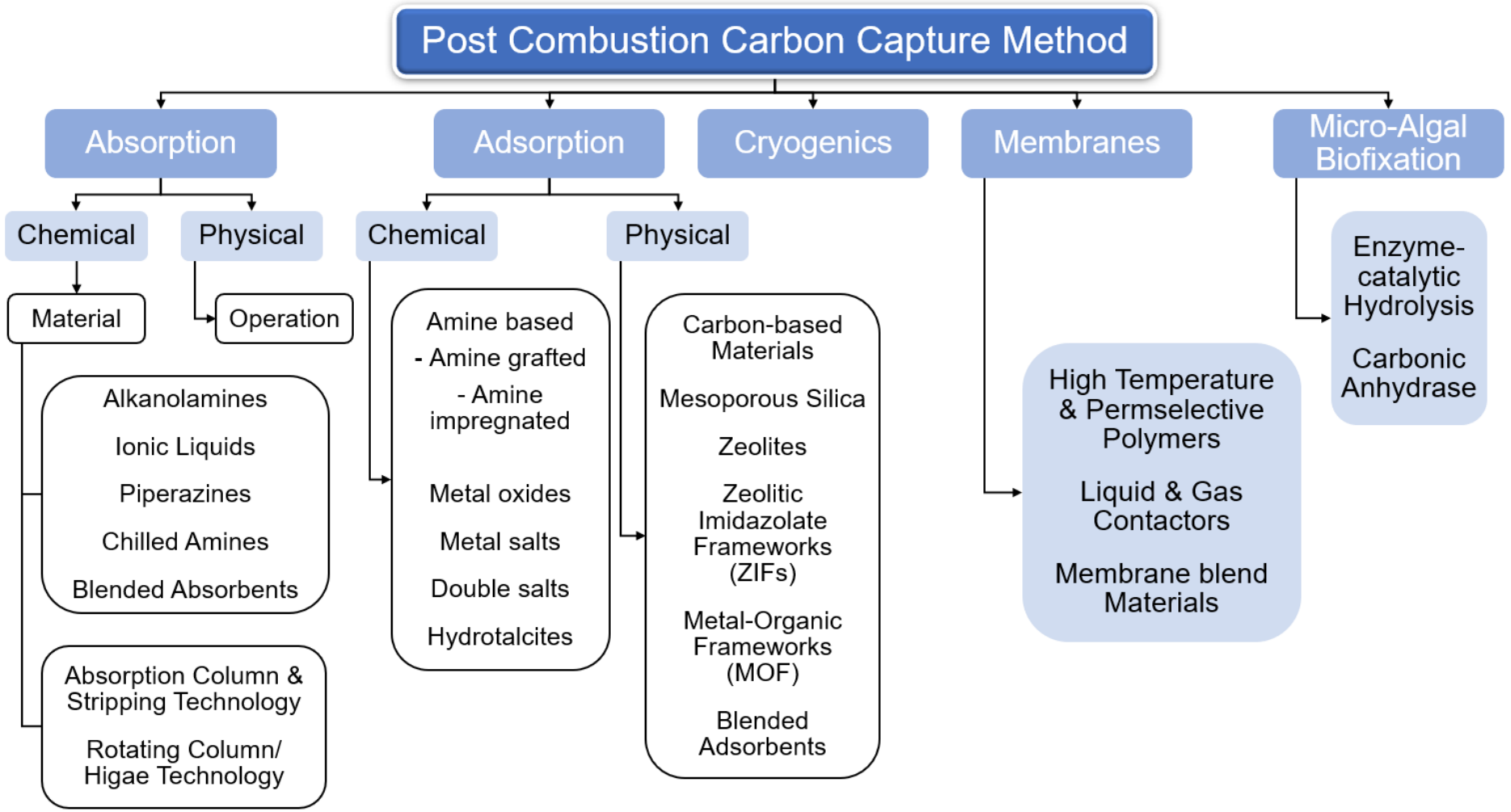

Figure 2-6 Summary of the post combustion capture methods (50).

By taking the industrial needs and literature into consideration, the research aim of this PhD is to produce porous microcapsules with highly permeable shells and high sorption capacity core for efficient CO_2 capture. As a widely known method for microencapsulation, the emulsion technique is chosen for the encapsulation process due to the potential of encapsulating hydrophobic and hydrophilic substances (43,44). Also, 2-amino-2-methyl-1-propanol (AMP), which is immiscible in oil for the encapsulation process, is chosen as the initial core material due to its high sorption capacity. This will then be followed by producing microcapsules with MEA to observe the effect of sorbent on the encapsulation process and absorption capacity. MEA was chosen due to its faster absorption kinetics compared to AMP (36). Additionally, the effect of stirring speed, emulsifier, emulsifier concentration and core-shell ratio on the formulation were also studied. The formulated microcapsules were then analysed in terms of physical, chemical and surface properties, payload, absorption capacity and absorption kinetics for its potential industrial applications. The results are expected to provide an alternative CO_2 absorption technique to the current CO_2 capture technologies.

Chapter 3 Methodology

3.1 Introduction

This chapter describes the materials used to prepare 2-amino-2-methyl-1-propanol (AMP), monoethanolamine (MEA) and triethanol amine (TEA) encapsulated microcapsules, as well as the formulation techniques, characterisation, and absorption capacity of these microcapsules.

A conventional emulsion polymerisation combined with a homogenisation system was used to prepare a water in oil (w/o) emulsion from which microcapsules were formed. During the formulation process, the following parameters were examined to identify the optimal conditions: stirring speed of the impeller, homogeniser speed, core-shell ratio, variety of amine adsorbents, different emulsifiers and emulsifier concentrations. To analyse the physical properties of the emulsion phase, the interfacial tension of the bulk and the surrounding phase were measured. Furthermore, the morphology and quality of the samples were observed with a scanning electron microscope (SEM) which was followed by investigating the mean size and size distribution of the microcapsules with a laser diffraction method (MasterSizer 2000). For the determination of the wall thickness, the sample was frozen before being crushed and observed under an SEM. After formulating the microcapsules, the thermogravimetry (TG) was used to determine the pay load to identify how much core materials were encapsulated. The thermal properties of the samples were investigated with differential scanning calorimetry (DSC) to identify the melting and freezing points of pure core materials and to identify a possible change in the core material after encapsulation. Similarly, to study the chemical composition to observe the effect of encapsulation on the core material a Fourier Transform Infrared spectroscopy (FTIR) was used. To analyse the effect of the surface area (SA), pore size and pore volume, the Brunauer-

Emmet-Teller (BET) was used. The thermal stability (over a range of temperature) of the samples was also investigated by use of a dilatometer. Lastly, to observe CO_2 capture by the microcapsules', initially the thermogravimetry is used, however, at a later stage, a pressure rig and continuous reactor are set-up to investigate the effect of particles size, temperature and core material on the CO_2 loading capacity and absorption kinetics.

The details of the individual techniques and instruments used will be discussed in this chapter.

3.2 Materials

As mentioned 2-amino-2-methyl-1-propanol (AMP; >98%), monoethanolamine (MEA, >99%) and triethanolamine (TEA, >98%) were chosen as the core materials due to their high absorption capacity and tetraethyl orthosilicate (TEOS; >99%) is chosen as the shell material due to its high permeability to gases, compatibility with the core as well as immiscibility with the formulation oil (51). Other chemicals used in the formulation process include sodium hydroxide, thymol blue, emulsifiers: polyglycerol polyricinoleate (PGPR) (>99%), Span85®, Tween80®, Span20® and mineral oil (>99%) (Table 3-1). All these chemicals were purchased from Sigma Aldrich, U.K.

Table 3-1 Important features of the materials used during the encapsulation process.

Function	Material	Features
Core	100% AMP	Highest CO_2 loading capacity, low regeneration temp, secondary amine
	10% MEA	Fast absorption kinetics, primary amine
	30% - 100% TEA	Tertiary amine
Shell	TEOS	Permeability to gas
Immiscible phase	Mineral oil	Immiscibility with core
Emulsifier	PGPR	Non-ionic, to reduce viscosity, low concentrations used (> 0.5%)
	Span85	Non-ionic emulsifier to stabilise aqueous phase; high molecular weight
	Tween80	Non-ionic emulsifier to stabilise aqueous phase; very high molecular weight
	Span20	Non-ionic emulsifier to stabilise aqueous phase; low molecular weight

3.3 Formulation

This section will first introduce the formulation procedure, then discuss the key formulation parameter including emulsifier selection, core-shell ratio, stirring speed, and reaction time, and lastly summarise all the samples formulated during the research period.

3.3.1 Encapsulation Process

Prior to starting the formulation, parameters are chosen for the formulation: emulsifier, emulsifier concentration, core-shell ratio, reaction time, homogeniser and mechanical stirrer speed. The following method is described based on the following constraints: 0.5 wt% PGPR, 6:4 core-shell ratio, 24 h reaction time, 1200 rpm homogeniser speed and 400 rpm mechanical stirrer speed. All the used materials and speeds can be adjusted to accommodate different formulation parameters. Table 3-2 shows all the microencapsulated samples formulated with different parameters.

As illustrated in Fig. 3.1, first of all, 0.35 g (± 0.01 g) of PGPR is weighed into a 100 mL beaker and then 70 g of oil is measured into it to give a 0.5 wt% emulsifier concentration. Subsequently, the beaker is placed on a magnetic stirrer (IKA RCT) and stirred for a minute before transferring the liquid over to a jacketed beaker. This beaker is then connected to a water bath (Julabo ME-F25) where the temperature is set to 20 °C (± 0.1°C) and placed under the homogeniser under fumehood conditions. The temperature of the water bath is kept constant at 20 °C throughout the whole encapsulation process.

In the meantime, the core material is prepared by weighing 1 g (± 0.1 g) of thymol blue and 15 g (± 0.1 g) of colourless, liquid AMP into a 100 mL bottle. The purpose of the dye is to enable a qualitative analysis of CO_2 capture into the encapsulated AMP. Then, the core solution is magnetically stirred until the entire solution becomes blue. Afterwards, the homogenisation is initiated by setting the speed to 1200 rpm and adding the core solution to the oil phase via slow pipetting (3 mL disposable pipettes). Small core dorplet are formed due to the to the immiscibility of the oil and core that provide an interface for the TEOS particles in a later stage. The blade of the homogeniser is placed at the bottom of the beaker due to the high density of the core material compared to the bulk phase to ensure homogenised mixing. The solution is left mixing for 30 minutes to disperse the core into the bulk phase.

In the next step. 10 g (± 0.1 g) of TEOS is measured into a 100 mL bottle along with 2 g (± 0.1 g) of 0.5% sodium hydroxide (NaOH) solution to start the alkaline polymerization of the silica precursor. This shell solution is then stirred via ultra-sonification for one minute. The homogenisation solution is transferred over to the

mechanical stirrer with a stirring speed of 400 rpm and the activated TEOS is added to the beaker via slow pipetting (3 mL disposable pipettes).

The whole system is covered up to prevent solvent evaporation. Furthermore, the whole process takes place under constant temperature and mechanical stirring for at least 24 h.

At the end of the formulation, the sample is centrifuged and repeatedly washed with hexane (≥99%) to remove excess oil, not capsulated AMP, oligomers of TEOS particles before the sample is vacuum dried with a Buchner funnel. Samples prepared for the continuous reactor set-up for CO_2 absorption testing were additionally washed with ethanol during the drying process to further reduce the agglomeration and improve the microcapsule quality.

Once the microcapsules are successfully formulated, the sample is ready for characterisation and CO_2 absorption testing.

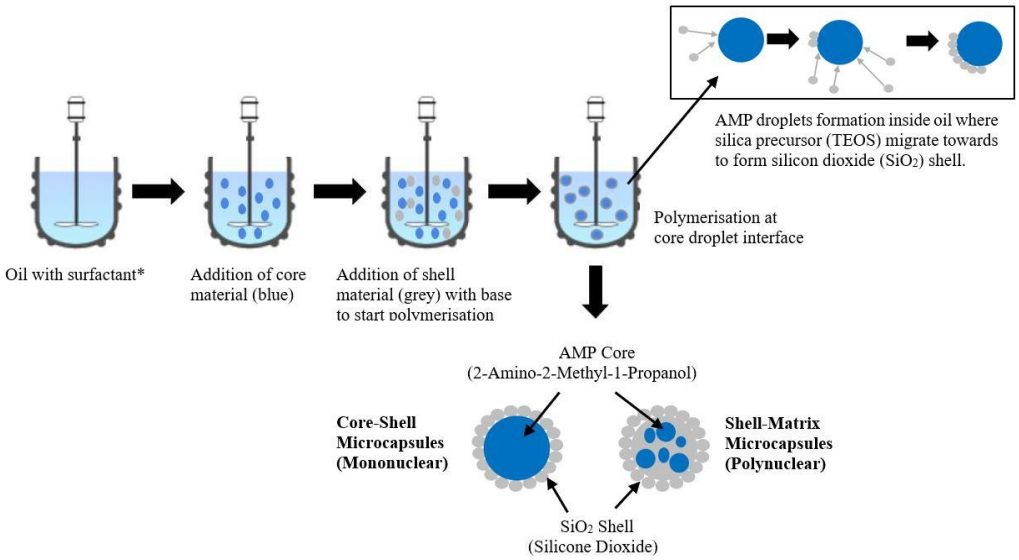

Figure 3-1 Schematic diagram of the microencapsulation of AMP with TEOS. Core material with thymol blue is added to mineral oil with an emulsifier under constant stirring. Then activated TEOS is added to the system to allow the formation of the silicon dioxide shell around the core droplet interface. This method can either form microcapsules with a core-shell or shell-matrix type which is dependent on the core material, shell material and polymerisation technique used (52).

Table 3-2 List of all the microencapsulated samples along with their different parameters used during the formulation process. (*formulation time:6 hrs; ** formulation time: 12 hrs; standard: 16 hrs).

Emulsifier	Emulsifier concentration (wt%)	Core-Shell Ratio	Homogeniser Speed	Mechanical Stirrer Speed	
PGPR	0.5	6:4	N/A	100	Effect of mechanical stirrer
PGPR	0.5	6:4	N/A	400	
PGPR	0.5	6:4	N/A	600	
PGPR	0.5	6:4	N/A	800	
PGPR	0.5	6:4	N/A	1000	
PGPR	0.5	6:4	1200	400	Effect of Homogenise
PGPR	0.5	6:4	1200	800	
PGPR	0.5	6:4	1200	1000	
PGPR	0.1	6:4	1200	400	Effect of Emulsifier Concentration
PGPR	0.2	6:4	1200	400	
PGPR	0.3	6:4	1200	400	
PGPR	1	6:4	1200	400	
PGPR	1.5	6:4	1200	400	
PGPR	0.5	5:5	1200	400	Effect of Core-Shell
PGPR	0.5	7:3	1200	400	
PGPR	0.5	8:2	1200	400	
Span85	0.3	6:4	1200	400	Effect of Emulsifier
Span85	0.5	6:4	1200	400	
Span85	1	6:4	1200	400	
Span85	1.5	6:4	1200	400	
Span85	1	5:5	1200	400	Effect of Core-Shell ration
Span85	1	7:3	1200	800	
Span85	1	8:2	1200	1000	

Span85	1	6:4	1200	100	Effect of Mechanical Stirrer
Span85	1	6:4	1200	600	
Span85	1	6:4	1200	800	
Span85	1	6:4	1200	1000	
Span85	1	6:4	600	400	Effect of Homogeniser
Span85	1	6:4	2000	400	
Span85	0.5	6:4	2000	400	
Span85*	1	6:4	1200	400	Effect of Reaction
Span85**	1	6:4	1200	400	
Tween80	0.5	6:4	1200	400	Effect of Emulsifier
Tween80	1	6:4	1200	400	
Tween80	1.5	6:4	1200	400	
Tween80	1	5:5	1200	400	Effect of Core-Shell Ratio
Tween80	1	7:3	1200	400	
Tween80	1	8:2	1200	400	
Tween80	1	6:4	N/A	800	Effect of Stirring Speed
Tween80	1	6:4	600	400	
Span20	1	6:4	1200	400	Effect of Emulsifier
Span85	1	N/A	N/A	400	Silica Particles

3.3.2 Emulsifier

To identify the best surfactant for the preparation of microcapsules with an amine core, four different emulsifiers were used with different concentrations (Table 3-3). The desired emulsifier concentration was achieved and ensured that the emulsifier was fully dissolved in the oil prior to the experiment. Initially, 0.5 wt% PGPR was used to make the microencapsulated AMP sample. Afterwards, a range of emulsifiers and concentrations were used to improve the quality of microcapsules and size. A wide range of concentration was used for the first emulsifier (PGPR) which was then narrowed down to a smaller range due to no successful encapsulation for >0.3 wt% emulsifier concentration.

In comparison, Span20 was only used at 1 wt% to control the change in microcapsule size due to prior testing showing best results for 1 wt% Tween80 and Span85.

Table 3-3 Variety of emulsifier concentrations used during formulation.

Emulsifier	Concentration (wt %)
PGPR	0.1 0.2 0.3 0.5 1 1.5
Span85	0.3 0.5 1 1.5
Tween80	0.5 1 1.5
Span20	1

3.3.3 Core-shell ratio

After preparing the emulsifier concentration and choosing the most effective one, the effect of different core-shell ratios on the encapsulation process was observed. A 6:4 ratio of core to the shell was decided on as the first ratio to be tested, i.e 15 g of core material with every 10g of shell material used which gives a 1.5:1 or 6:4 ratio. This was then followed by the following ratios: 5:5, 7:3 and 8:2. These ratios were first tested with 0.5 wt% PGPR and AMP as emulsifier and core material respectively Afterwards,

formulations tests were undertaken by changing the emulsifier to 1 wt% Span85, Tween80 and the core material to MEA and 30 wt% TEA (Table 3-4).

Table 3-4 The different core materials, emulsifiers and core-shell ratios used during the formulation process.

Core Material	Emulsifier	Core-Shell Ratio			
AMP	0.5% PGPR	5:5	6:4	7:3	8:2
	1% Span85	5:5	6:4	7:3	8:2
	1% Tween80	5:5	6:4	7:3	8:2
	1% Span20		6:4		
100% MEA	1% Span85		6:4		
30% TEA	1% Span85		6:4		

3.3.4 Homogeniser and mechanical stirrer speed

During the encapsulation process, both a homogeniser and mechanical stirrer were used to identify the best parameters to formulate good quality microcapsules. These microcapsules were not only investigated for their quality but also size distribution.

A Silverson L4RT homogeniser was used to stabilise the bulk phase by mixing the core material into the oil phase for 30 minutes, and an IKA mechanical stirrer was used to stir the bulk phase with the core during the addition of the shell material and left running until the formulation ended. The homogenizer and mechanical stirrer speeds are listed in Table 3-5.

Table 3-5 Homogeniser and mechanical stirrer speeds used during formulation.

Homogeniser Speed (rpm)	Mechanical Stirrer Speed (rpm)
N/A	400
1200	100
1200	400
1200	600
1200	800
1200	1000
600	400
2000	400

3.3.5 Reaction time

The encapsulation process requires time to finish formulating microcapsules since it is reliant on the shell material polymerisation. This reaction time can both affect the microcapsule quality as well as reduce the overall formulation time. If the formulation is left to run for longer than required, i.e. microcapsules are already formed, then more particles will get attached onto the surface and the samples will be left in the system for longer than required. Similarly, if the process is stopped too early the encapsulation process might not have finished yet and the encapsulation process will be unsuccessful. The aim is to find the reaction time that successfully formulates microcapsules in the shortest amount of time.

The following reaction times were considered during the encapsulation process: 6 hrs, 12 hrs and 16 hrs.

However, the reaction time experiments were only carried out with parameters that gave the best quality capsules: 1 wt% Span85 emulsifier and 100% AMP as the core.

3.4 Microcapsule Characterisation

Prior to formulating microcapsules with different core material (AMP, MEA, TEA) and emulsifiers, the interfacial tension of the bulk phase is measured. The formulated microcapsules are then characterised in terms of morphology, structure, size, surface properties, chemical and thermal properties. These tests are followed by post-formulation analysis including formulation yield and payload.

3.4.1 Pre-Formulation Characterisation – Interfacial Tension

During the formulation process, different quality microcapsules were produced with different emulsifiers and core material. Certain combinations resulted in no microencapsulation like 0.5 wt% PGPR and 100 % MEA or 1 wt% Span85 and 100 % TEA core, while all other combinations like 0.5 wt% PGPR and 100% AMP or 1 wt% Span85 and 100% AMP core were successful in the microencapsulation. To examine this phenomenon and to get a better understanding of the limiting factors, the interfacial tension of the bulk phase, i.e. core droplets inside the oil phase, was measured.

To this end, an optical tensiometry (KRÜSS GmbH) with the pendant drop method was used for analysis (Figure 3-2). For this method, the oil along with the emulsifier is placed inside a square, open cuvette (2 cm x 2 cm, 20 mL of oil) and the core material (450 μL) is added to a syringe with a needle. The syringe is dropped down until it is inside the middle point of the cuvette where a drop of the core material is hanging from. For this method, the drop size is important, and should either be pendant or tear shaped.

The interfacial tension is correlated to the shape of the drop hanging from the needle and can be expressed by Equation 3-1.

$$\gamma = \frac{\Delta\delta \; g \; R_0}{\beta} \qquad \textbf{Equation 3-1}$$

where γ is surface tension, $\Delta\delta$ is density difference between the two fluids, g is the gravitational constant, R_0 is the drop radius of the curvature of the drop apex and β is the shape which is defined by the Young-Laplace equation (53).

The software of the tensiometer uses iterative approximations for the Young-Laplace equations which allow the interfacial tension of two immiscible fluids to be determined if their densities are known (taken form their material safety data sheet (MSDS)).

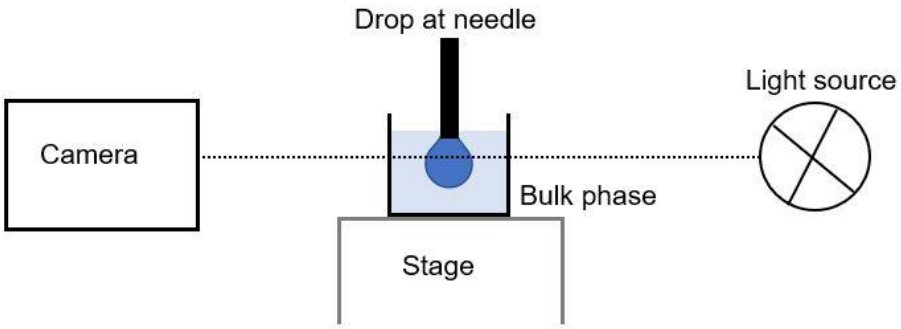

Figure 3-2 Schematic illustration of pendant drop method based on the optical shape analysis. A drop of the tested material is hung from a needle and light passes through it which is caught by the camera and the interfacial tension measurement is given. The bulk phase contains the emulsifier and mineral oil, whereas the core material is hung as a drop from the needle. The densities of the materials are used by the instrument software to calculate the interfacial tension of the system.

3.4.2 Morphology, Microstructure and Size Characterisation

3.4.2.1 Scanning Electron Microscopy - Morphology

To examine the internal structure, morphology, size uniformity and aggregation of the formulated samples, a Hitachi Tabletop TM3030 SEM was used.

The samples were spread as a thin layer across a double-sided carbon tape on a metal stub which was then transferred to a gold sputter for a 3 nm gold coating to make the sample electricity conductive. After preparing the sample, the stub is inserted into the SEM where the vacuum process is carried out prior to the start of observation. The following SEM conditions were used for sample observation: secondary electrons (SE) and 15 kV.

3.4.2.2 Shell thickness

Measuring the shell thickness of small-sized sample (>100 μm), which is not a core-shell type, is challenging and hard to obtain without the proper tools. Through numerous trials, the shell thickness of 3 individual samples was acquired though it

should be kept in mind that this is not a representation of the sample but purely an indication of the thickness.

To obtain the shell thickness, samples were placed in a mortar. Afterwards, liquid nitrogen is added to freeze and harden the capsules which are then broken with a pastel. The broken samples were then placed on a stub with double-sided carbon tape, coated with 3 nm gold and analysed under the SEM. Accordingly, the thickness of the three samples was calculated with the help of ImageJ.

3.4.2.3 Bruner-Emmet-Teller (BET) Method - SA Analysis

The surface area along with the pore sizes and pore volume affect gas absorption onto a surface. A larger surface area for the microcapsules will give a higher absorption capacity. To determine the surface area properties (m^2/g), pore size (Å) and pore volume (cm^3/g), the samples were submitted to physisorption tests and analysed by the Bruner, Emmett and Teller (BET) method by the Particle Analytical (Micrometrics TriStar II Plus). This BET method in majority cases applies the Langmuir Type II isotherms to obtain the solid specific surface calculations. For solid materials, the following BET calculation is used to determine the SA:

$$\frac{1}{W(\left(\frac{P}{P_0}\right)-1)} = \frac{1}{W_m C} + \frac{C-1}{W_m C}\ (\frac{P}{P_0}) \qquad \textbf{Equation 3-2}$$

where W is the weight of the absorbed gas at a relative pressure of P/P_0, W_m is the weight of the adsorbate creating a monolayer of the surface coverage, C is the BET constant which is related to the energy adsorption in the first absorbing layer, consequently the value indicates the magnitude of the aerobate/absorbent interactions.

The linear plot of $\frac{1}{W(\left(\frac{P}{P_0}\right)-1)}$ vs $(\frac{P}{P_0})$ is required to for the BET equation which is the adsorbate when using nitrogen with solids where $(\frac{P}{P_0})$ is usually restricted to 0.05 to 0.35.

Additionally, the microporous structure of the materials is characterised based on the pore size distribution (PSD), pore volume, and surface area. Barrett, Joyner and Halenda (BJH) procedure was applied to measure the pore volume and pore area distributions for mesopore samples. Micropore distribution was given by the application of the total micropore volume and MP method plotted by the t-plot method (54).

The instrument is composed of two different testing units. The first one being the vacuuming unit and the other being testing unit. In the first unit a degassing process, a vacuum pump, is conducted to remove any liquids to ensure the sample is completely dry for accurate measurement. For the degassing process, samples are measured out as 1 g ± 0.1 g and placed inside glass sample-holder (12 mm long, bulb-shaped end) before connecting it to the vacuum system. Subsequently, after 200 mTorres is reached, the sample is considered properly vacuumed and the holder is transferred over to the testing unit. In the testing unit, a dewar is present that needs to be filled up with liquid nitrogen which is moved upwards to immerse the holder in the liquid nitrogen the for cooling down process of the testing. This allows a stronger gas molecule interaction with the sample during the adsorption stage. The standard measurement points used are $(\frac{P}{P_0})$ of 0.1, 0.2 and 0.3. The absorbed gas volume on the particle surface is measured at the boiling point of nitrogen (-196°C). The amount of adsorbed and desorbed gas is then correlated to the total surface area including the pore volume

and size at the surface. The calculated results values are based on the BET theory (55).

The surface area for the tested samples refers to the surface area of the microcapsules which includes the whole particle, i.e. the surface, pores and internal structures. Additionally, the average pore size displayed in the tables are the BHJ Adsorption average pore diameter. The BET is not able to identify the macropores and nanopores.

3.4.2.4 Laser Diffraction – Size Distribution

The laser diffraction is a technique used to determine the size and size distribution of particles in the range of 0.02 µm to 2000 µm in a solution. The size distribution of the microcapsule was determined by utilising a Malvern MasterSizer 2000 that uses the static light scattering (SLS) and the Mie scattering theory.

The Mie theory predicts the light scattered by spherical particles as well as the passing or adsorbing of light through the particle. This theory assumes that all particles are spherical where larger particles scatter light at a smaller angle than smaller particles and are known to be accurate if the refractive index (RI) of the liquid and particle is known. Hence, the MasterSizer works backwards from the Mie theory as it uses the optical bench to capture the scattering pattern of the particles. Afterwards, the theory is used to calculate the particles size that created the detected pattern. The sample measurement in the MasterSizer follows three distinct procedures that must be followed:

1) Sample preparation. The optical bench is filled with ethanol prior to testing and then the sample is dispersed into the optical bench at the correct concentration (2-10%). This step is very important because if it is poorly done, i.e. bad dispersion of the sample, the data given by the software will be incorrect.
2) Measurement. The various detectors of the instrument capture the scattering patterns of the sample where each detector collects a specific range of angle form the scattered light. The detector array, i.e. the channels, captures these scattering patterns as “snapshots”. For good sample representation, the MasterSizer takes several snapshots, known as snaps, and displays the average.
3) Data analysis. The raw data is analysed by the Malvern Software after the measurement is complete with the Mie theory to display the size distribution (56).

Prior to sample testing, the MasterSizer is cleaned with ethanol and the unit is then filled up with the liquid to be used during the experiment. The stirrer speed of the MasterSizer is set to 2500 rpm and the light intensity is measured. Only when the light intensity is above 80%, a small quantity of sample is added into the liquid (2-10%). For measuring the sample’s particle size distribution, the RI for both silicon dioxide (shell material) and ethanol (liquid phase) are taken from literature which are 1.45 and 1.36 respectively.

The results are shown as the average values of 3 data sets.

3.4.3 Chemical and Thermal Properties of Microcapsules

3.4.3.1 Fourier Transform Infrared Spectroscopy (FTIR) - Chemical Composition

The primary focus of this experiment was to identify the functional groups of the microcapsules. This would allow a better understanding of the chemical reactions taking place during the formulation process, i.e. polymerisation.

Hence, a Bruker Tensor 27 FTIR spectrometer (Bruker) was set with the following conditions: 10 scans, 4 cm^{-1} optical resolution and spectral range of 4000 – 400 cm^{-1}. The data were recorded on the OPUS software ((version 4.0, build: 4.0.24 (20020320)).

Before the start of the experiment, a background spectrum is run on an empty cell, however, for a solution spectrum, the solvent is run as the background first. A sample cell consists of a Pike Miracle single-bounce attenuated total reflectance (ATR) cell with a ZnSe single crystal. To run a measurement, the sample is placed directly onto the small crystal so that it is covering it completely inside the cell and the arm is rotated and pressed down onto the sample so that it touches the crystal with the sample in-between. As soon as the experiment is started, the IR beam from the arm penetrates 60 μm into the sample and is detected by the crystal. The ATR crystal can work with solid, liquid, solutions and gel materials.

The patterns in the spectrum help to identify bonds present inside the sample since each molecule exhibits a specific IR fingerprints (57). For comparison purpose, the encapsulated samples are run against their counterpart, pure core material.

Due to the absence of a chemical library in the OPUS software, data evaluation to compare the compounds represented in the spectra were based on the data available in the literature (58).

3.4.3.2 Differential Scanning Calorimetry (DSC) - Thermal Properties

To characterise and identify materials for their thermal properties like melting and freezing temperatures, a differential scanning calorimetry (DSC2, STAR^e System; Mettler Toledo) is used. The DSC measures the enthalpies associated with the reactions and transitions along with the temperature at which these processes occur. This method is known to be fast but very sensitive with easy sample preparation (59). In the DSC, the samples are tested in two different temperature ranges: 1) from 25 °C to -60 °C and 2) 25 °C to 60 °C to examine the effect of low and high temperatures on the encapsulated core compared to the pure core material by measuring the heat flow to and from the sample under controlled conditions. A small amount of sample (5-10 mg) is sealed in a 40 μL aluminium crucible before placing it into the DSC. A second empty crucible is used as a reference, also known as 'blank'. The sample is then cooled down to the desired temperature in the furnace.

3.4.3.3 Dilatometer - Thermal Cycling

An optical dilatometer (DIL 806) is generally used for measuring the change in length of a thin, plastic material without contact in relation to temperature. Nevertheless, the dilatometer of the research group was used to observe the effect of low temperature cycling on the morphology of the microencapsulated samples.

The dilatometer was connected to a 25 L cylinder filled with liquid nitrogen and nitrogen gas was used as a purge gas due to its inertness. In terms of the sample preparation, a small quantity of sample was placed on an SEM stub which was inserted into the dilatometer chamber and closed afterwards. Then the temperature profile is set from 25 °C to -100 °C and to 25 °C again at a cooling/heating rate of ± 10 °C/min and the

sample is subjected to 10 continuous thermal cyclings. Additionally, in the temperature profile, the use of liquid nitrogen is switched to manual control to allow liquid nitrogen to be used only during cooling.

After the cycling, the samples are observed for any changes in morphology under the SEM.

For statistical relevance the thermal cycling tests were repeated with three different batches for each sample conditions.

3.4.4 Post-formulation analysis – including formulation yield and payload calculation

3.4.4.1 Formulation yield

After the formulation process, the batch sample is dried and then weighed to compare the dry mass of the formulated sample at the end of the encapsulation process, i.e. the formulation yield, of the different formulating parameters, through the following calculations:

$$Amoung\ fo\ dry\ sample\ formulated = yield, \gamma\ (\%) = \frac{dry\ batch\ sample\ (g)}{raw\ materials *\ (g)} \quad \textbf{Equation 3-3}$$

where * indicates the used core material, pH indicator volume, sodium hydroxide and TEOS (sodium hydroxide was used to activate the TEOS particles).

This allows the formulation process to be compared based on the encapsulated sample, giving a better understanding for a potential scale up.

3.4.4.2 Thermogravimetric Analysis (TGA) - Pay Load

The thermogravimetric analysis (TGA, Mettler Toledo) was used to measure the core material encapsulated inside the microcapsules as the core is crucial for the carbon capture research for correlations between the absorbent and the absorbed CO_2.

Moreover, this technique was selected to evaluate the initial CO_2 absorption capability of the first encapsulated sample.

In order to calculate the pay load of the sample, i.e. the amount of core material present inside the sample, the sample needs to be heated up above the melting temperature of the core material so that it evaporates and leaves the shell material behind. Before the samples are tested for pay load, a correction file was created containing all the corresponding setting required for heating above the melting temperature of the core material inside the sample, hence the following temperature profile was chosen:

- start temperature: 20 °C
- heating: 10°C/min to reach 250 °C
- hold temperature: 250 °C for 2 hrs

The sample is weighed in the range of 10-20 mg into TG crucible (Pt).

Prior to the start of the temperature program for the sample testing, the balance is tared, and the gas flow is started. For payload testing, the chosen gas was nitrogen (50 mL/min flow rate), whereas for the CO_2 absorption testing the gas used was carbon dioxide with 50 mL/min as the flow rate. Platinum crucibles were used during all the testing's (both correction and sample).

The payload is then calculated as follows:

$$\emptyset = \frac{m_I - m_S}{m_I} \; x \; 100 \qquad \textbf{Equation 3-4}$$

where ∅ is payload (wt %); m_I is the initial weight of the sample; m_S is the weight of shell after the core evaporation process.

Each sample for both payloads and initial CO_2 absorption capacity were tested three times where then the average is taken for comparison and analysis.

Some limitations of the instrument were observed during the CO_2 absorption tests (discussion in later chapter) which necessitated the need for a better CO_2 absorption method. This led to the set-up of a pressure rig as well as a continues reactor for the CO_2 absorption measurements.

3.5 CO_2 Absorption Capacity of Microcapsules

In the beginning, CO_2 absorption testing were done by setting up the TGA by connecting it to a CO_2 cylinder (50 L). However, the initial result showed the unsuitability of the TGA for the determination of the CO_2 loading capacity and kinetics for the microencapsulated samples. Hence two methods were established to measure the absorption capability, one static method for high pressure testing, and one continuous method to investigate the effect of temperature in a dispersed sample (dynamic process).

3.5.1 Pressure rig (set-up)

A pressure rig is set up to test the CO_2 absorption loading capacity of the microcapsules. The piping and instrumentation diagram (P&ID) is shown in the schematic diagram in Figure 3-3.

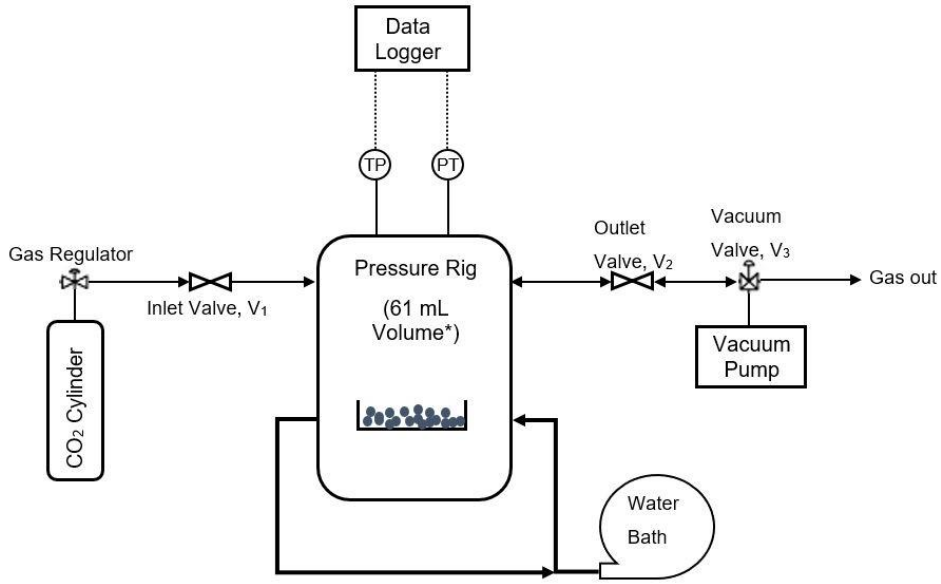

Figure 3-3 Schematic diagram of pressure rig set-up for CO_2 absorption testing. (* Working volume of pressure rig = 61mL, including pressure cell, connections, valves and tubings; TP: temperature probe; PT: pressure transducer).

For all the CO_2 sorption experiments with the pressure rig, 0.5 g (± 0.01 g) of sample was used. The sample holder is a glass crucible to allow observation of the sample (quantitative analysis) from any perspective. For comparison purposes, images of the samples are taken both before and after sorption. Before exposing the sample to CO_2, the pressure rig chamber is vacuumed to ensure absorption occurs when pressure is introduced. The whole system is cooled down to the desired temperature before the chamber is pressurised. The end of the absorption experiment is identified once the pressure does not drop anymore an reaches an equilibrium where then the sample is removed from the rig after depressurising the vessel, and the sample is weighed for comparison in weight change.

The experiments were performed at ten barA pressure and a range of temperatures (24 °C to -40 °C ± 0.1 °C). A circulating water bath connected to the pressure rig was used to ensure constant temperature during the testing.

A data logger recorded the pressure and temperature during the experiments. The pressure was measured by a transducer (Omega, model no: PX309-300AI) in volts with the Data Logger which was then converted to Bara for CO_2 absorption calculations.

To validate the data, CO_2 sorption tests for each sample are repeated at least three times. Furthermore, the calculated values and the physical weight change measured between before and after CO_2 exposure are compared. Only once the calculated values agree with the physically measured values (within a 5% error margin), the CO_2 absorption system and sample loading capacity are considered valid. However, it is important to mention that some measurement results were invalid due to sealing issue of the rig as it is not designed for low temperature use.

For an accurate result, the CO_2 sorption calculations using the Peng Robinson equation of state (PREoS) reduced form were compared with the weight increase of the sample after CO_2 exposure. Only if the calculation values are within 5% error margin of the physical weight measure is the calculation accepted and used for comparison. The calculated method assumes that the pressure loss over time is correlated to the absorption of the gas by the sample, hence:

$$absorbed\ pressure\ by\ Sample, P = P_I - P_E \qquad \textbf{Equation 3-5}$$

where P_I is the initial pressure at the start of experiment and P_E is the pressure at the end of the experiment.

The first step involved in the conversion of the measured pressure of CO_2 into mass is through the help of PREoS (60):

$$P = \frac{RT}{v-b} - \frac{a\alpha}{v(v+b)+b(v-b)} \quad \textbf{Equation 3-6}$$

with $a = \frac{0.45724R^2T_c^2}{P_c}$ **Equation 3-7**

$$b = \frac{0.07780RT_c}{P_c} \quad \textbf{Equation 3-8}$$

$$\alpha = [1 + k(1 - T_r^{0.5})]^2 \quad \textbf{Equation 3-9}$$

$$k = 0.37464\omega + 1.5422\omega - 0.26992\omega^2 \quad \textbf{Equation 3-10}$$

$$T_r = \frac{T}{T_c} \quad \textbf{Equation 3-11}$$

where the coefficient “a” and “b” are critical properties, ω is the acentric factor (taken from literature according to the material/gas), T_r is reduced temperature, T_C is critical temperature, P_C is critical pressure, *R* the universal gas constant which is $Jmol^{-1}K^{-1}$ (60).

The above equation is then translated into a polynomial form:

$$Z^3 - (1-B)Z^2 + Z(A - 2B - 3B^2) - (AB - B^2 - B^3) = 0 \quad \textbf{Equation 3-12}$$

$$Z = \frac{PV}{RT} \quad \textbf{Equation 3-13}$$

$$a = 0.45724\ \alpha\ \frac{P_r}{{T_r}^2} \quad \textbf{Equation 3-14}$$

$$b = 0.7780\ \frac{P_r}{T_r} \quad \textbf{Equation 3-15}$$

where, P_r is reduced pressure ($= \frac{P}{P_c}$), T_r is reduced temperature ($= \frac{P}{P_c}$). Equation 3-12 is then solved for Z by using the Newton-Raphson method:

$$Z^3 - CZ^3 + DZ - E = 0 \quad \textbf{Equation 3-16}$$

$$Z = \frac{PV}{RT}$$ **Equation 3-17**

$$C = (1 - B)$$ **Equation 3-18**

$$D = (A - 2B - 3B^2)$$ **Equation 3-19**

$$E = (AB - B^2 - B^3)$$ **Equation 3-20**

where P is the pressure (10 barA), V is volume of CO_2, R is the universal gas constant ($Jmol^{-1}K^{-1}$), T is temperature and A and B are the polynomial forms:

$$A = \frac{a\alpha\rho}{R^2T^2}$$ **Equation 3-21**

$$B = \frac{b\rho}{RT}$$ **Equation 3-22**

where a" and "b" are critical properties and p is the density of CO_2.

The values for Z, C, D and E are be looked up in the from the excel spreadsheet of Chemical Engineering's guide (61) along with the density of CO_2 where Z is the compressibility factor, C, D and E are the ratios of critical properties. This given density is then converted to mass:

$$m = \rho * V$$ **Equation 3-23**

where m is absorbed CO_2 mass, ρ is the density of CO_2 and V is the volume at the experimental temperatures and 10 barA.

In the pressure rig the following parameters were investigated: A) effect of temperature and B) effect of size/ SA on the absorption capacity.

It is important to note that CO_2 absorption of the sample occurs as soon as it is exposed to air. This means that CO_2 absorption already starts prior to the testing chamber becoming pressurised, thus the corresponding results are to be taken with caution.

3.5.2 Continuous Reactor

To identify the effect of temperature, SA, different cores on the absorption capacity and kinetics of the microencapsulated samples, a 500 mL Radley-Reactor™ (UK) vacuum glass jacketed vessel is connected to a mixture of CO_2 (30%) and N_2 (70%) , a Huber chiller unit (Germany) and an ABB Gas Analyser (UK). The mixture of gas is introduced into the vessel by inserting a tube through one of the connections of the reactor lid into the bottom of the vessel, whereas for the outlet gas a gas connector is attached to the lid connection which is then connected to the ABB through a silicone tube where the CO_2 measured values at the outlet are recorded. Additionally, a temperature probe, connected to the chiller unit, is inserted into the vessel for accurate process temperature control. A P&ID is shown in the schematic diagram in Figure 3-4.

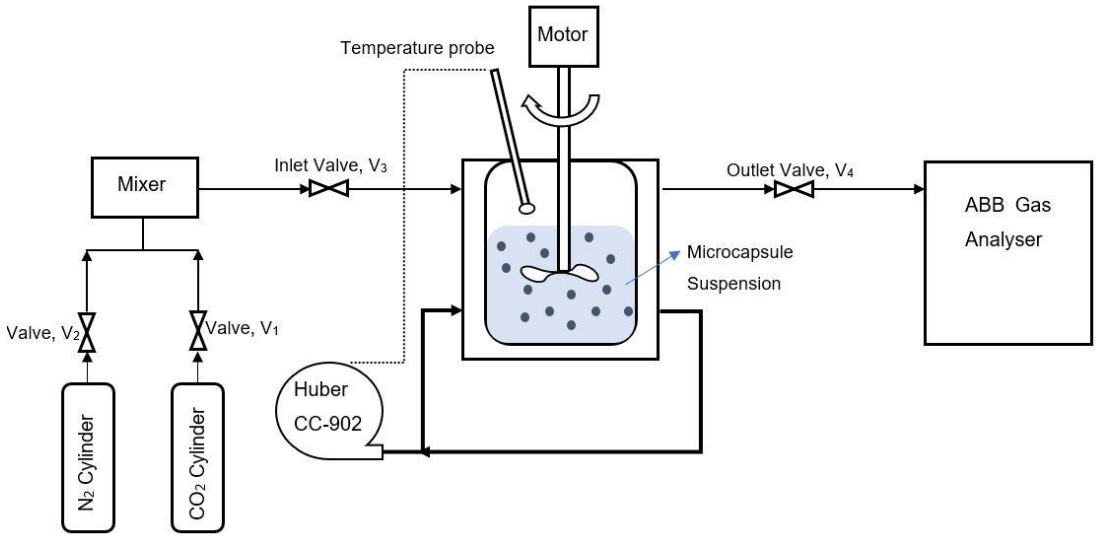

Figure 3-4 Schematic diagram of a Radley™ Reactor for continuous CO_2 absorption testing. Nitrogen and carbon dioxide are mixed together to create the desired gas mixture before introducing it to the microcapsule suspension. A temperature probe is connected to the Huber CC-902 chiller to control the temperature of the reaction.

For the continuous reactor, a slurry of the sample is prepared by dispersing 20 g (± 0.1 g) of the sample into 200 g (± 0.1 g) ethanol to create a 10 wt% solution. This slurry is then added to the reactor. Afterwards, the reactor is cooled down to the desired

temperature (20 °C to -60 °C) before the gas mixture (200 mL/min) is bubbled into the slurry. Throughout the whole experiment, the ABB records the CO_2 concentration (vol%) at the outlet. Once the CO_2 concentration at the outlet reaches an equilibrium, the experiment is stopped. The ABB measures the CO_2 vol % of the outlet gas which necessitates the conversion of the vol % into the absorbed CO_2 mass by sample. To ensure that the absorption values are corresponded to the sample, first the CO_2 vol% at the outlet is measured with varying temperatures (20° C to -60 °C) with the reactor only containing 200 g EtOH (no sample). The CO_2 that is bubbled into the liquid and then comes out is measured overtime at the set temperature. This CO_2 gas at the outlet is then subtracted from the absorption result of the microcapsules. The following calculations were used to convert CO_2 vol% to absorbed CO_2 mass (g):

$$\frac{a}{100} = f_{CO_2}(out) \qquad \textbf{Equation 3-24}$$

where a is the CO_2 volume % out measured by the ABB gas analyser and $f_{CO_2}(out)$ is the CO_2 volume fraction at the outlet. This then allows the N_2 flow at outlet and inlet to be calculated as well as the N_2 fraction out and CO_2 flow (L/min) in:

$$F_{CO_2,in} = F_{Gas,in} * f_{CO_2}(out)_{max} \qquad \textbf{Equation 3-25}$$

$$F_{N_2,in/out} = F_{Gas,in} - F_{CO_2,in} \qquad \textbf{Equation 3-26}$$

$$1 - c(out) \qquad \textbf{Equation 3-27}$$

where $F_{Gas,in}$ is the gas mixture flow into the reactor (set to 0.5 L/min) and the N_2 flow is the same at inlet and outlet as it does not get absorbed by the sample, hence allowing the flow of the gas mixture at the outlet to be calculated:

$$\frac{f_{N_2}(out)}{F_{N_2,in/out}} = F_{gas\ mixture,out} \quad \textbf{Equation 3-28}$$

where $F_{gas\ mixture,out}$ is the flow of the gas mixture at the outlet in L/min. This then gives the CO_2 flow at the outlet:

$$F_{CO_2,out} = F_{gas\ mixture,out} * f_{CO_2}(out) \quad \textbf{Equation 3-29}$$

The absorbed CO_2 (L/min) is then calculated by subtracting the CO_2 flow out from the CO_2 flow out:

$$\gamma, CO_2 absorbed = F_{CO_2,in} - F_{CO_2,out} \quad \textbf{Equation 3-30}$$

Afterwards, CO_2 absorption graphs are plotted to show the absorption kinetics of different samples to observe the effect of temperature on different sizes, emulsifiers and core materials. Additionally, the absorbed CO_2 (L/min) flow is converted to the absorbed CO_2 mass to compare the different CO_2 loading capacities of the samples. After obtaining the absorption graph, the area under the graph is found through integration with the help of a trendline (with $R^2 > 0.99$) which gives the CO_2 loading capacity in L. The absorption capacity is then converted into mass through the following equations with the help of CO_2 density (δ) at the set temperature:

$$\frac{CO_2 absorbed\ [L]}{1000} = CO_2\ absorbed\ [m^3] \quad \textbf{Equation 3-31}$$

$$\frac{CO_2 absorbed\ [m^3] * \delta_{CO_2}{}^*}{1000} = CO_2\ absorbed\ [g] \quad \textbf{Equation 3-32}$$

$$\frac{g\ CO_2 absorbed}{g\ Sample} = g\ CO_2\ absorbed\ /\ g\ Sample \quad \textbf{Equation 3-33}$$

Chapter 4 Formulation Process Analysis

4.1 Introduction

This chapter analyses the microcapsule formulation process described in chapter 3.3. Amine cores were selected as the CO_2 adsorbents due to their high absorption capacity with secondary amines (AMP) having the highest loading capacity and primary amines (MEA) having the fastest absorption kinetics (62). Afterwards, the shell material was chosen according to the following properties: inertness, selective CO_2 diffusion and ability to form a porous shell. An *in-situ* polycondensation inside an emulsion was chosen due to the relatively simple formulation process. An immiscible phase is required for microencapsulation, hence, a water-in-oil (w/o) emulsion was used, where the core material acted as the surrounding phase (water) and the mineral oil acted as the bulk phase (oil). The polycondensation of TEOS at the core droplet interface results in the formation of silicon dioxide shell at the end of the formulation process. To this end, the polymerisation reaction is studied in detail. Additionally, the interfacial tension of the bulk phase was measured to further give insight into the limiting parameters of the formulation process.

Furthermore, the effect of the formulation parameters was investigated in terms of microcapsule quality. Different emulsifiers and their concentrations were studied to optimise the encapsulation process of amine adsorbent for carbon capture.

Lastly, the formulation process will be critically appraised with suggestions for potential future work.

4.2 Result and Discussion

4.2.1 Formulation Principles and Process

The most common precursors used for making silicon dioxide are silicon alkoxides which are characterised by the strong covalent Si-O bonding (63) These bonds are hydrophobic and thus immiscible with water. Tetraethyl orthosilicate (TEOS) is such a silica precursor. The advantage of using TEOS as a precursor is its polymerisation ability in alkaline, acidic and neutral conditions to form silicon dioxide. During formulation, alkaline conditions were chosen due to the high alkalinity of the core material (63). In this case, the polymerisation of TEOS would occur through alkaline catalysed hydrolysis and condensation which are caused by the hydroxyl ions (OH^-) of the sodium hydroxide. These OH^- ions have a strong nucleophilicity. The alkoxides silicon atom carries the highest positive charge and are therefore the target of the nucleophilic attack from the deprotonated hydroxyls (OH^-) (64). This mechanism leads to the formation of a pentacoordinate intermediate as shown in Figure 4-1. Typically condensation nucleation occurs under mild to extreme alkaline conditions (65,66).

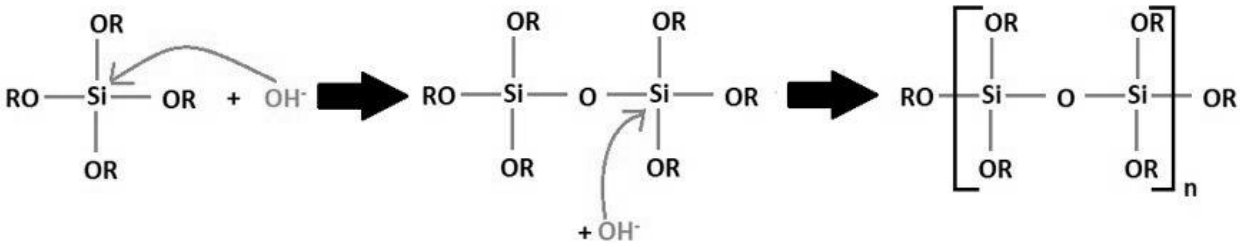

Figure 4-1 Polycondensation of TEOS with hydroxyl ions to form an intermediate (4), where R represents the alkyl group, C_2H_5.

The TEOS reaction to produce silica shell can be described in the following general equations:

$$Si(OC_2H_5)_4 + NaOH \rightarrow Si(OC_2H_5)_3OH + C_2H_5OH$$ **Equation 4-1**

hydrolysis

$$\equiv Si - O - H + H - O - Si \equiv \rightarrow Si - O - Si \equiv + H2O$$ **Equation 4-2**

water polycondensation

$$\equiv Si - OC_2H_5 + H - O - Si \equiv \rightarrow \equiv Si - O - Si \equiv + C_2H_5OH$$ **Equation 4-3**

alcohol polycondensation

In the first step silanol groups (Equation 4-1) are formed through the hydrolysis of the TEOS particles which is then followed by the polycondensation (Equation 4-2, Equation 4-3) between these silanol groups that creates the siloxane bridges to form the silica structure. These two steps can be divided into the nucleation and growth phases which have been described in the literature by two models: the monomer addition and controlled aggregation for the silica growth. In the monomer addition model, the growth phases are described by an initial nucleation burst followed by a particle growth through the addition of the hydrolysed monomers at the capsule surface (67). In contrast, the aggregation model is described by continuous nucleation throughout the reaction where the resulting nuclei aggerate together to form larger particles. However, both models lead to the formation of either spherical or gel silicon dioxide formation depending on the conditions. As can be seen from Figure 4-2, the use of sodium hydroxide as the catalyst for the TEOS with an amine core creates spherical microcapsules with a porous shell which also agrees with the finding in (67).

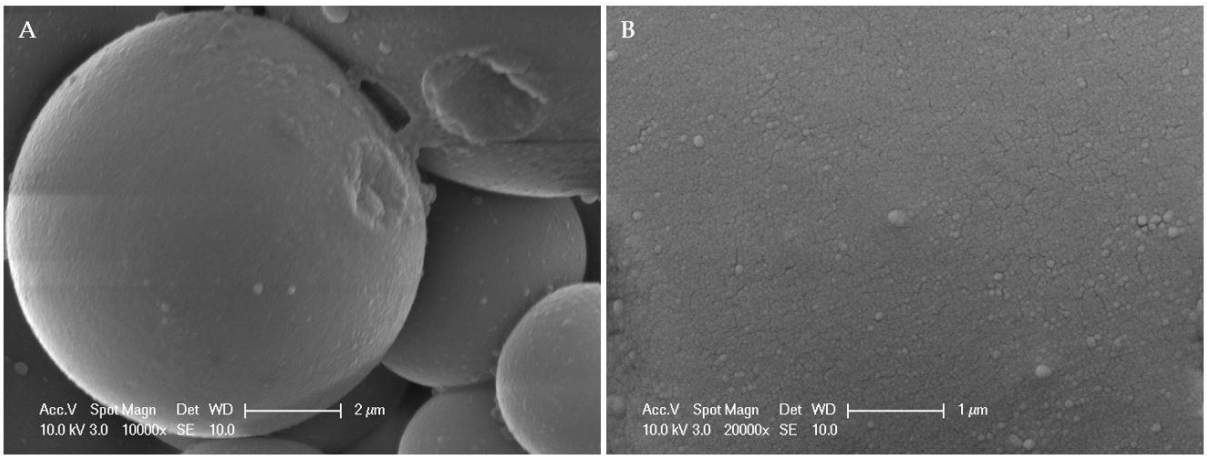

Figure 4-2 Surface structure of microcapsules (JEOL6060). (A) Surface Structure of microcapsules (B) High magnification of microcapsule surface. (100% AMP core, 6:4 core-shell ratio, 1200 rpm homogeniser speed and 400 rpm mechanical stirrer speed).

The in-situ polymerisation used to formulate the microcapsules was a two-step process since it involved the preparation of the pre-condensate by adding sodium hydroxide to TEOS. This is then followed by the encapsulation of the core material under alkaline environment. Such a two-step process is necessary for the shell formation and cannot be achieved with a one-step in-situ polymerization (68). This produced porous, spherical shaped microcapsules with a matrix internal structure rather than a core-shell type as can be seen in Figure 4-3, called monolithic (matrix) microcapsules due to the migration of the activated TEOS towards the AMP interface inside the oil. However, due to the force created by the mechanical stirrer, the shell particles come into contact to form a stable polymeric system, leading to a more or less uniform core material distribution across the polymer matrix. Another possible reason could be the reactivity of the hydroxyl (-OH) group of AMP with the activated TEOS forming bonds which leads to the core material distribution inside the polymer matrix. This core distribution may be in micronised particle form or particles with a substantial fraction of the microcapsule itself (69).

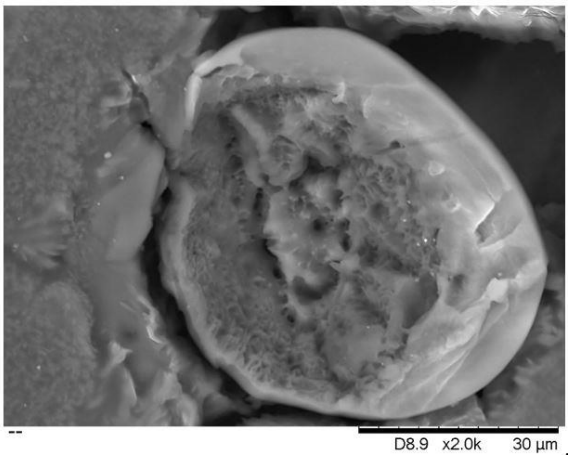

Figure 4-3 Internal structure of microcapsule observed as a matrix of sample 0.5 wt% PGPR (100% AMP core, 6:4 core-shell ratio, 1200 rpm homogeniser speed and 400 rpm mechanical stirrer speed) (TM3030Plus).

From the view of applications, the advantage of these matrix microcapsules is the ruggedness where the dissolution properties are less likely to be either affected or altered by the abrasion or pressure (70). The surface properties of the formulated samples will be analysed and discussed further in 5.2.2.2.

The drying process of the formulated sample is simple. The samples are dried with the use of a Buchner funnel attached to a vacuum dryer. This step is very important as it could potentially reduce agglomeration. Initially, samples were only washed with n-hexane to remove oil droplets, but the samples formulated for the continuous reactor were washed additionally with at least 150 mL ethanol to remove particles from the surface of the microcapsules, i.e. the polymeric silica species and non-encapsulated core material.

During the ethanol washing, the microcapsules lost their blue colour (Figure 4-4), indicating that the pH indicator, Thymol Blue, is not bound inside the capsules, hence it gets washed away easily. However, the thymol blue was only required for initial confirmation of CO_2 absorption capability of the microcapsules. The test from the TGA confirmed the samples ability to capture CO_2. Nevertheless, to keep the ratio between

the core solution (AMP + pH indicator) and the shell solution (TEOS + NaOH) the same, thymol blue is still used throughout all the formulation processes. Additionally, the samples washed with ethanol show slightly lower amount of agglomeration compared to samples washed only with n-Hexane.

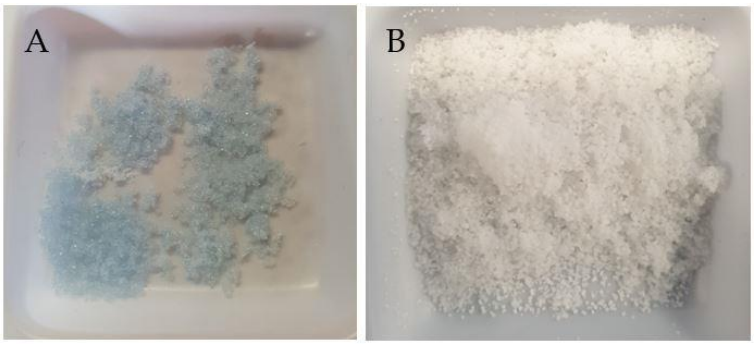

Figure 4-4 Images of samples formulated with 1 wt% Span85, 6-4 core-shell ratio, 1200 rpm homogeniser and 400 rpm mechanical stirring speed. A) washed with n-Hexane only; B) washed with n-Hexane then with ethanol.

Figure 4-5 compares the different emulsifiers in terms of agglomeration after ethanol washing. Agglomeration is present in all the formulated samples, however, sample formulated with 1 wt% Span85 shows the lowest agglomeration with a smoother surface compared to the other two samples. The main factors that govern the agglomeration inside the emulsion system are the collisions and coalescence of the polymeric species of silica and core material droplets (67). In this study, the shell of the microcapsule is synthesised from the hydrolysis of TEOS in a non-ionic w/o emulsion which is then followed by the polycondensation, i.e. polymerisation, of the hydrolysed silica species, i.e. monomeric and polymeric units, in the presence of a base catalyst, sodium hydroxide. These polymeric species are not only found as small particles on the surface of the capsules but can also lead to the formation of larger species through dynamic fusion which leads to the sample being bonded to each other.

However, the samples separate easily when dispersed into ethanol which is advantageous for the CO_2 absorption testing in the continuous Radley^{TM} reactor (71).

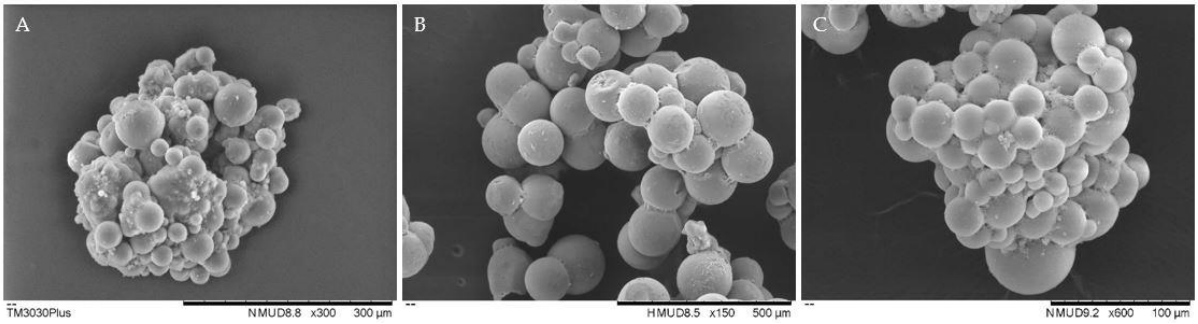

Figure 4-5 Agglomeration observed in samples formulated with different surfactants: A) 0.5 wt% PGPR; B) 1 wt% Span85; C) 1 wt% Tween80 (100% AMP core, 6:4 core-shell ratio, 1200 rpm homogeniser speed and 400 rpm mechanical stirrer speed) (TM3030Plus).

4.2.2 Formulation parameters

During the encapsulation process, the formulation parameters were varied to optimise the microcapsule quality. The examined parameters are emulsifiers and their concentrations, core-shell ratio, core materials, and homogeniser/mechanical stirrer speeds.

4.2.2.1 Emulsifiers

To form and stabilise an emulsion, surfactants, also referred to as emulsifiers, are required. The core phase inside the bulk phase (mineral oil) is unstable due to the immiscibility and repulsion of the two phases, hence the need to stabilise the system with surfactants (72).

PGPR, Span and Tween were chosen as the emulsifiers to formulate the bulk emulsion. PGPR was used due to its strong ability to reduce the interfacial tension inside an w/o emulsion due to its non-ionic property (49). Both Span and Tween are mild non-ionic emulsifiers that offer a range of advantages over the ionic emulsifiers like increased stability, wider compatibility and formulation flexibility (Figure 4-6).

These surfactants can be used at different ratios to allow the production of the oil phase. To this end, a range of surfactant concentration was tested from 0.1 to 1.5 wt%.

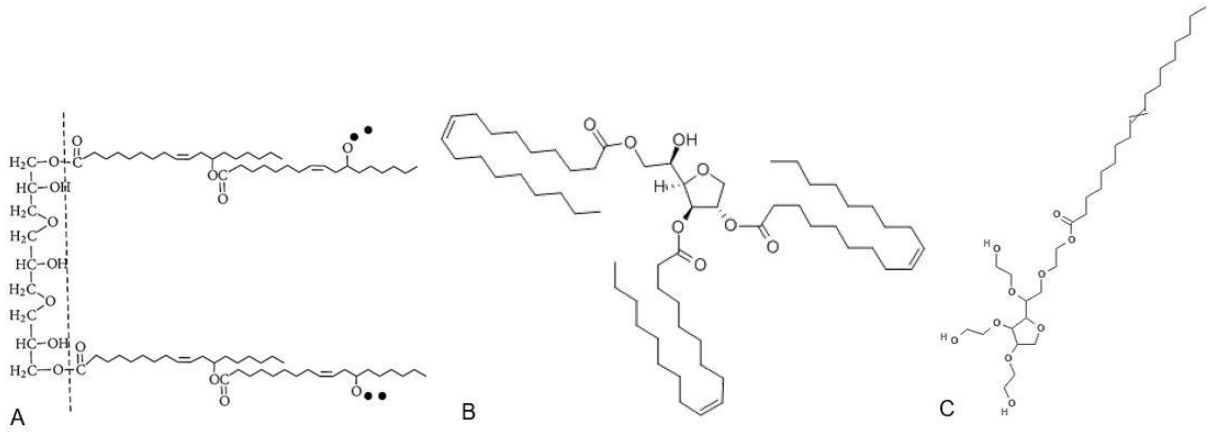

Figure 4-6 Chemical structure of the different emulsifiers used during formulation. A) PGPR (black dots represent polyricinoleic acid chains); B) Span85; C) Tween80 (49,73,74).

Overall, microcapsules formulated with PGPR have a rougher surface and higher agglomeration compared to sample formulated with Span85 (Figure 4-7). This is due to the difference in the structure as well as the molecular weight of the surfactants (Table 4-1).

Table 4-1 Different surfactants used during formulation with their molecular weight.

Surfactant	Molecular weight [g/mol]	Reference
PGPR	390.6	(75)
Span85	957.49	(73)
Tween80	604.8	(76)
Span20	346.46	(77)

The molecular weight of a surfactant, as well as the methyl group, is decisive for its efficiency. The methyl group at the end of an emulsifier provides a strong hydrophobicity for the surfactant and is an important characteristic of an amphiphile, i.e. hydrophilic and lipophilic properties. An example would be PGPR. Ideally, the surfactant should have maximum hydrophilicity at the polar head and maximum hydrophobicity at the hydrophobic tail to minimise the loss into the bulk phase. As can

be seen from Figure 4-6, PGPR has a long hydrophobic tail and a small hydrophilic head. However, there is a limit to the surfactant's effect. A too high increase in surfactant concertation slows its diffusion into the bulk phase which is likely the case with 1.5 wt% emulsifier concentration as these microcapsules show higher agglomeration compared to ≤ 1.5 wt% emulsifier concentrations. This leads to less stable emulsion formation than with 1 wt% Span85/ Tween80/ PGPR. These samples have a higher amount of agglomeration, i.e. particle attached on the surface of the microcapsules. The quality of microcapsules detoriates with higher agglomeration. This occurs due to the instability of the system where the core droplets coalesce upon collision during the stirring process (78).

Additionally, the surfactant needs to align properly at the interface, hence the molecular structure is important. To obtain emulsion stability, the geometry at this interface should be so that the polar head matches the hydrophobic tail. By looking at the molecular structure, the volume of the hydrocarbon tail needs to be larger compared to the polar head for an emulsifier for w/o system. This is the case for all the used surfactants. For each emulsifier, the hydrophobic chains are larger than the hydrophilic chain.

In comparison, non-ionic surfactants like Span and Tween are based on the alcohol branches to have a more balanced geometry which enhances the interaction between the emulsifier and the oil phase. The long chains of the hydrophobic chains help prevent coalescence due to the steric repulsion between the droplets inside the emulsion (78). It seems that 1 wt% Span can provide the best stability for the emulsion compared to the other two emulsifiers and their concentrations, hence why less coalescence and in turn less agglomeration is seen (Figure 4-7). However, with 0.5

wt% Span85 some broken microcapsules and higher agglomeration is found in the formulated sample. Tween80 shows similar results for 0.5 wt%, i.e. higher agglomeration, suggesting that concentrations less than 1 wt% lead to unstable emulsions due to not enough steric repulsions leading to the coalescence of the particles in the bulk phase (78).

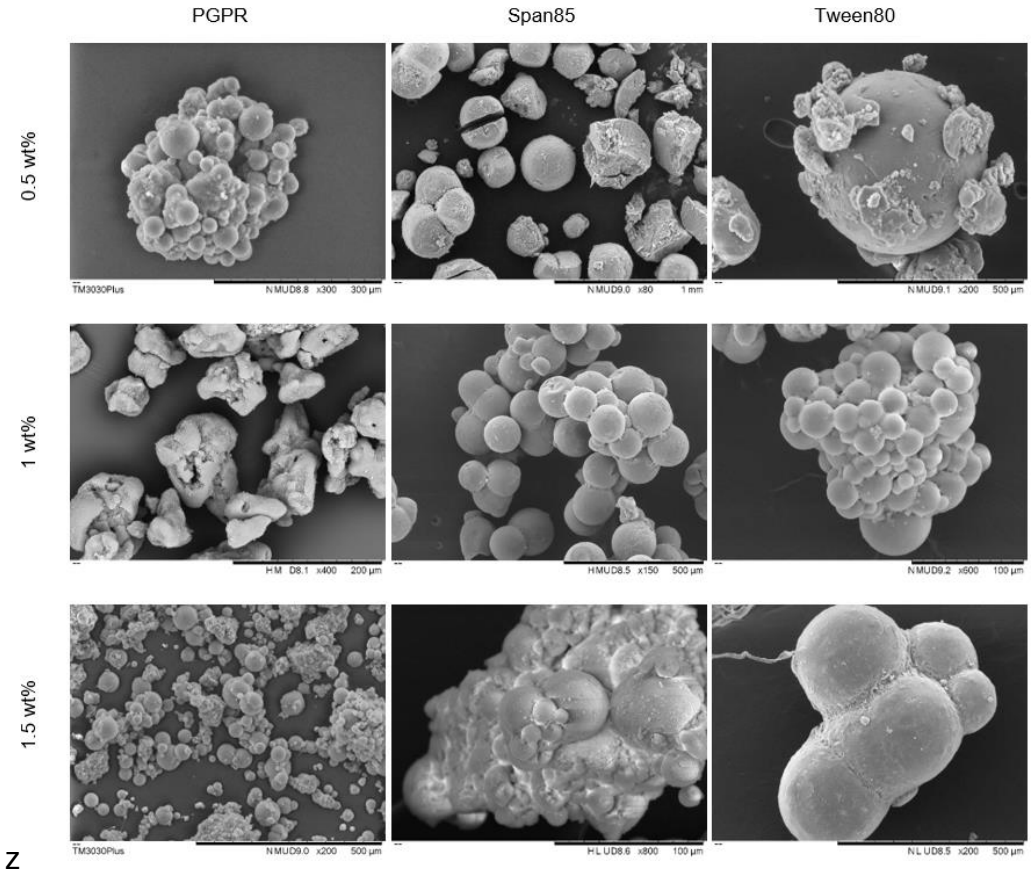

Figure 4-7 Effect of different emulsifiers and emulsifier concentration on sample formulation with 100% AMP core, 6:4 core-shell ratio, 1200 rpm homogeniser speed and 400 rpm mechanical stirrer speed (TM3030Plus).

Comparing the microencapsulated sample from Figure 4-8, 0.1 – 0.3 wt% PGPR concentration do not produce any microcapsules, only broken shells that do not have any core, whereas in comparison 0.5 wt% to 1.5 wt% PGPR is able to produce spherical shaped microcapsules with 0.5 wt% showing the best result. Similarly, 0.3 wt% Span85 only produces broken particles.

Concentrations of ≤ 0.3 wt% surfactant lead to no encapsulation due to the shortening of the emulsion lifetime. The core droplets are too unstable in the bulk phase leading to the formation of a cream or a coalescence. Creaming is observed when the core material either ascends or descends to the top and bottom respectively inside the jacketed beaker. Due to the higher density of the core material (AMP: 0.934 g/cm^3, MEA: 1.01 g/cm^3, TEA: 1.13 g/cm^3,), the creaming during formulation with not enough stabilised emulsion occurs at the bottom as it is heavier than the oil (0.83 g/cm^3) (78).

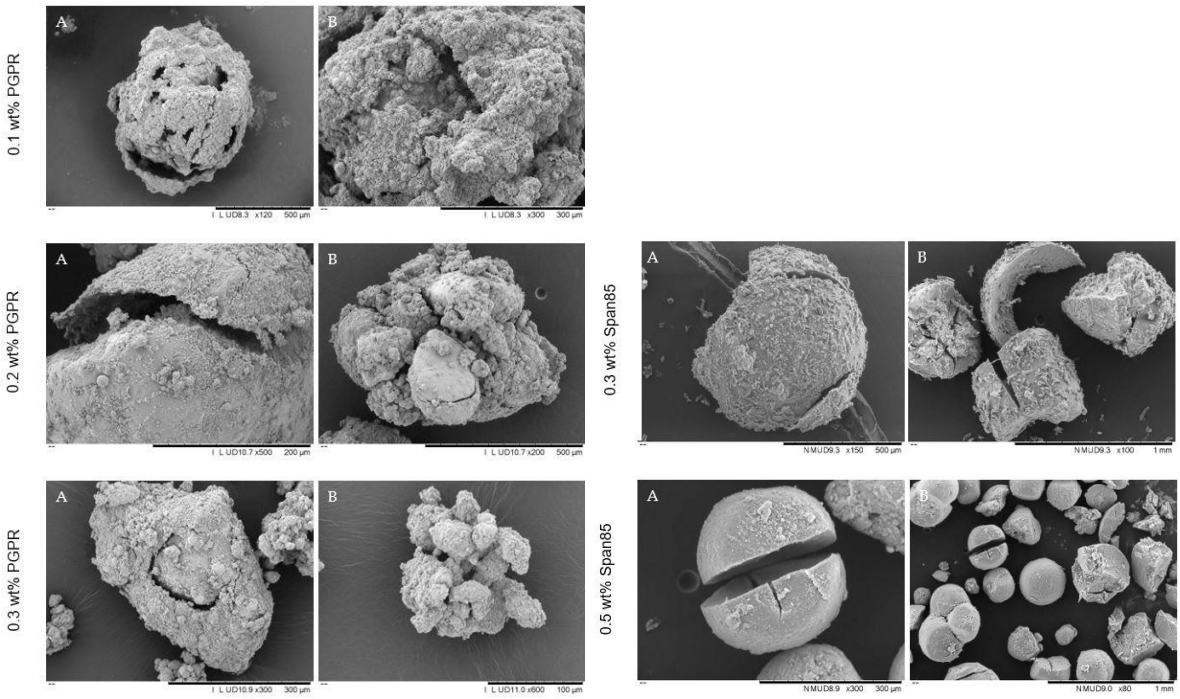

Figure 4-8 Emulsifier concentrations that were unsuccessful in encapsulating AMP core with hydrolysed TEOS (6:4 core-shell ratio, 1200 rpm homogeniser speed and 400 rpm mechanical stirrer speed). A) single microcapsules; B) cluster of microcapsules (TM3030Plus).

Overall, it can be observed that the emulsifiers affect the surface properties. 0.5 wt% PGPR seems to be the best sample due to the formulated microcapsules containing less agglomeration, having a more uniform morphology, with less broken microcapsules found inside the sample and giving a rougher surface with higher pore number compared to 0.5 wt% Span85 and 0.5 wt% Tween80 formulated samples.

However, both 1 wt% Span85 and 1 wt% Tween80 are the best concentrations for the respective emulsifiers due to more uniformly sized microcapsules and less agglomeration being present inside the sample compared to the other concentrations. 1 wt% Span85 seems to have a smoother surface finish compared to the other two emulsifiers, whereas 1 wt% Tween80 formulated sample had the highest quantity of agglomeration. This is due to the differences in the interfacial tension produced by the different emulsifier and concentrations.

4.2.2.2 Emulsifier Concentrations and Interfacial Tension

Figure 4-8 shows the emulsifier concentrations that were not able to produce any encapsulation. This is due to the concentration of the emulsifier not being strong enough to stabilise the bulk phase sufficiently so that hydrolysed TEOS can migrate towards the core droplet interface as described previously (4.2.1).

In comparison the other concentrations (≥0.5 wt%) were successful in encapsulating AMP. However, there is not only a lower limit for emulsifier concentration but one for higher concentrations as well. Concentrations of 0.5 wt% for PGPR and 1 wt% for Span85/Tween80 show the least amount of agglomeration, i.e. at these concentrations, the quality of microcapsules is best. The higher the agglomeration, the more likely it will not only interfere with the CO_2 absorption later but also affect the surface properties of the microcapsule. Agglomeration might cover the pores on the surface, more on this in chapter 5.

The emulsifier concentration is related to its effect on the interfacial tension between the bulk and surrounding phase. The stabilising mechanisms are generally very

complex and vary from system to system, however, the following two parameters always play a role in the stabilisation (72):

1) Low interfacial tension. The adsorption of surfactant at the interface in the bulk phase leads to the lowering of the interfacial energy of the emulsions, thus, easing the emulsion development and improving the stability of the emulsion.
2) Mechanically, strong interfacial film. The stability of the emulsion is provided by the mechanical protection formed by the adsorbed emulsifier film around the core droplet (72).

For example, if Span85 is dispersed into the oil, the interfacial tension of the bulk phase reaches up to 4.6 mN/m with 0.5 wt%, however, as the surfactant concentration is doubled to 1 wt% the interfacial tension is lowered to 2.78 mN/m (Figure 4-9). The trend of the higher the surfactant concentration, the lower the interfacial tension is followed by PGPR as well with the exception of Tween80. An increase in Tween80 concentration leads to a slight increase in interfacial tension, suggesting that Tween80 works differently from the other two surfactants. To either reduce or increase the interfacial tension of the system with Tween80, a higher or lower concentration than 0.5 wt % and 1.5 wt% are required. The interfacial tension results support the observations from the SEM images (Figure 4-7) of suggesting higher surfactant concertation giving more stable emulsions due to lower interfacial tension leading to better microcapsule formulation. However, a too low interfacial tension also gives an unstable emulsion as the surfactant concentration is too high which is the case for all emulsifiers with 1.5 wt% concentrations. But the lower interfacial tension limit varies with different surfactants due to their differences in their chemical structure and hence the way they stabilise the emulsion system (78).

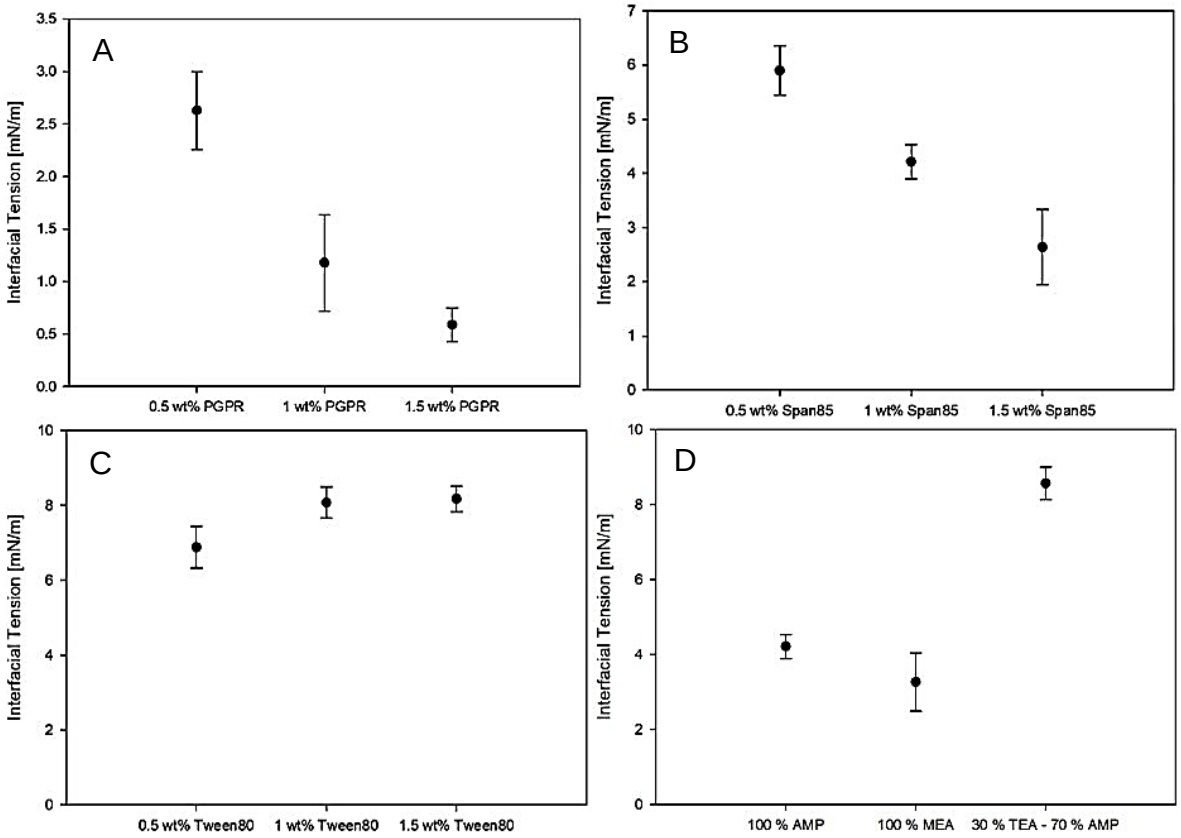

Figure 4-9 Graphs showing measured interfacial tension for different emulsifiers, emulsifiers concentrations and different core materials: A) PGPR concentrations; B) Span85 concentrations; C) Tween80 concentrations; D) AMP, MEA and TEA core material.

Emulsifier concentration is not the only factor affecting the interfacial tension. The success of encapsulation is also depended on the density of the core material. It was found that no samples were formulated by using pure TEA as a core material. The density of pure TEA (1.13 g/cm^3) is too high to measure the interfacial tension of the surrounding and the bulk phase. The bigger the difference between the bulk and surrounding phase is in terms of density, the more unstable the emulsion is going to be and might prevent the encapsulation of the core due to higher surface tension. But if the TEA concentration is lowered to 30% by mixing it with AMP a stable enough emulsion can be formed to produce microcapsules, though, the shape of the capsules

is not spherical (Figure 4-10). This suggests that the interfacial tension of the emulsion with TEA is still too high with 8.8 mN/m (Figure 4-9).

Table 4-2 Density of the different core materials and mineral oil.

Material	Density [g/cm$^{3]}$	Reference
AMP	0.934	(79)
MEA	1.01	(80)
TEA	1.13	(81)
Mineral oil	0.834	(82)

In the case of MEA, the viscosity of the material is lower than that of the oil (24.1 mPa.s) and the density is higher than that of the oil with 1.01 g/cm^3 which hinders the encapsulation of the material. The high density of MEA prohibits a proper core droplet formation where the emulsifier can diffuse into which meant that the emulsion is only creamed, i.e. core descends to the bottom (82), hence the formulated sample with MEA core had an elongated shape rather than a spherical shape (Figure 4-10). However, this disadvantage of lower viscosity can be overcome with the use of a homogeniser, i.e. homogenisers with the correct emulsifier and emulsifier concentration can still stabilise core materials with lower viscosity than the bulk phase. By comparing the formulated sample from Figure 4-10, it can be concluded that an AMP core gives the best-formulated sample, suggesting that an interfacial tension around 4.6 mN/m is favourable for creating a stable emulsion.

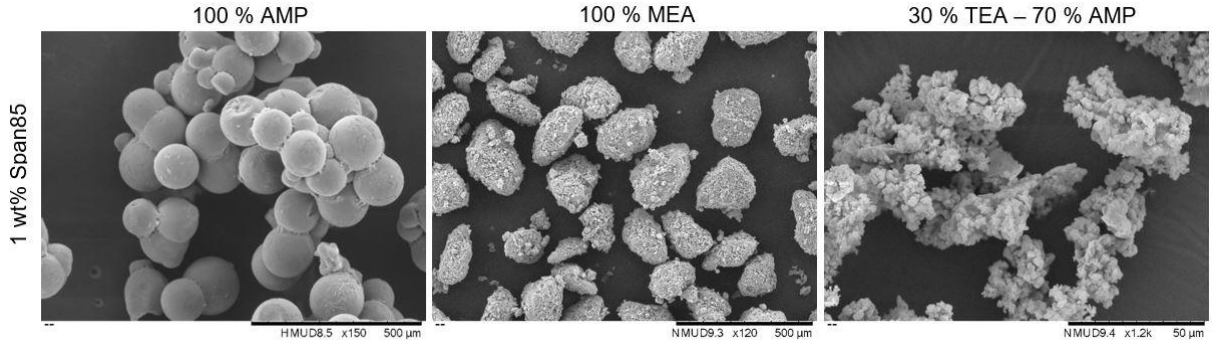

Figure 4-10 Comparison of formulated sample with 1 wt% Span85, 6:4 core-shell ratio and different core materials (AMP, MEA, TEA) (TM3030Plus).

4.2.2.3 Core-Shell Ratio

Different core to shell ratios were used in the microcapsule formulation to optimise and investigate its effect on the formulation process. The ratios were defined by the core and shell material mass used during the encapsulation process, e.g. a 15g core material with 10g of shell material gives a 6:4 or 1.5:1 core-shell ratio. The aim was to find the best ratio to reduce the agglomeration, hence, produce better quality microcapsules and also to increase the payload while maintaining the capsule quality

The higher the core to shell ratio is going to be, i.e. more core material compared to shell material, then a rougher surface is achieved, whereas lower differences in the ratio of the two material, the higher the agglomeration. For example, samples with 5:5 core-shell ratio (Figure 4-11) show more polymeric species attached on the surface of the shell compared to samples with 8:2 ratio as these samples have a very rough surface, higher agglomeration and the formed microcapsules are either elongated or have a ‘neck’ formed (67).

A higher hydrolysed TEOS availability will give a higher rate of reactant which will enhance the silica nucleation which leads to the formation and growth of many relative species at the same time which is advantageous, however, in this case, the core concentration is too low, hence the coalescence of the reactive species with each other without being able to encapsulate anything as well as provide overall a higher amount of polymeric species in the emulsion. In contrast, if the core concentration is too high, there is not enough hydrolysed TEOS to encapsulate all the core material, hence leaving a high concentration of core material inside the emulsion which leads to the agglomeration of the microcapsules due to coalescence (71). From Figure 4-11, it can be concluded that a ratio of 6:4 gives the best quality microcapsules due to low

agglomeration with more uniformly shaped microcapsules and lower amount of broken capsules.

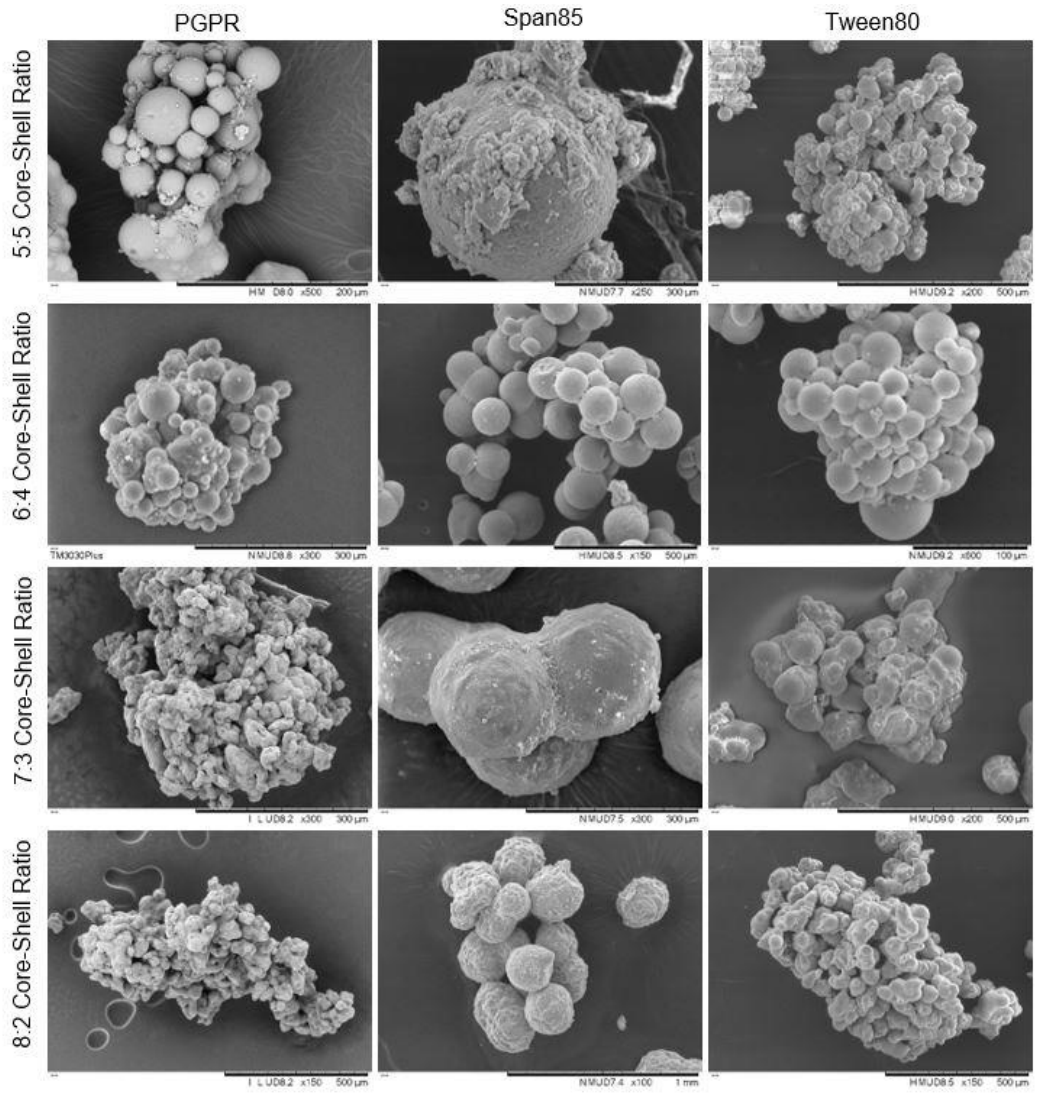

Figure 4-11 Effect of core-shell ratio on sample formulated with different emulsifiers (100% AMP, 1200 rpm homogeniser speed and 400 rpm mechanical stirrer speed) (TM3030Plus).

4.2.2.4 Homogenisation

Another requirement for a stable emulsion is the use of a homogeniser. For this purpose, samples were prepared both with and without a homogeniser.

As mentioned previously, the use of a homogeniser is advantageous when the density difference between the surrounding and bulk phase is large, e.g. MEA and mineral oil.

MEA has a higher density than the oil which means that emulsifiers alone are not enough to form a core droplet interface for the shell material, resulting in the material depositing at the bottom and forming a slurry at the end of the formulation process when a homogeniser is not used.

Homogenisers are used to reduce the size of droplets in a liquid-liquid dispersion by disrupting the core droplet formation in the oil, i.e. the core droplet are broken to smaller ones before rapid adsorption of the surfactant around the core surface leads to the formation of stable droplets. Hence, homogenisation can overcome the difference between the surrounding and bulk phase density. However, TEA has a too high density where the surfactant adsorption onto the surface is too slow, preventing spherical core droplet formation inside the oil, hence descending down to the bottom due to their higher density (83).

It can be seen from Figure 4-12 that the morphology of the microcapsules does not vary much from each other with the various homogenisation and mechanical stirring speeds used. The samples only differ in the surface roughness and the amount of agglomeration present inside each sample. Samples formulated with 1200 rpm and 400 rpm homogeniser and mechanical stirrer speed respectively, show the lowest amount of agglomeration along with a smooth surface. However, in comparison, if the homogenisation speed is increased from 1200 rpm to 2000 rpm the microcapsule get a rougher surface, whereas microcapsules produced without a homogeniser and a 800 rpm mechanical stirrer speed produces vast clusters of microcapsules with large pores visible to the naked eye.

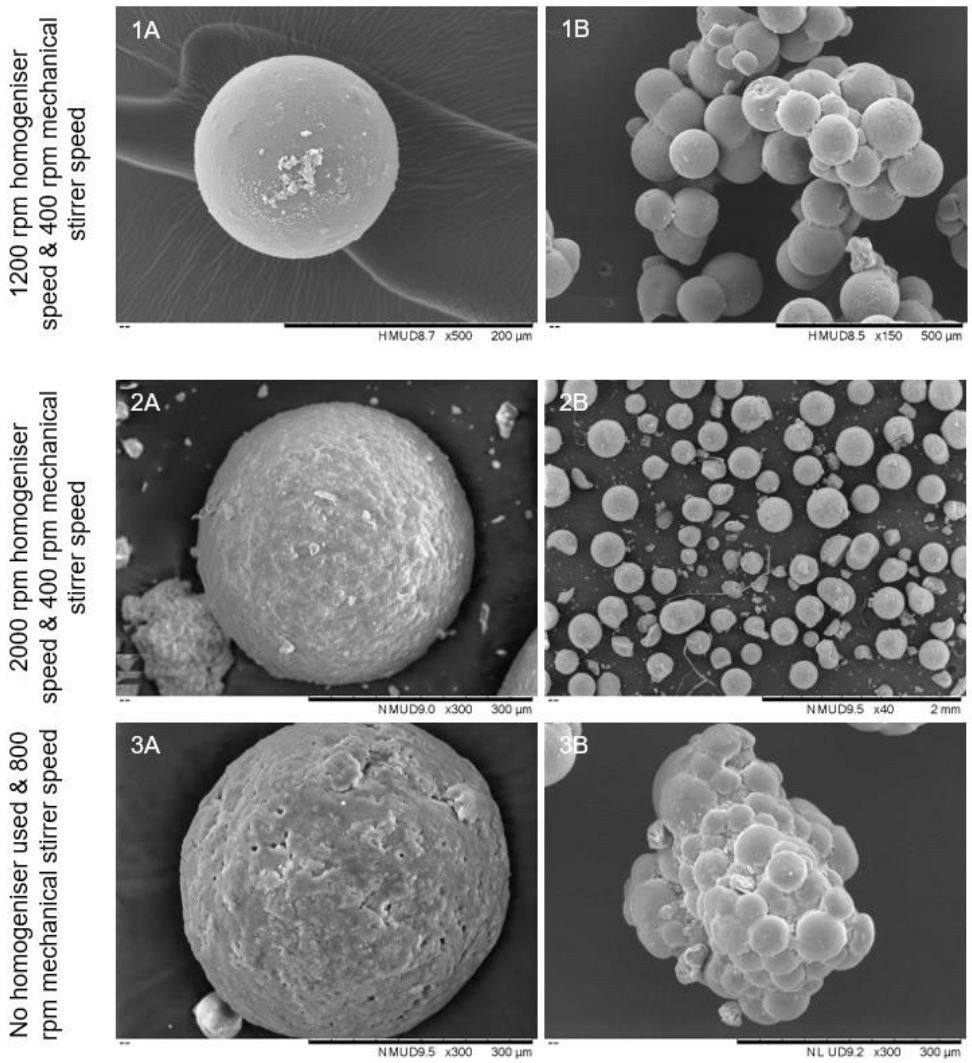

Figure 4-12 Effect of homogeniser and mechanical stirrer speed on microcapsules formulated with 1 wt% Span85. A) single microcapsule; B) cluster of microcapsules (100% AMP and 6:4 core-shell ratio) (TM3030Plus).

In comparison samples produced with the lowest stirring speed (100rpm) showed the highest particle attachment on capsule surface compared to samples formulated with higher stirring speeds (600 rpm) (Figure 4-13). Lower stirring speeds, lead to more traces of monomers and oligomers of TEOS to be found with the final product which are very hard to remove from the sample (70).

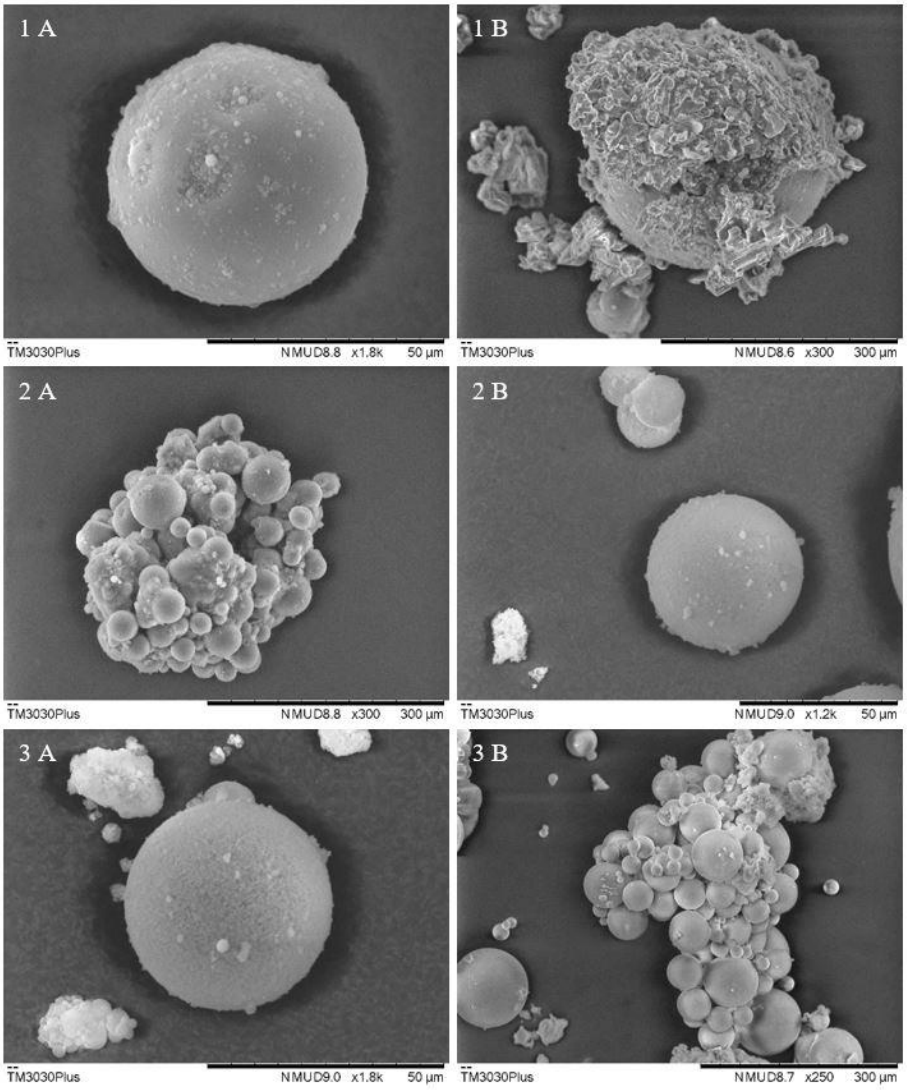

Figure 4-13 Effect of mechanical stirrer on microcapsules formulated with 0.5 wt% PGPR and 6-4 core-shell ratio. (1A) 100 rpm - Single microcapsule; (1B) 100 rpm - Single microcapsule with agglomeration; (2A) 400 rpm – Single microcapsule; (2B) 400 rpm – Microcapsule with agglomeration, (3A) 600 rpm – Single microcapsule; (3B) 600 rpm – Microcapsule with agglomeration (100% core, 6:4 core-shell ratio) (TM3030Plus).

The use of a homogeniser cannot fully negate the effect of viscosity on the encapsulation process if the viscosity of the surrounding phase is too low or too large. If the viscosity of the continuous phase is high than the formed droplets will the spherical due to slow droplet formation which is the case for AMP (Figure 4-10). In comparison with highly viscous continuous phases like TEA, the formed capsules will be deformed. Similarly, If the continuous phases' viscosity is too low like MEA, the

material flows too easily in the homogeniser, making it harder for the core droplet to retain their spherical shape, hence ‘necks’ formed capsules are created (82).

4.2.2.5 *Core Material Yield*

After formulating the sample with the different parameters, the sample is dried and measured in terms of weight to identify the amount of core material found inside the dry sample, i.e the formulation yield. It is advantageous to have a high yield to reduce the amount of time required to formulate samples, especially if large quantities are required for running a reactor.

As can be seen from Table 4-3, samples formulated with low surfactant concentrations show a lower yield, whereas higher concentration give higher yield, e.g. 0.5 wt% PGPR, 100% AMP core and a 6:4 core-shell ratio gave a yield of 51.7% but in comparison sample 1.5 wt% PGPR, 100% AMP core and a 6:4 core-shell ratio gave a yield of 56.6%. This is due to the higher agglomeration present in the samples formulated with 1.5 wt% surfactants. A higher amount of both unencapsulated core material and polymeric species after the drying process gives a higher sample weight and thus a higher yield.

Similarly, a higher core-shell concentration gives a higher yield. Higher amounts of the core are present in the emulsion that cannot be encapsulated due to lower hydrolysed TEOS concentration. For example, a 9% yield difference between samples formulated with 1 wt% Span85, 5:5 and 8:2 core-shell ratio is seen. As can be seen from Figure 4-11, higher core-shell ratios give more agglomeration in the sample with elongated or neck formed microcapsules, which agrees with the findings in (67).

In comparison, 100% TEA shows the lowest yield with 5.6% due to the low quantity of formed microcapsules. As mentioned previously, TEA has unsuitable properties that prevent it from being encapsulated. However, the yield can be improved by lowering the TEA concentration by mixing it with AMP. By using a 30% TEA and 70% AMP concentration more sample can be formulated with a better yield of 38.4%, though the yield is still lower compared to the other core materials and formulation parameters.

For encapsulated MEA a lower yield is observed (40.5%) compared to encapsulated AMP (44.8%) even though MEA has a higher density (1.01 g/cm^3) than AMP (0.934 g/cm^3). The density difference would indicate sample formulated with MEA should have a higher yield just based on the density. However, as discussed previously, the formulation is also highly depended on the viscosity of the material and emulsion stability. Since emulsions with MEA have lower stability, they formulate less sample, hence the lower yield.

The first test for the formulation of AMP with TEOS was left running for 24 hrs and produced good microcapsules. However, to optimise and potentially narrow down the required time for the reaction, the formulation is repeated for 6 hrs and 12 hrs. Figure 4-14 shows that after 6 hrs most of the microcapsules are not fully formed yet, hence the high amount of broken particles and agglomeration is observed. Similarly, after 12 hrs there is still a considerable amount of broken microcapsules and agglomeration found compared to samples left running for 24 hrs, suggesting that both 6 and 12 hrs are not enough time for the formulation to finish, hence, a lower yield is observed for both (34.5% and 41.3% respectively) compared to the 16 hrs sample as generally without an increase in temperature the silica formation is slow (67) (Table 4-3). Therefore, an increase in the temperature of the jacketed beaker could lead to the

faster formulation, however, the low melting temperature of AMP (30 °C) prevents the change of the formulation temperature above 20 °C for safety measure. Hence it was decided to continue formulating sample with 24 hrs (84).

Table 4-3 Comparison of the calculated yield from formulated, dry sample with different core materials, emulsifiers and core-shell ratios.

Core Material	Emulsifier	Core-shell ratio	Yield (%)
100% AMP (16 hrs)	0.5 wt% PGPR	5:5	45.6
		6:4	51.7
		7:3	56.4
		8:2	60.4
	1 wt% PGPR	6:4	54.4
	1.5 wt% PGPR	6:4	56.5
	0.5 wt% Span85	6:4	42.9
	1 wt% Span85	5:5	40.2
		6:4	44.8
		6:4 (ethanol dried)	39.7
		7:3	44.5
		8:2	49.2
	1.5 wt% Span85	6:4	45.1
	0.5 wt% Tween80	6:4	38.4
	1 wt% Tween80	5:5	27.6
		6:4	39.5
		7:3	41.6
		8:2	45.6
	1.5 wt% Tween80	6:4	42.4
100% MEA	1 wt% Span85	6:4	40.5
100% TEA	1 wt% Span85	6:4	5.6
30% TEA – 70% AMP	1 wt% Span85	6:4	38.4
100% AMP (6hrs)	1 wt% Span85	6:4	34.5
100% AMP (12hrs)	1 wt% Span85	6:4	41.3
Silica particles with no core	1 wt% Span85	N/A	16.7

Additionally, silica particles without a core were formulated for later CO_2 absorption testing. Trying to formulate silica particles without a core material is quite challenging. Without core droplets in the oil phase, silica particles need to rely on the collision to each other for polymerisation, whereas with a core, the core provided a site for the hydrolysed particle to migrate towards and start forming nuclei to further the growth of the species into silicon dioxide. Hence, a very low yield is observed with silica particles

(16.7%). In order to overcome this phenomenon, the hydrolysed TEOS weight is quadrupled from 12 g to 48 g for the formulation which then improved the yield to 67%. All in all, due to the good emulsion stability with 0.5 wt% PGPR, 1 wt% Span85 and 1 wt% Tween80, these samples show the highest yield, whereas a core material with high density or viscosity is able to reduce the yield of the formulated samples.

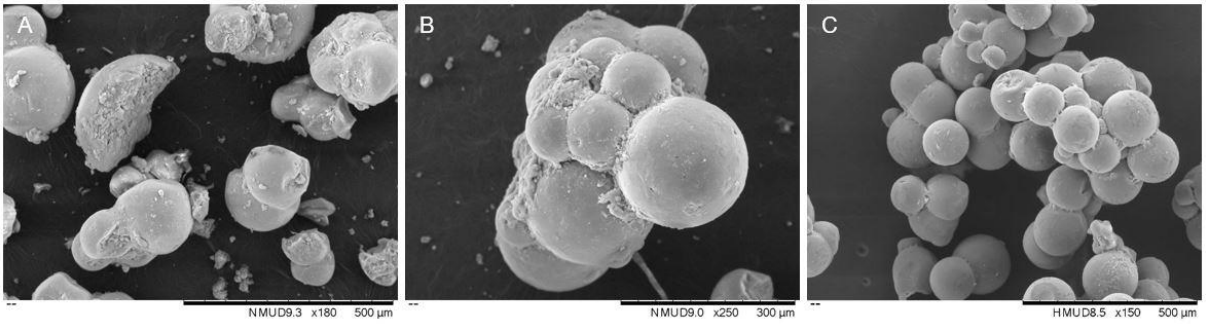

Figure 4-14 Effect of reaction time of morphology on formulated sample (100% AMP, 6:4 core-shell ratio, 1200 rpm homogeniser speed and 400 rpm mechanical stirrer speed) (TM3030Plus): A) 6 hrs; B) 12hrs; C) 24 hrs.

4.3 Summary and Method Analysis

To conclude a wide range of formulation parameters were investigated where in most cases it lead to a successful encapsulation with the exception of < 0.3 wt% PGPR emuslifier concentrations and pure TEA core material. However, comparing the samples in terms of quality 1 wt% Span85 with a 6:4 core-shell ratio (400 rpm and mechanical stirrer 1200 rpm mechanical stirrer speed) showed the least amount of agglomeration with a smoother surface finish. A summary of the formulation process is provided in Figure 4-15.

In-situ polyermisation was selected as this method is simple and easy to set-up as well as allows the size distrbution of the sample to be controlled to a certain degree, however, it gives very little control over the polymerisation. It also produces agglomeration which is hard to dispose of. Additionally, only the external factors like

the stirring speed and core-shell ratio can be controlled during the formulation process. The use of homogenisation systems and mechanical stirrers results in non-uniform, wide size distribution. The polymerisation reaction itself cannot be influenced unless the temperature of the formulation process is changed. However, this is not an option for amine-based core materials as they possess low melting temperatures (85). This limits the method as the growth of silica particles from the condensation of polymeric species is rate-limited and extremely slow with hydrolysed TEOS at low temperatures. This can lead to fast inter-droplet matter exchange, leading to silica nucleating too early which could limit the size of the final microcapsules (71).

Additionally, the use of amines as CO_2 adsorbent cores limits the use of polymerisation due to the potential loss of amine group during the polymerisation reaction. Even though the set-up used during formulation gives a wide size distribution and agglomeration, a microfluidic device is not suitable for the purpose of amine encapsulation. This is mainly due to the use of u-v induced polymerisation which would polymerise the amine group essential for the carbon capture (64).

Even though a wide variety of factors were investigated, an alkaline pH of the emulsion could potentially improve the formulation process. During the encapsulation process, the pH was not measured, however, due to the alkalinity of amine cores, an alkaline polycondensation was chosen. Previous research has shown that a constant pH during the polymerisation is advantageous (86). Hence, it is recommended that future work include monitoring of pH during the formulation. Other future work could include replacing the TEOS with a different shell material to form a shell-core type of microcapsules rather than a matrix internal structure.

Moreover, a highly dispersed microcapsule formulation with hydrolysed TEOS inside an emulsion is highly challenging along with the drying process due to the polymeric species being highly sensitive to the processing conditions (67). It is demanding to try to find a solvent that will only dissolve the polymeric species and will not affect the microcapsule at all to reduce the agglomeration of the formulated sample.

After formulating the microcapsules, the influence of the formulation conditions on the microcapsule properties will be further investigated in the following chapter, including the size distribution, microcapsule composition, thermal properties, thermal cycling, payload, surface area and shell thickness.

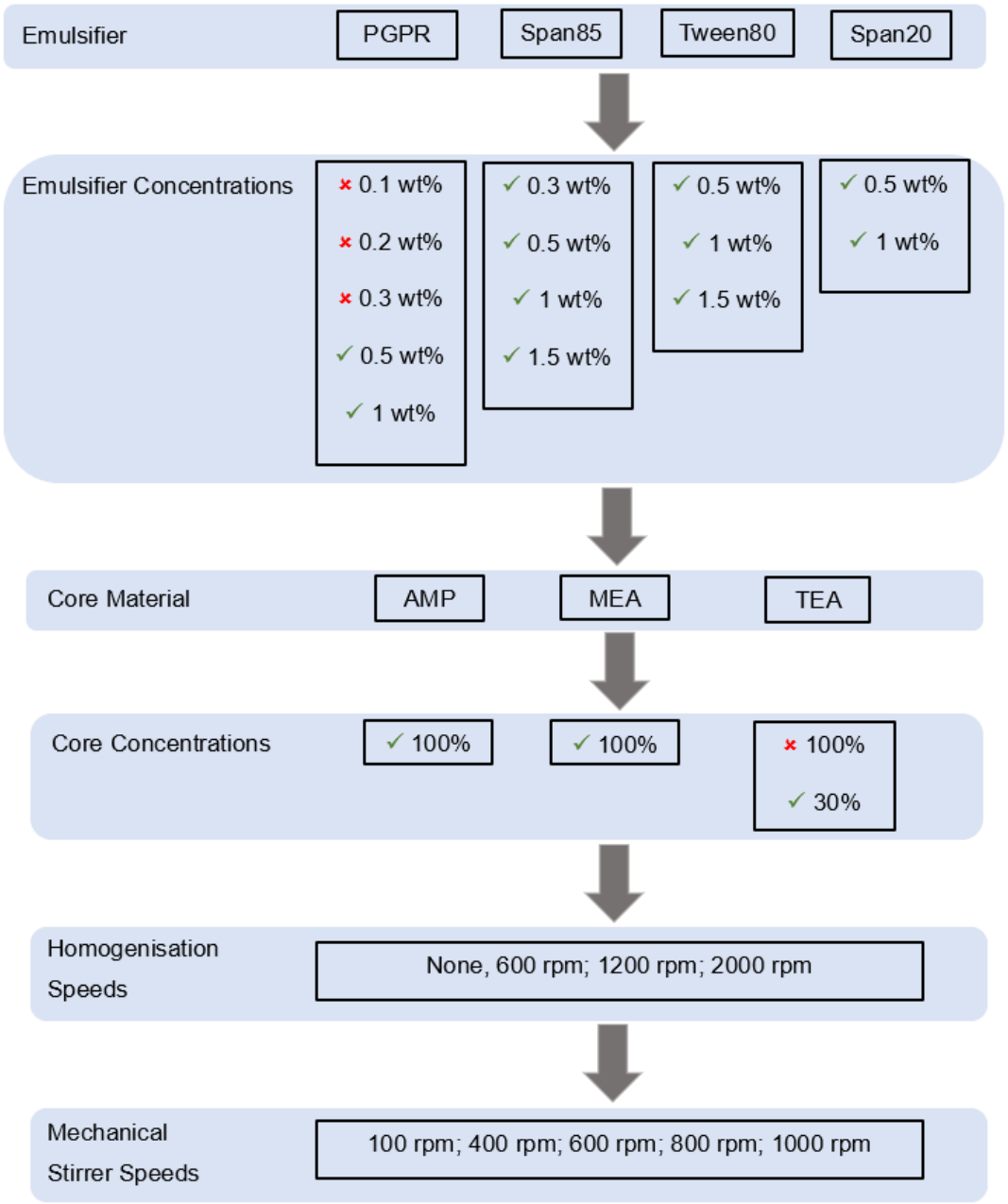

Figure 4-15 Flow diagram summary of the different formulation parameters to show which ones resulted in successful encapuslation (where × indicates failure of encapsultaiton and ✓ successful encapsulation).

Chapter 5 Microcapsule Characterisation

5.1 Introduction

In this chapter, the physio-chemical and structural properties of the formulated microcapsules from chapter 4 are characterised by using different measurement techniques like thermal analysis, thermal cycling, Malvern particle sizing and Brunett-Emmet Teller analysis. The most important characteristics of the microcapsules are their ability to capture CO_2 as they are being produced for this purpose. To this end, a TGA instrument, thermogravimetric analysis, was used to verify the absorption ability of the encapsulated sample. Additionally, the payload is studied as well as it influences the absorption capacity, whereas the core material influences the absorption kinetics and thus was investigated as well. Furthermore, factors like homogenisation and stirring speeds along with surfactants that influence the microcapsule properties in terms of size, pore size and surface area are also investigated. Moreover, not only are the different measurement techniques discussed but also the microcapsules' properties effect on applicability and limitation.

5.2 Results and Discussion

5.2.1 Physio-chemical characterisation of microcapsules

5.2.1.1 Thermal Properties

The thermal properties of the formulated samples are measured and compared against the pure core materials to observe the effect of encapsulation, specifically the stability of microcapsules at low temperatures.

Figure 5-1 conveys the various melting and freezing points of the core material as a response to temperature. Pure, liquid AMP showed freezing at -22 °C and at -16 °C and a melting point is seen at 8 °C. The peaks at -22 °C and-16 °C represent the

crystallisation before melting takes place at 8 °C, despite the material having a melting point around 30°C (literature value). This lower melting temperature occurred most likely due to the freezing of the material previously which allowed the material to melt earlier. The two freezing points could be due to either impurities or water vapour inside the material despite pure, liquid material being used for testing (52).

Similarly to pure AMP, pure MEA showed freezing as well but at -25 °C and -53 °C and then a corresponding melting point at 13 °C, whereas pure TEA showed a freezing point at -16 °C. Comparing these results for the pure core materials with literature, no freezing point has been stated in literature to the best of our knowledge; even the melting temperature of pure AMP and TEA at 30 °C and 19.5 °C respectively is not seen (comparison values from MSDS of materials). But from the DSC result (Figure 5-1) the freezing points are suggesting the core materials undergoe crystallisation at the highlighted points. Similarly, the endothermic peak (melting of material) of both MEA and AMP is not found in the literature (84) which is explained by the re-melting of the AMP from the crystalline state that shifts the melting point of the material to a lower temperature. Pure TEA has been reported to show melting around 19.5 °C, however, this melting point is not seen in the experiment.

The discrepancies in the result and literature values can be explained by impurities and the limitations of the DSC instrument. For all three core materials, only 10 µL was pipetted into the crucible instead of measuring out the weight of the material. The DSC is dependent on the sample weight, a higher sample weight is preferred to lower the possibility of errors due to artefacts being present in the pure material as well as lowering the background noise. As the pure core material is a liquid, it is easier to distribute the same amount of liquid by using a 100 µL than try to weigh the exact

sample weight for every measurement, however, this small quantity of sample makes the testing more susceptible to errors through small vibrations, too low sample mass and impurities (59).

In contrast, the decrease in freezing point has been observed previously when the pore size diameter was lower than 100 nm, suggesting a porous structure might lower the freezing point of the material which seems to be the case here (87), suggesting a change in material properties compared to pure, liquid core.

In comparison, no melting or freezing is observed with all the encapsulated samples irrespective of their stirring speed, core-shell ratio, different core material and different emulsifiers and emulsifier concentrations, indicating no phase change occurred which is advantageous as it may lead to a decrease in the CO_2 sorption capability of core materials (also for MEA encapsulated sample) to ensure good stability over the range of 25 °C to -60 °C which is supported by the findings of the SEM images from thermal cycling (Figure 5-1) (5.2.1.2).

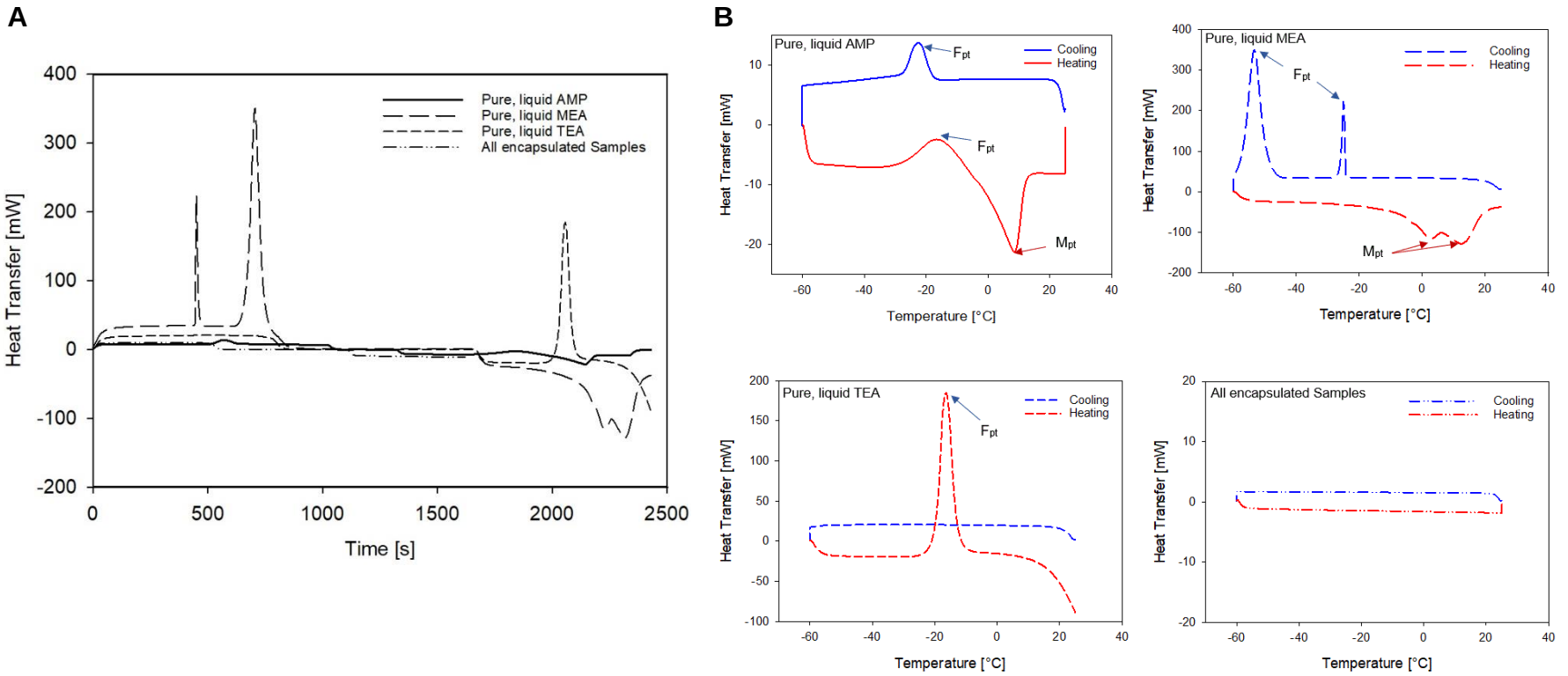

Figure 5-1 Thermal property comparison of pure core materials (liquid) against the encapsulated sample. The following temperature profile was used: start at 20 °C then cool down to -60 °C at 10 °C/min and leave sample at -60 °C for 10 min before heating up again to 25 °C. **A** Heat transfer against time profile; **B** Heat transfer against temperature profile.

5.2.1.2 Thermal Cycling

The formulated samples were repeatedly exposed to low temperatures through 10 continuous thermal cycling by alternating heating and cooling from 20 °C to -100 °C with a high-temperature change (10 °C/min) to evaluate the samples' reliability thermal fatigue which is important for application. If the sample can be recycled and reused, then the production cost can be lowered which is advantageous in industry. Fatigue can be defined by the weakening or breakdown of the microcapsules due to repeated or prolonged stress exposure. This is a gradual and irreversible process that most often leads to deformation of the formulated microcapsules (88).

Thermal cycling overall does not change the morphology of the samples, but it does introduce cracks and indentations on some microcapsules inside the samples. The sample formulated with 100 rpm stirring speed only showed cracks on the surface of the microcapsules, whereas microcapsules produced with the other two stirring speeds only had indentations with 600 rpm showing the largest and highest amount (Figure 5-2). This indicates that the shell produced with lower and higher stirring speed than 400 rpm is weaker and hence more susceptible to thermal damage (88).

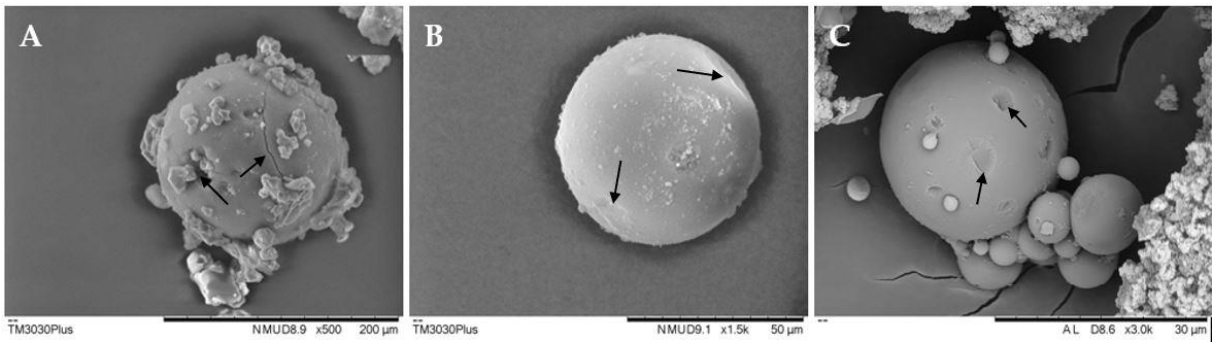

Figure 5-2 Microcapsule morphology of sample formulated with 0.5 wt% PGPR and different stirring speeds after ten continuous cycles. A) 100 rpm stirring speed - Microcapsule with crack and indentations; (B) 400 rpm – Microcapsules with indentations; (C) 600 rpm – Microcapsule with indentations.

In contrast, by changing the emulsifier from PGPR to Tween80, similar indentations are seen with some microcapsules, whereas samples formulated with Span85 show less to no depressions. These indentations occur most likely due to solvent evaporation from the surface of the particles during the repeated cycling process. This suggests that microcapsule produced with Span85 have a better ability to withstand continuous temperature changes, hence produce better quality microcapsules (Figure 5-3).

Figure 5-3 Effect of different emulsifiers on microcapsule morphology after thermal cycling. A) 0.5 wt% PGPR; B) 1 wt% Span85; C) 1 wt% Tween80.

Bigger changes in morphology are observed when the core-shell ratio is changed from 6:4 during the thermal cycling. Both increasing or decreasing the core concentration has a negative effect where a decrease from 6:4 leads to very large hollowing of the microcapsules (Figure 5-4 A)., whereas thermal cycling introduces several cracks for microcapsules with a 8:2 core-shell ratio. This suggests that the shell created with an 8:2 core-shell ratio is more susceptible to shrinkage compared to the other ratios and hence more susceptible to fatigue (Figure 5-4 D).

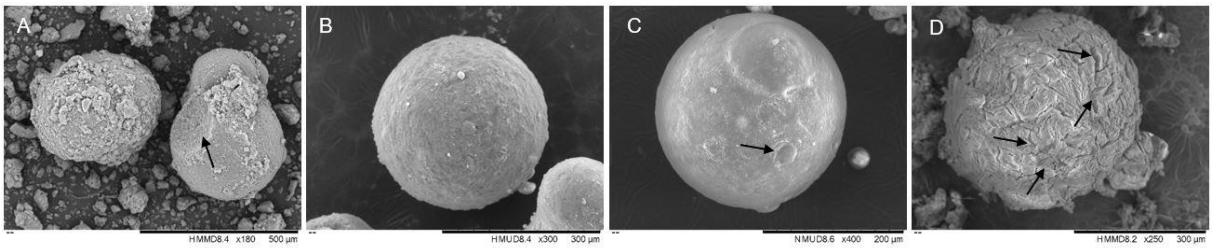

Figure 5-4 Effect of core-shell ratio on the morphology of microcapsules formulated with 1 wt% Span85 after thermal cycling. A) 5:5 core-shell ratio; B) 6:4 core-shell ratio; C) 7:3 core-shell ratio; D) 8:2 core-shell ratio.

The presence of indentations and cracks after thermal cycling is partially influenced by the surface structure as can be seen from Figure 5-5. When the core material is changed from AMP to MEA or TEA, a more porous and rougher surface is produced which is more likely to resist crack and dent formations.

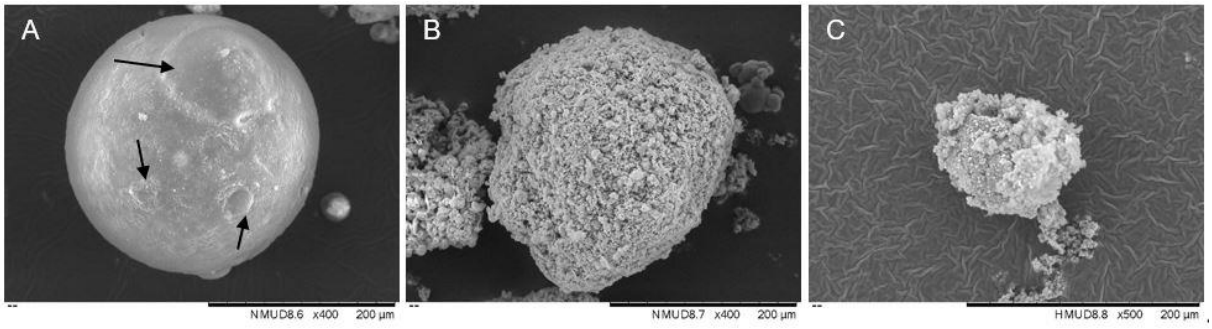

Figure 5-5 Effect of different core material on the morphology of microcapsules formulated with 1 wt% Span85 after thermal cycling. A) AMP core; B) MEA core; C) TEA core.

It has been reported in literature that thermal cycling is often followed by indentations or crack formation on the surface of a material which tends to grow with an increase in thermal cycle number, indicating that 10 thermal cycling is not enough to conduct fatigue studies to identify the limitations of the microcapsules. Normally fatigue studies repeat more than 100 thermal cycles to get an indication about the failure conditions, hence for future work it is suggested to repeat thermal cycling for at least 100 cycles. It is important to recognise the thermal stability properties of microcapsules as it

estimates their endurance limit and strength and how the capsule responds to external damage (88).

Overall, most samples did not show many changes in morphology after 10 continuous cycles from 20 °C to -100 °C apart from the occasional crack or indentation, indicating all produced microcapsules irrespective of the formulation parameter are able to retain their shape after intensive, low-temperature exposure.

5.2.1.3 Size and Size Distribution

To optimise the formulation condition, the different parameters affecting the encapsulation need to be considered so that the method can produce homogeneous and similar sized microcapsules. In principle, the size of microcapsule can be obtained by changing the emulsifier concentration, stirring/ homogeniser speeds and core-shell ratio (71).

Effect of stirring speed. The stirring speed of the mechanical stirrer and the homogeniser speed both affect the size and size distribution during the formulation. At first the size of the formulated sample is tried to be varied by changing the mechanical stirrer speed from 100 rpm to 600 rpm which leads to the production of a sample with varying sizes. The average size distribution of the individual samples is represented in Figure 5-6. It can be seen that 600 rpm sample has the smallest overall capsule size with the narrowest size distribution (5-40 μm) out of all the three samples. In comparison, 100 rpm sample yielded the largest capsules with the broadest size distribution among all the samples. The mean particle size for the various samples were 20 μm, 105 μm and 140 μm for 100 rpm, 400 rpm and 600 rpm sample respectively.

As the stirring speed is increased from 100 rpm to 600 rpm, smaller microcapsules with smaller size distribution but higher agglomeration are produced (5). However, between 400 rpm and 600 rpm sample a smaller difference in particles size and size distribution spectra is observed. The main difference between the samples is the apparent shift of average particles size (APS) from 105 μm (400 rpm sample) to 140 μm (600 rpm sample) (Figure 5-6). The APS shifts from right toward the left as stirring speed increases. These differences occur due to the force created by the mechanical stirrer that involves core drop breakup by the generated shear stresses. These stresses are not uniform across the system, hence the highly polydispersed sample (42). The higher the stirring speed, the more force distributes the internal phase into smaller droplets (600 rpm sample), thus, decreasing the mean diameter of the formed microcapsules (89,90).

However, at the same time higher stirring speed causes higher core droplet collisions resulting in agglomeration during the encapsulation process. Hence 600 rpm sample showed higher agglomeration compared to 100 rpm and 400 rpm sample. In contrast, the broad particle size distribution at lower stirring speed is most likely due to the varying energy distribution of the stirring depending on the position of the microcapsules within the jacketed-beaker. This unevenly distributed shear force produced causes reduced control over the surface force of the drops as well as minimises the surface tension that pulls the core solvent into spherical shapes (91).

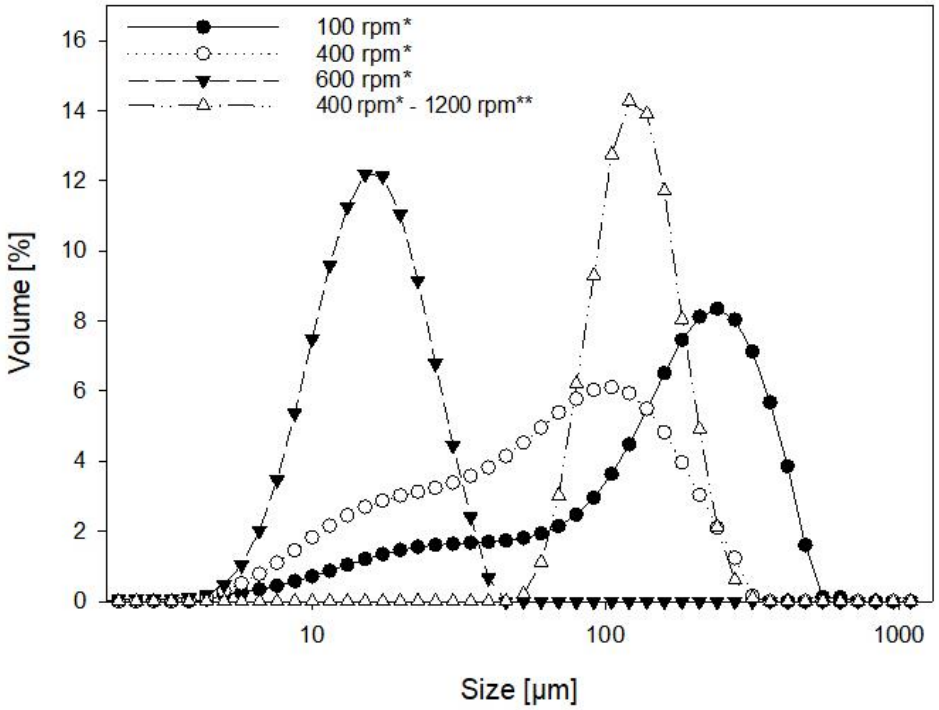

Figure 5-6 Effect of varying mechanical stirrer and homogeniser speeds on the size distribution of formulated sample (core-shell ratio of 6:4, 0.5 wt% PGPR, AMP core). The graphs show the average size distribution where * indicates the mechanical stirrer speed with no homogenisation speeds and ** indicates the homogenisation speed used.

To have a better control over the size distribution, homogenisers are used in emulsion to reduce the droplet size in a liquid-liquid dispersion by disrupting the core droplet formation inside the emulsion, i.e. the adsorption of the emulsifier around the core droplet is disrupted which is then followed by a rapid emulsifier adsorption to form more stable droplets, whereas a slow adsorption leads to coalescence. Hence, less polydispersed particle size is given for sample formulated without a homogeniser as can be seen from Figure 5-6. The use of a homogeniser narrows the size distribution of the sample (400 rpm – 1200 rpm*) from 4 µm – 300 µm to 70 µm – 300 µm with the average size being larger (122 µm). However, uniform size distribution is still not achieved with the use of a homogeniser and mechanical stirrer due to the uneven force distribution inside the system (92).

Formulating silica particles. The size distribution of the encapsulated sample is compared to the produced silica particles to observe and to better understand the encapsulation process with and without a core. As is expected, the silica particles had a smaller average size (60 μm) with a wider size range (6 μm – 500 μm) (Figure 5-7). This is due to no core material being present. The core material gives the hydrolysed TEOS during the encapsulation process a place to migrate towards due their immiscibility, however in a situation where there is nothing for them to attach onto the particles must rely on the turbulence of the stirrer to collide with each other to form clusters of silica particles (67).

To change the size of the silica particles, the polycondensation reaction needs to be either faster or slowed down by manipulating the reaction parameters, e.g. it has been shown that an increase in ammonia concentration increases particle size (67). If the reactant concentration and temperature of the reaction are fixed, then the particle size distribution of silica particle formulation is dependent on the mixing mode used. During this formulation process the mechanical stirrer speed is the same that was used to form encapsulated sample, i.e. 400 rpm (67).

These silica particles (without a core) were formulated to help better understand the carbon dioxide absorption of the encapsulated sample, i.e. to allow comparison of chemical and physical adsorption.

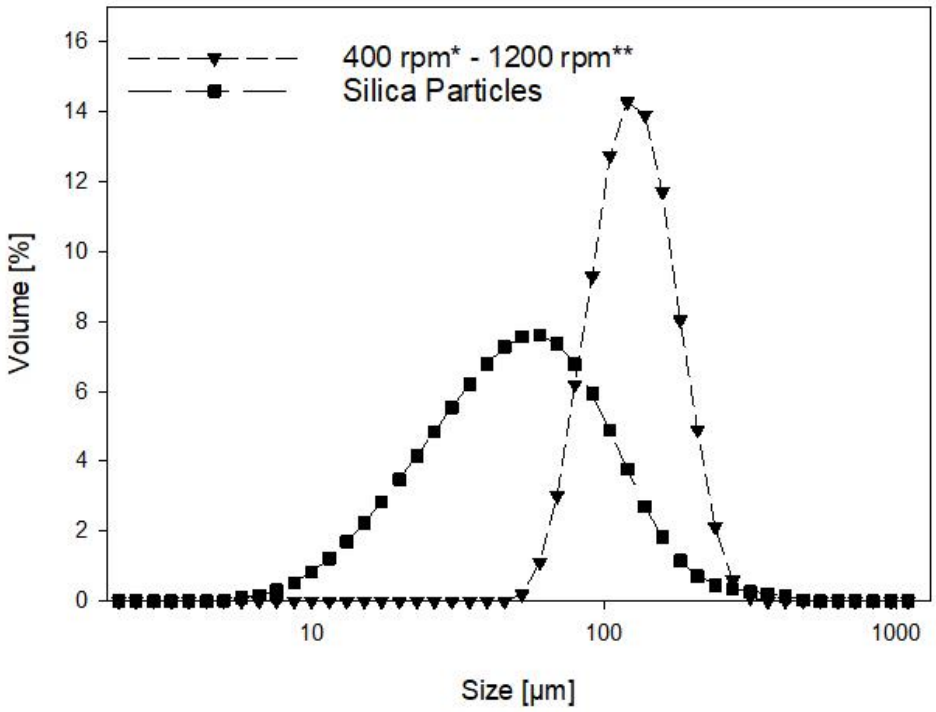

Figure 5-7 Comparison of silica particles and encapsulated sample with 800 rpm mechanical stirrer speeds (core-shell ratio of 6:4, 1200 rpm homogeniser, AMP core) where * indicates the mechanical stirrer speed and ** indicates the homogenisation speed used.

Change in size distribution with varying homogeniser speed. As mentioned earlier, homogenisation is important not only for stabilising the emulsion phase, but it also affects the size distribution. Previous studies (82,93) have shown that the use of a homogeniser provides a better w/o interfacial tension and thus improved the stability of the emulsion by de-creasing the droplet size. To form emulsion for smaller droplet size, more mechanical energy was applied to the system, i.e. the homogenisation speed is increased which leads to intense turbulent and shear flow that normally tends to break the core droplets further into smaller ones. Similarly, if the homogenisation speed is decreased, bigger core droplets should be formed. However, it can be seen from Figure 5-8 that a change in homogenisation speed did not change the size distribution of the formulated sample (range of 100 µm – 900 µm), indicating that the emulsion is stable enough to withstand those forces. The difference in microcapsule

size (ploydispersion) occurs due to the energy distribution from the stirrer not being homogenous across the system. The core droplet near to centre is more likely to be smaller than those that are near the beaker thus further away from the homogenisation blade (92).

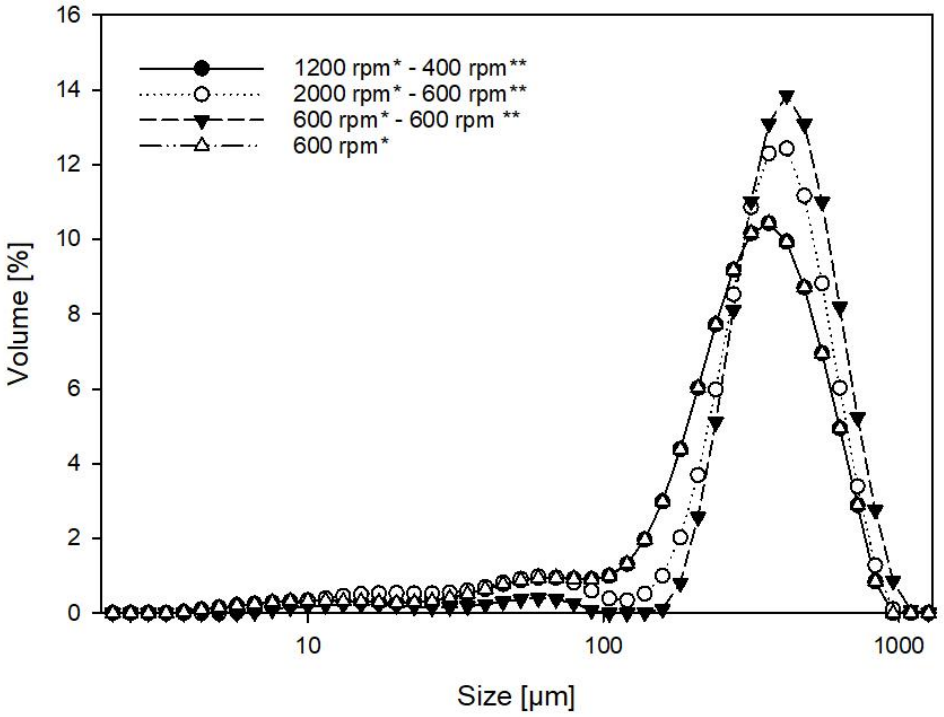

Figure 5-8 Effect of homogeniser speeds on the size distribution of formulated sample (core-shell ratio of 6:4, 1 wt% Span85, AMP core). The graphs show the average size distribution where * indicates the homogeniser speed and ** indicates the mechanical stirrer speed used.

Consequently, the emulsifier was changed from Span85 to Span20 due to Span20 providing the emulsion with lower stability. This resulted in a more polydisperse size distribution (4 µm - 1600 µm) of the sample compared to the sample formulated with Span85, thus a change in emulsifier was not advantageous. The mean size and size distribution of the microcapsules can also be changed by decreasing the emulsifier concentration during the formulation process, as it affects the emulsion stability through the interfacial tension.

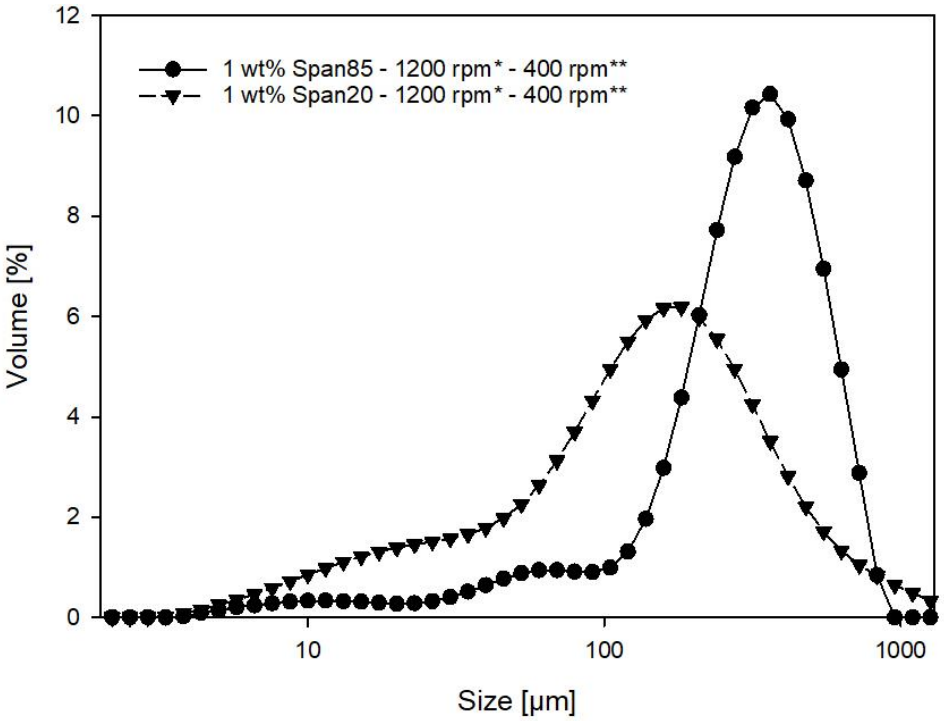

Figure 5-9 Comparing two different Span emulsifiers with the same core-shell ratio (6:4), AMP core, homogenisation (1200 rpm) and mechanical stirrer speed (400 rpm).

Effect of Emulsifier Concentration. Figure 5-10 shows the different sized microcapsule produced by controlling the emulsifier concentrations. The surfactant concentration, as well as different emulsifiers, effect the size distribution. The formulated sample show a wide size distribution irrespective of the emulsifier and emulsifier concentration used. 0.1 – 0.3 wt% PGPR produced microcapsule with a similar size distribution range (5 µm – 900 µm), whereas a higher concentration like 0.5 wt% and 1 wt % produced overall smaller microcapsules where 1 wt% showed the narrowest size distribution of 50 – 500 µm. Furthermore, using PGPR as an emulsifier gave the samples two peaks for the size distribution (0.5 wt% PGPR). These double peaks occurred due to the lower interfacial tension of the oil phase compared to both Span85 and Tween80. A lower interfacial tension allowed the core droplets to break down more easily and coupled with the varying energy distribution inside the

formulation system, hence smaller microcapsules being formed near the stirrer blade, whereas the microcapsules near the beaker (on the outside) are smaller in size (71).

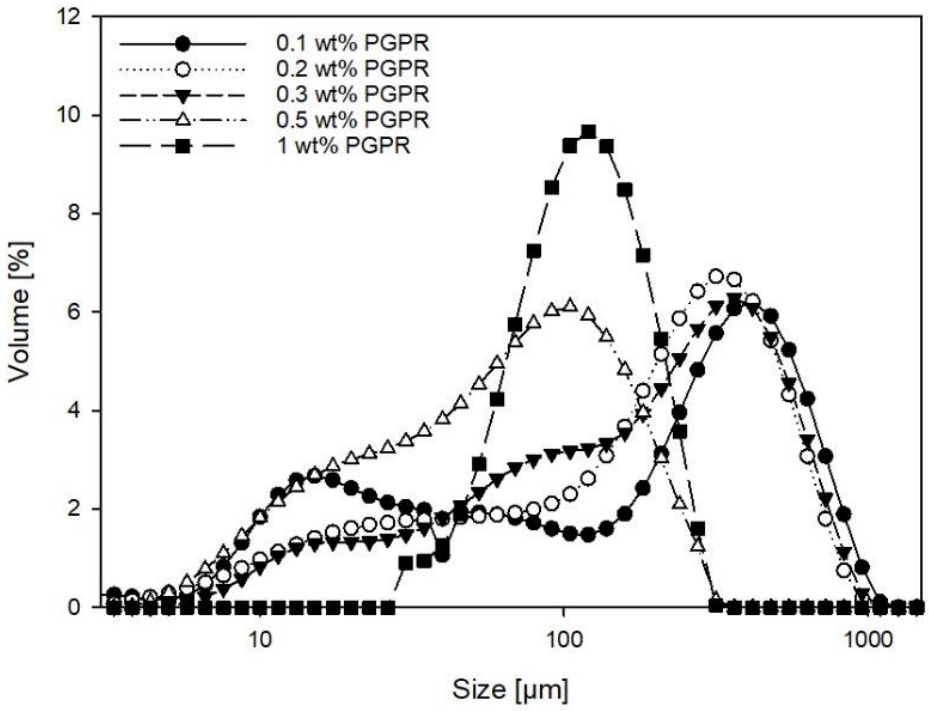

Figure 5-10 Effect of PGPR concentrations on the size distribution of the formulated sample (core-shell ratio of 6:4, AMP core and a mechanical stirring speed of 400 rpm). The result is shown as the average size distribution.

A similar trend in size distribution is seen with Span85 and Tween80 where the size distribution is narrower and smaller microcapsules are produced as the emulsifier concentration is increased from the lowest concertation to the highest with 1 wt% Span85 and 1.5 wt% Tween80 showing the best size distribution, indicated by the APS more towards the left (

Figure **5-11**, Figure 5-12).

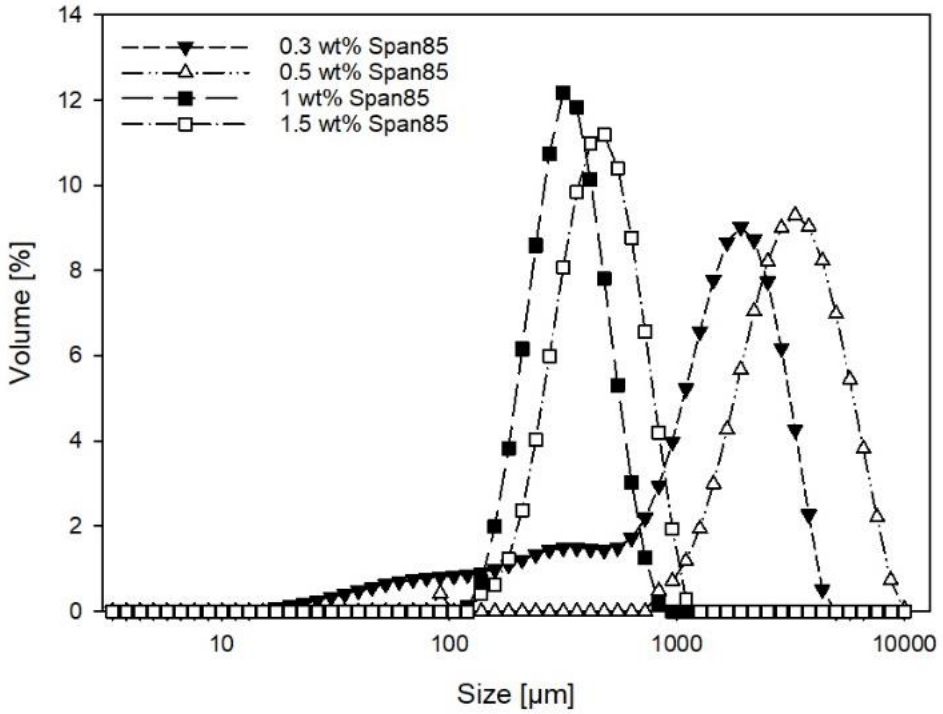

Figure 5-11 Effect of Span85 concentrations on the size distribution of the formulated sample (core-shell ratio of 6:4, AMP core and a mechanical stirring speed of 400 rpm). The result is shown as the average size distribution.

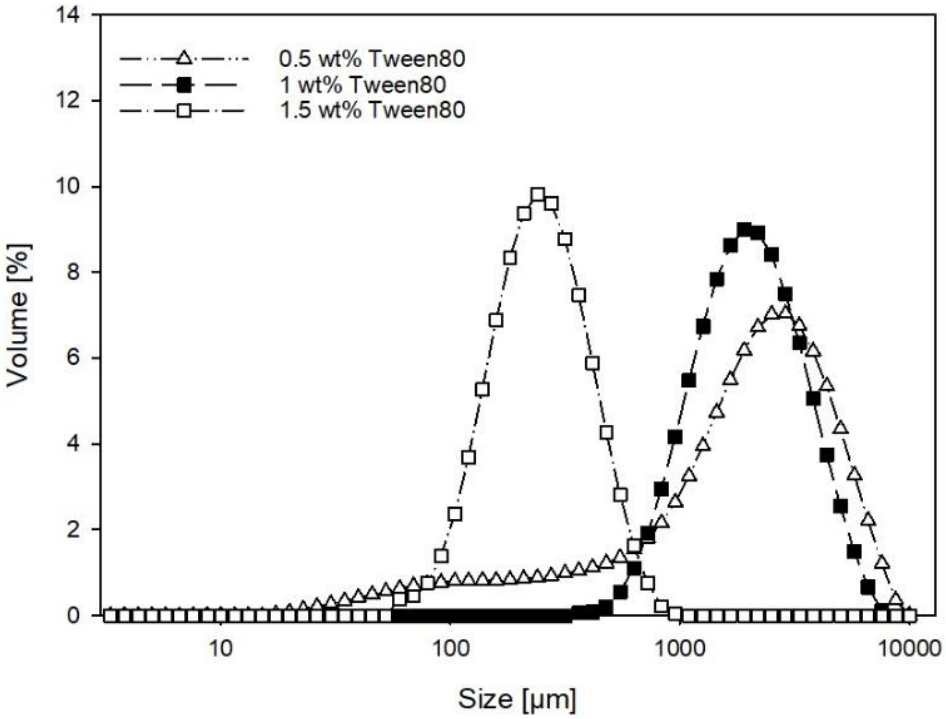

Figure 5-12 Effect of Tween80 concentrations on the size distribution of the formulated sample (core-shell ratio of 6:4, AMP core and a mechanical stirring speed of 400 rpm). The result is shown as the average size distribution.

Previous research has shown that molecular structure affects the size of the emulsion droplets (71). Emulsifiers like Span85 have a longer head and tail groups that can provide a stronger interaction with the core and silica particles inside the emulsion. Consequently, these stronger interactions lead to more nuclei being formed that become into smaller particles, thus higher emulsifier concentration give smaller microcapsules, e.g. 1.5 wt% Tween80 produced microcapsule with an average size of 250 μm and a size distribution range of 50 μm – 900 μm compared to 0.5 wt% Tween80 that produced an average particle size of 2000 μm and a size distribution range of 400 μm – 7000 μm (Figure 5-12). Smaller sized microcapsules are formed with a 1 wt% and 1.5 wt% PGPR/ Span85 and Tween80 concentration. If the concentration is varied from this value, then a more polydispersed and larger particle size are formed as the silica particles are more condensed and thus form larger particles (71).

Figure 5-13 compares the size distribution of the different emulsifier concentration that produced the best quality microcapsules in their respective concentrations. It can be observed that 0.5 wt% PGPR produced a sample with a very wide size distribution compared to the other two surfactants, whereas 1 wt% Tween80 (900 μm) produced larger microcapsules compared to 1 wt% Span85 (360 μm). These differences occur due to the difference in the interfacial tension achieved in the emulsion. 1 wt% Span85 has shown the best properties due to a better emulsion stabilisation. The reason for choosing 1 wt% tween80 from the other three concentrations is due to better microcapsule quality (4.2.2) despite larger microcapsule size. In comparison 0.5 wt % PGPR is chosen as a good parameter as well as it allows the size of the microcapsules to be changed with varying stirring speeds. This is important in order to analyse the effect of size on the absorption capacity of the sample. Though a better size distribution

is achieved with 1 wt% PGPR the sample showed higher agglomeration as seen from the SEM images in the previous chapter, hence less advantageous properties.

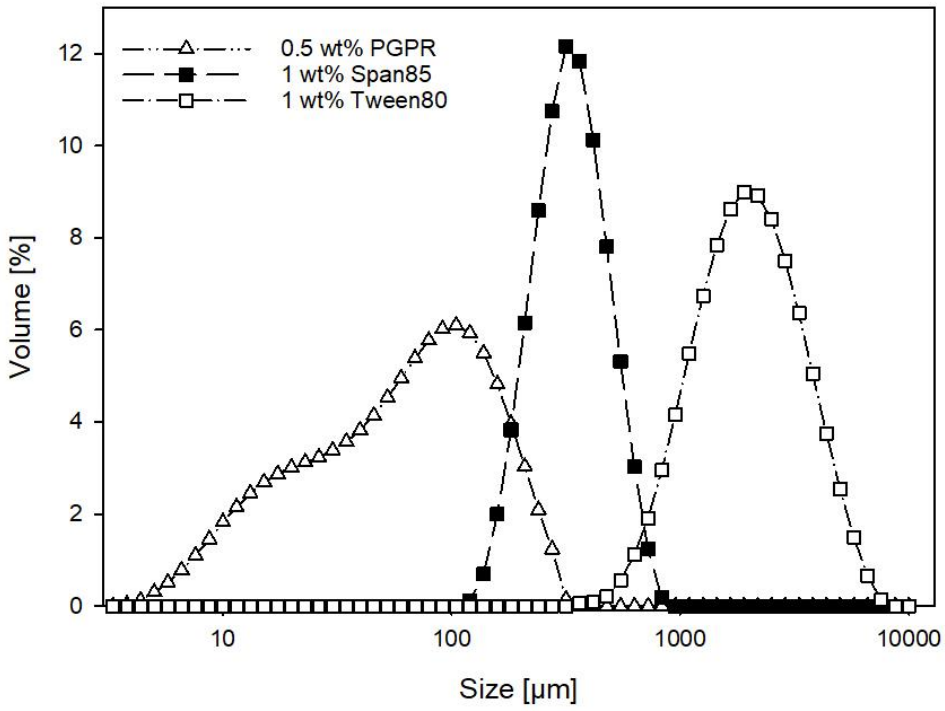

Figure 5-13 Comparison of best quality formulated microcapsule with a core-shell ratio of 6:4, AMP core and a mechanical stirring speed of 400 rpm). The result is shown as the average size distribution.

Effect of core-shell ratio. Another possible parameter that could affect the size distribution is the core-shell ratio, hence its effect is investigated. As can be seen from Figure 5-14, a 5:5 and 6:4 core-shell ratio for 0.5 wt% PGPR formulated sample gave a narrower size distribution with 5:5 ratio giving the largest average microcapsules size (200 µm) in comparison to 6:4 ratio (120 µm). The other two ratios (7:3 and 8:2) showed a wider size distribution with both having a similar size range (5 µm – 500 µm). In contrast, a 5:5 ratio for 1 wt% Span85 produced microcapsules with a very large size range compared to the other ratios for the same emulsifier concentration, whereas the other three ratios had a similar average size (300 µm – 500 µm) and size range (100 µm – 1200 µm) (Figure 5-15). The sample produced with 1 wt% Tween80 showed that

all ratios except 6:4 produced a similar size average (200 μm) and size range (50 μm – 800 μm) with the size range of 6:4 being shifted towards larger ones (1800 μm) (Figure 5-16).

A 5:5 core-shell ratio indicates that the quantity of core material is the same as the shell material which allows most of the core material to be encapsulated. However, from the SEM images (4.2.2.3) it was concluded that a 5:5 ratio gives a high amount of agglomeration where very small particles are attached on the surface. This suggests that the shell material concentration is higher than required, hence more hydrolysed TEOS particle collide with each other to form larger microcapsules. In comparison a 6:4 ratio had a higher core quantity, hence more encapsulated sample which is shown by the lower agglomeration of the dried sample. A 7:3 or 8:2 ratio had a too-large quantity of core material present so that not all of it can be encapsulated which not only lead to higher agglomeration inside the formulated sample due to the core material. The difference in size distribution with varying emulsifiers occurs due to the different interfacial tension produced inside the emulsion. 0.5 wt% PGPR showed less stable emulsion compared to the other two emulsifiers, hence a higher core concentration leads to more break of core droplets inside oil phase, hence a wider size distribution is seen with a larger than 6:4 core-shell ratio. In comparison 1 wt% Span85 can stabilise the emulsion better, hence a similar size distribution is seen for a ≥ 6:4 core-shell ratio. However, a wider size distribution with 5:5 ratio is seen due to higher possibility of the shell material encountering each other compared to other ratios, hence faster nuclei are produced that lead to smaller microcapsule formation. Regarding samples produced with 1 wt% Tween80, the emulsion is less stable than the one produced with

1 wt% Span85 but still more stable than the emulsion with 0.5 wt% PGPR, hence why Tween80 produces a less wide size distribution (94,95).

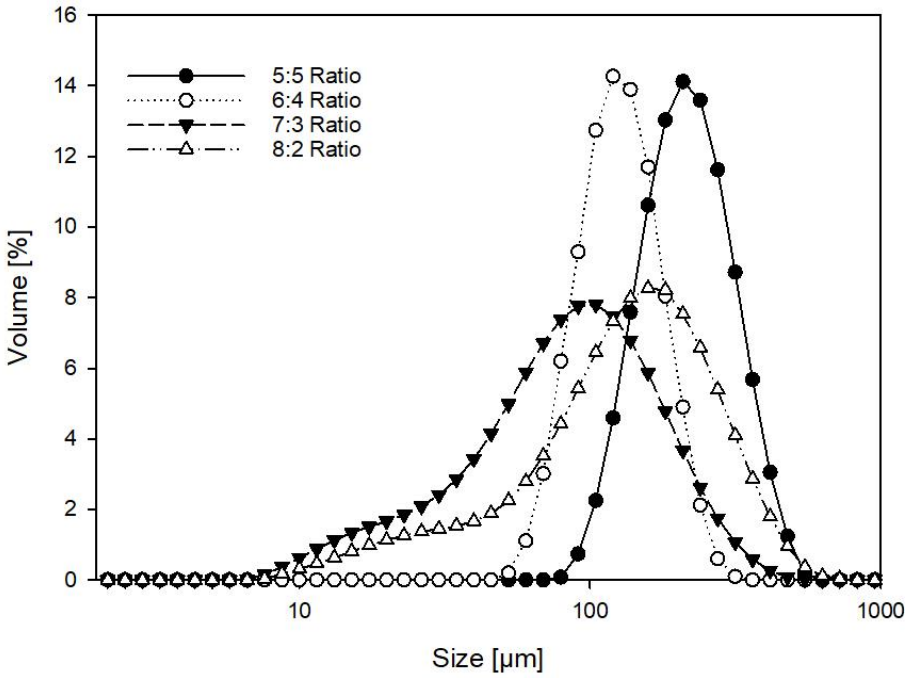

Figure 5-14 Effect of core-shell on the size distribution of 0.5 wt% PGPR formulated sample (AMP core, mechanical stirring speed of 400 rpm and homogeniser speed of 1200 rpm). The result is shown as the average size distribution.

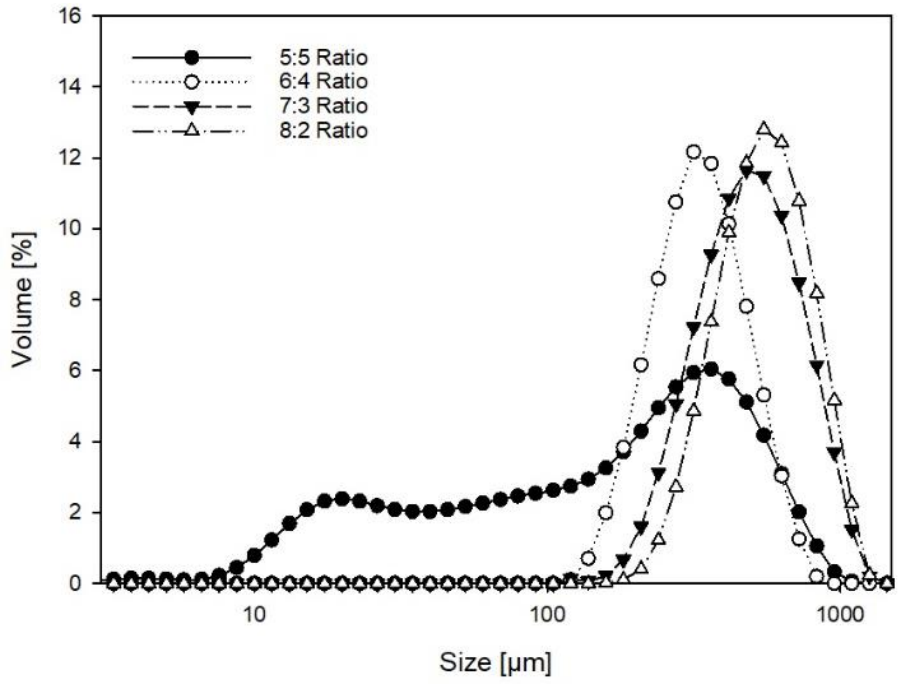

Figure 5-15 Effect of core-shell on the size distribution of 1 wt% Span85 formulated sample (AMP core, mechanical stirring speed of 400 rpm and homogeniser speed of 1200 rpm). The result is shown as the average size distribution.

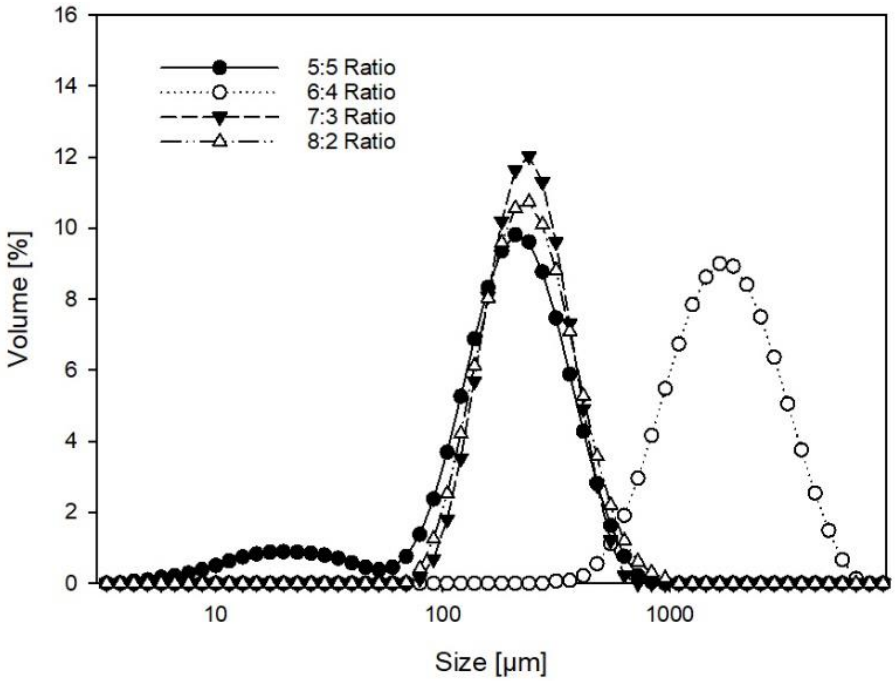

Figure 5-16 Effect of core-shell on the size distribution of 1 wt% Tween80 formulated sample (AMP core, mechanical stirring speed of 400 rpm and homogeniser speed of 1200 rpm). The result is shown as the average size distribution.

Effect of the core material. By changing the core material, the size distribution is changed as well as the core droplet inside the emulsion had a different size due to varying densities and viscosities. Pure MEA core samples produced the narrowest size distribution, whereas both pure AMP and 30 wt% TEA had a wider size distribution with a shift towards slightly smaller and larger respectively (Figure 5-17). Due to the mixing of TEA and AMP, formulated sample with 30% TEA showed a wide size distribution which could indicate that only AMP is being encapsulated as it showed a similar size distribution to a 5:5 core-shell ratio. There is a possibility of TEA separating from AMP once it was inside the emulsion phase where TEA might drift towards the bottom of the system due to its higher density. However, this is unlikely due to the use of a homogeniser. Homogenisers ensure good mixing and small core droplet formation. Another possible reason could be the structure of TEA. TEA has three ethanol groups that can all provide the necessary H+ protons for the polymerisation,

hence more nuclei sites present. This leads to bigger microcapsule production if the process encapsulated TEA, whereas microcapsule that contains the AMP would have a smaller size, resulting in more polydisperse size distribution. In comparison, MEA has the lowest density from the three amine cores, hence are more likely to break up more, hence the slight shift of the APS towards smaller microcapsules with a smaller number the same sized microcapsule production (82).

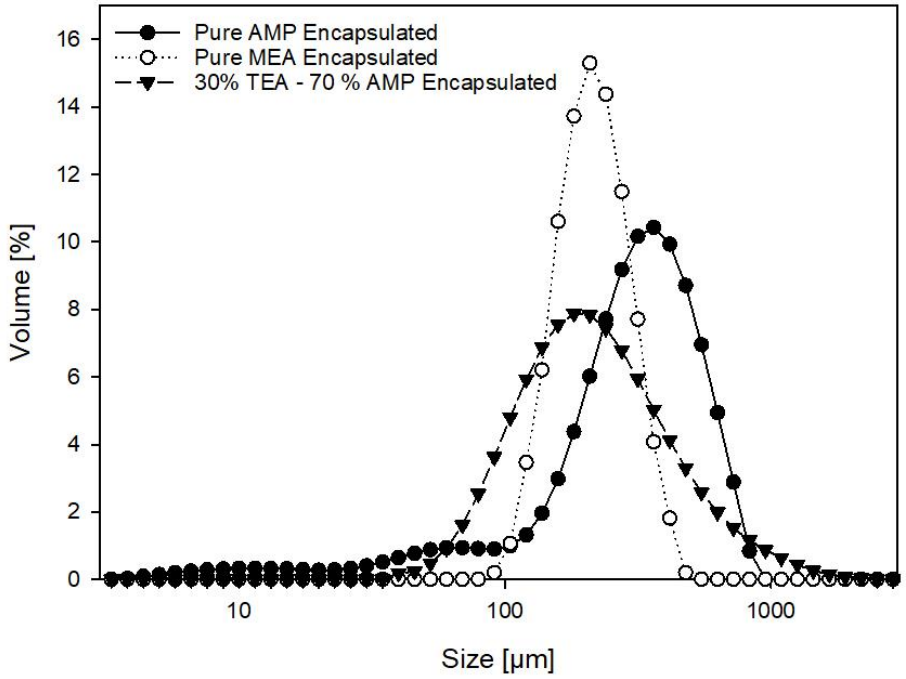

Figure 5-17 Size distribution of sample formulated with varying core materials (1 wt% Span85, 6:4 core-shell ratio, 400 rpm mechanical stirrer and 1200 rpm homogeniser speed).

Effect of reaction time. A change in reaction time does not affect the size distribution, as the size distribution is depended on the emulsifier, emulsifier concentration and mechanical stirrer/ homogeniser speeds. Particles smaller than < 100 µm are believed to be silica particles that were not able to encapsulate any core. However, the reaction time seems to affect the morphology as well as the payload (Figure 5-18).

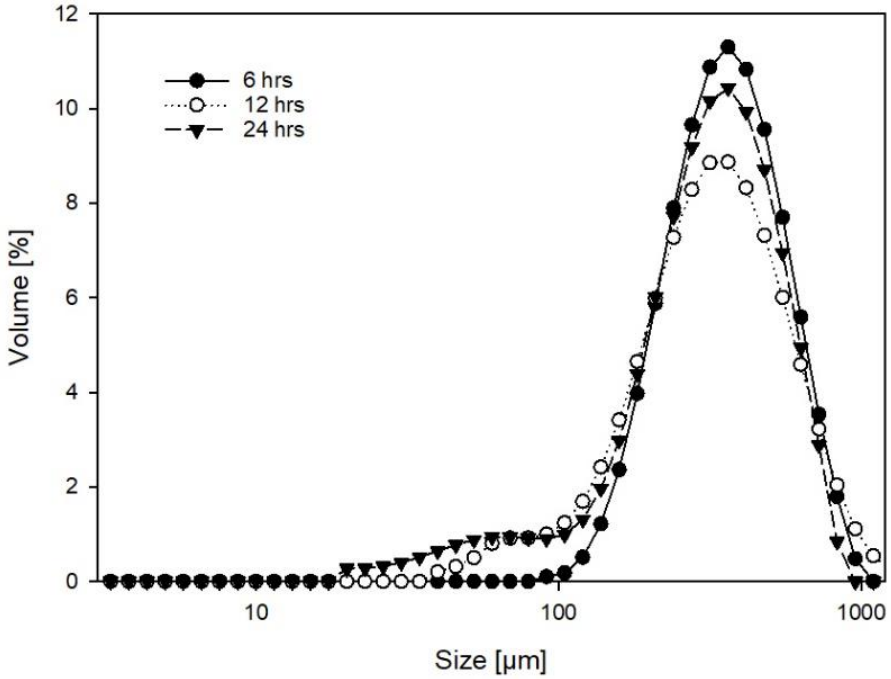

Figure 5-18 Effect of reaction time on the size distribution of formulated sample (1 wt% Span85, 6:4 core-shell ratio, 400 rpm mechanical stirrer and 1200 rpm homogeniser speed).

5.2.1.4 Chemical Composition

To investigate the chemical composition of the different encapsulated samples in comparison to the pure material, a Fourier Transform Infrared spectrometer (FTIR) was used. For easier comparison purpose all the encapsulated sample are simplified to one spectrum as there was no distinct difference in their spectra. Similarly, for the effect of core-shell ratio on the IR spectra, only one IR graph is shown for each ratio that represents 0.5 wt% PGPR, 1 wt% Span85 and 1 wt% Tween80. The FTIR spectrum obtained for pure AMP, MEA and TEA matched with the spectra reported in the literature (58).

The primary interest in the FTIR spectra is the N-H bonds from the amine groups and the O-H bonds from the propanol group of AMP. Both the N-H bonds and the O-H bond are present during in the FTIR spectra for all the encapsulated samples (Figure 5-19) in the range of 3500-3200 cm^{-1}, making it harder to distinguish between the two bonds

as they have overlapping infrared transmittance absorbance. However, the bimodal nature of the first peak, suggests the presence of primary amines rather than the hydroxyl group. The N-H bond stretch transmittance in the range of 3250 cm^{-1} to 3650 cm^{-1} decreases after encapsulation, which is suggesting a reduction in the free AMP due to polymerisation reaction between the amine and shell material (96). This reduction in AMP is not favourable because it would significantly affect the CO_2 absorption as less AMP is available to react with CO_2 to form carbamate ions. However, the most likely reason for the reduced peaks compared to the pure liquid AMP is due to a lower amount of the encapsulated adsorbent. Though there is the possibility of in-situ polymerisation of the amine group from AMP (97), amine and the hydroxyl group (-OH) both have the same probability of providing the required hydrogen for the formation of the shell material. However, this theory can be discarded due to the CO_2 absorption results acquired.

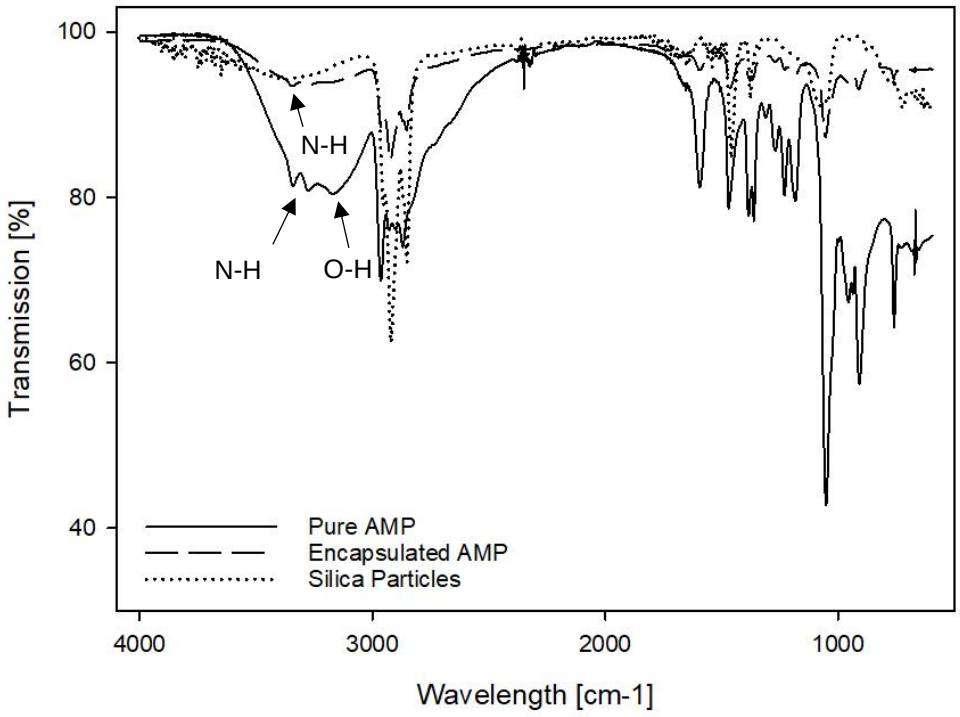

Figure 5-19 FTIR spectra of pure AMP, encapsulated AMP (PGPR, Span85, Tween80 emulsifiers and 6:4 core-shell ratio) and silica particles.

By comparing the silica particles to the encapsulated sample, it can be observed that the absorption spectra of AMP bonds in sample overlap with that of the bonds from pure AMP (Figure 5-19), making it harder to understand the chemical composition of the encapsulated sample.

In contrast, pure MEA showed a similar spectrum graph to AMP when it is compared to the encapsulated MEA with pure MEA showing the typical absorption peaks for O-H and N-H, whereas the N-H bond for encapsulated MEA has a very small transmission (Figure 5-20). In comparison, the N-H bond is not distinguishable from the O-H bond in TEA due to the higher quantity of ethanol being present in the amine compound, i.e. three ethanol groups are attached to the amine (Figure 5-21).

Investigating the effect of core-shell ratio on the chemical composition, it can be observed that the higher the core ratio is, the higher the transmission for the N-H bond due to more amine being present in the sample. However, both 7:3 and 8:2 ratio show a similar transmission spectrum (Figure 5-22), indicating that both have the same quantity of amine present in the formulated sample which can be verified with the payload results.

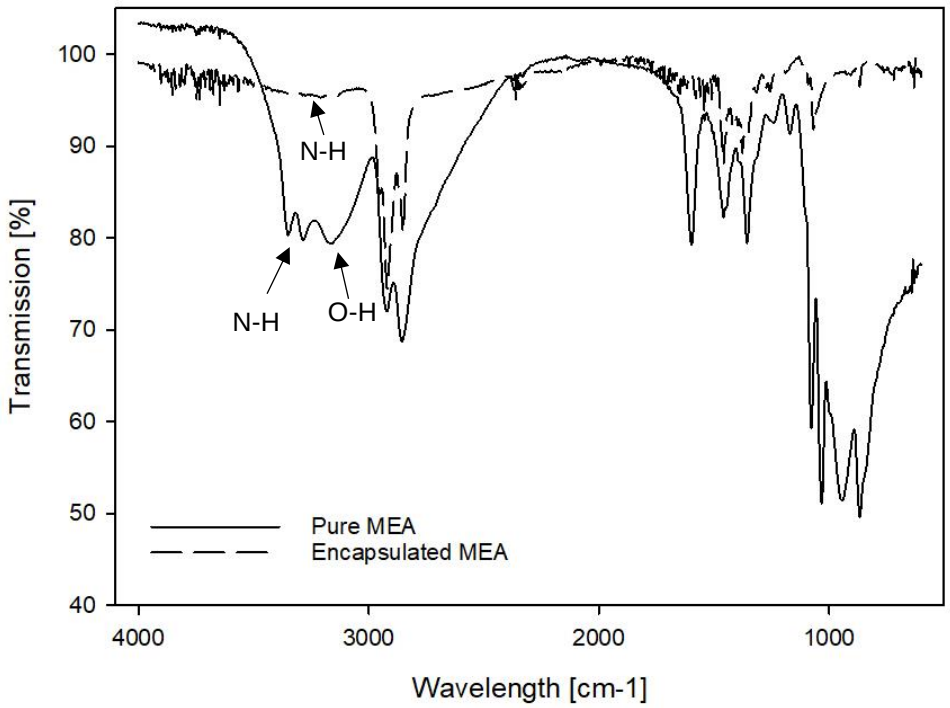

Figure 5-20 FTIR spectra of pure MEA and encapsulated MEA (1 wt% Span85, 6:4 core-shell ratio, 400 rpm mechanical stirrer speed and 1200 rpm homogeniser speed).

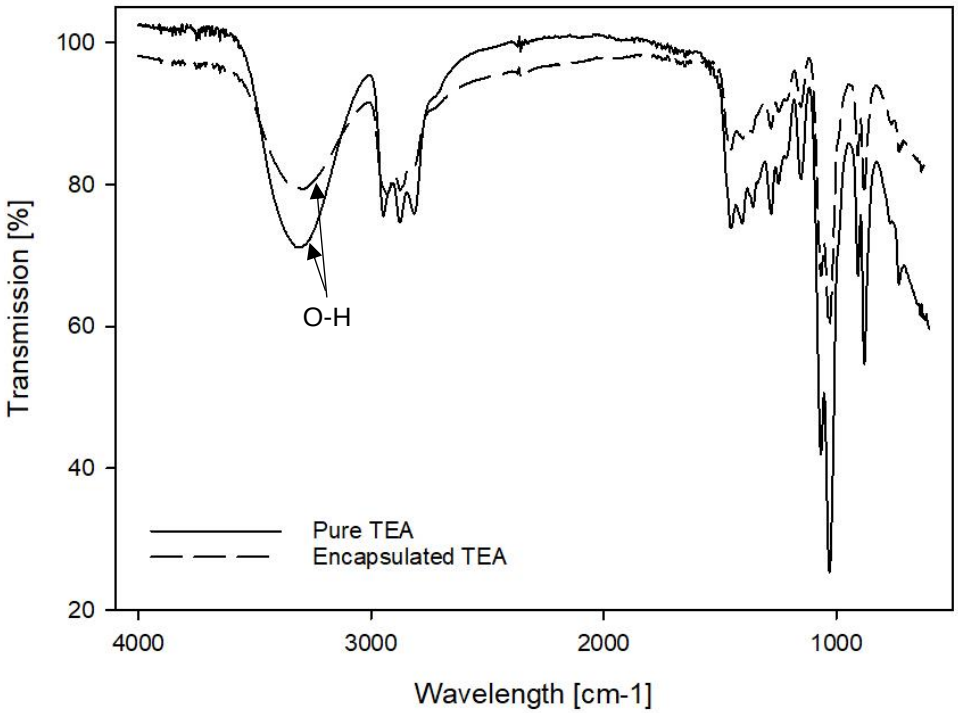

Figure 5-21 FTIR spectra of pure TEA and encapsulated TEA (1 wt% Span85, 6:4 core-shell ratio, 400 rpm mechanical stirrer speed and 1200 rpm homogeniser speed).

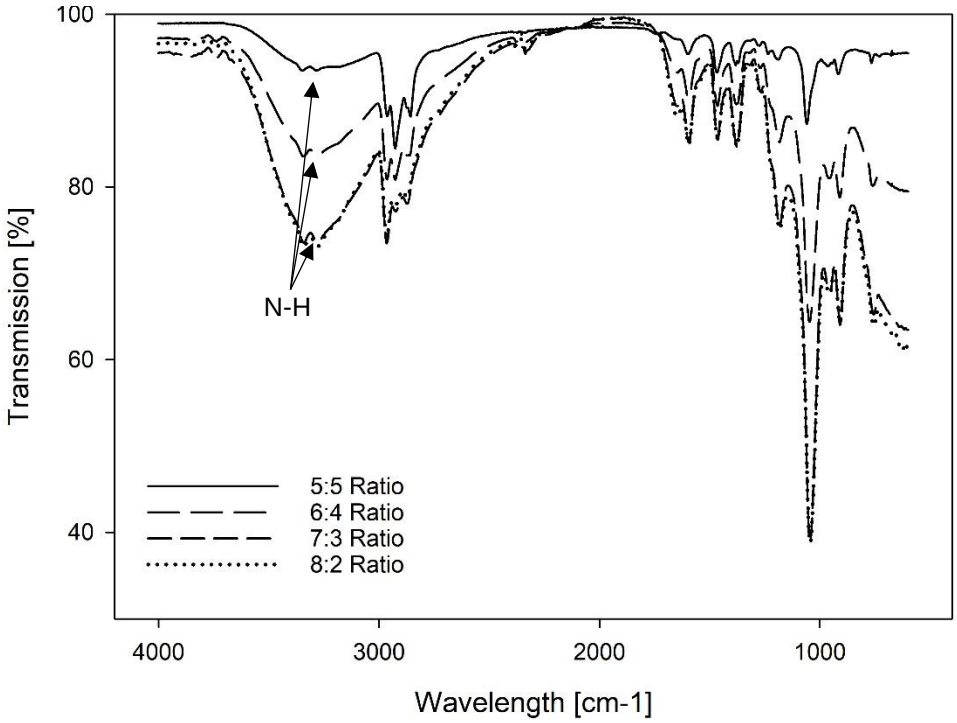

Figure 5-22 FTIR spectra of encapsulated samples with different core-shell ratios (1 wt% Span85, 400 rpm mechanical stirrer speed and 1200 rpm homogeniser speed).

This issue of overlapping bonds (with silica particles) and core material sensitivity (different core-shell ratio samples) occurred due to the used FTIR transmission sampling technique. Most commercially available cell spacers are 6 μm in thickness which gives an absorbance of 3 units, leading to the linearity of the detector being corrupted which in turn gives not completely useful information in the region of 2800 cm^{-1} to 3700 cm^{-1}. The bands in the aforementioned region tend to overlap with more intense and broader bond stretching like the overlapping of O-H stretching with N-H stretching, hence making further exploitation more complicated since to the non-linear detector is unable to perform a good subtraction. Furthermore, the penetration of the laser into the sample might not be deep enough considering the size of the microcapsules and silica particles. The attenuated total reflection (ATR), an FTIR technique, would be an alternative solution to the described problem which has a better

penetration depth as the light is totally reflected internally, leading to the interaction of the sample with the evanescent wave. This small light penetration of the ATR technique has been described as ideal for absorbing samples, surfaces and thin films (98). However, the school of engineering was not in possession of an FTIR that had the ATR mode and thus, measurements with ATR were not possible to be conducted.

5.2.2 Structural Properties

5.2.2.1 Shell thickness

Initially, to identify the shell thickness of the microencapsulated sample, microcapsules were embedded into a resin where the resin containing the sample is observed under an SEM. But due to poor contrast between the resin and embedded capsules, it was not possible to identify the shell thickness of the sample. This is likely because of the polishing of the surface with sandpapers. No instruments were available to cut the resin, hence the need to polish the surface to look at the embedded sample. However, the polishing not only made it hard to distinguish the microcapsules from the resin but also modified the surface at the same.

An alternative technique was tried to identify the shell thickness by freezing the microcapsules with liquid N_2 in a mortar. This allows the sample to instantly freeze, hardening the sample to make it easier to crush with a mortar. After crushing the particles, the sample is mounted onto a stub for shell thickness observation in an SEM. The process seems easy and straightforward, but it is challenging to identify the shell when the structure of the microcapsule is a matrix. Additionally, the crushing of microcapsules produced high debris, i.e. a lot of small particles, further making it harder to recognise the shell. Hence only the shell thickness of three different samples were

able to be measured which can be seen in Figure 5-23. It can be observed that the used formulation method produced microcapsule with uneven shell thickness across the diameter. Sample created with 0.5 wt% PGPR showed a shell thickness of 3.3 – 7.6 μm, whereas sample created with 1 wt% Tween80 had a shell thickness of 14.9 – 20.1 μm and sample 1 wt% Span85 showed a shell thickness of 6.2 – 7.2 μm (the shell thickness of the microcapsules is measured at point A and B by applying image analysis, ImageJ). This implies that the wall of the microcapsules is uneven. However, these shell thickness values are just an indication as the experiment was not reproducible, hence the actual thickness might be different if an average were to be taken from the formulated sample.

Generally, a thinner shell is preferred due to the faster CO_2 kinetics it will provide. However, due to the *in-situ* polymerisation used during polymerisation, the shell thickness is limited due to the formation of a matrix. Unless the method and/or the shell is changed to produce a core-shell type of microcapsule, the thickness can not be varied much by changing the surfactant. The surfactant only helps stabilise the emulsion phase, from section 4.2.2 it was concluded that 1 wt% Span85 had the best properties for the emulsion, hence the sample showed a more uniform shell thickness, however, overall the shell is thicker compared to sample 0.5 wt% PGPR. This might be due to the higher the interfacial tension, hence the quicker the shell deposit, the larger the thickness of the shell at end of formulation. This hypothesis is supported by sample 1 wt% Tween80 as it has the highest shell thickness with 15 – 20 μm (99).

To obtain a better understanding of the shell thickness or internal structure of the formulated sample, it is proposed to use a CryoTEM where the microcapsules are frozen before being sliced and observed under a TEM. This would allow different sliced

sections to be examined to give an average shell thickness for better analysis. Additionally, after obtaining an average, the wall thickness can be compared with the model developed by Liu M. (92) to find correlations and explanations on whether all the precondensate was used during the formulation by using the core-shell ratios (92).

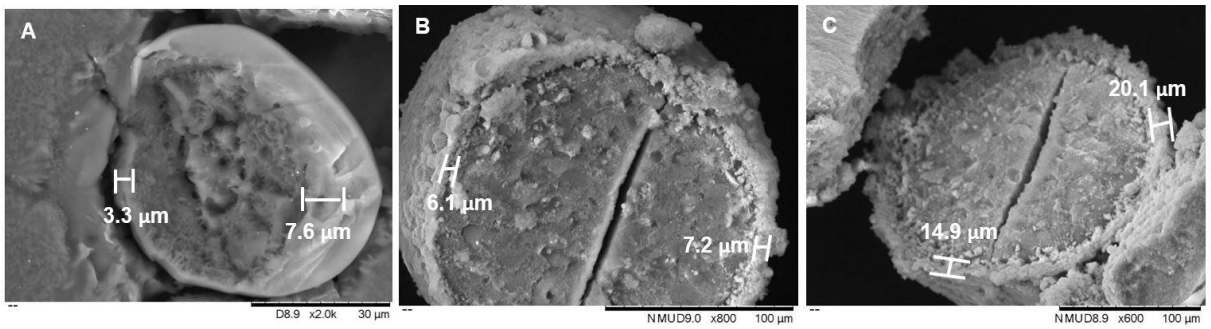

Figure 5-23 SEM Image showing the shell thickness of different samples: A) 0.5 wt% PGPR; B) 1 wt% Span85; C) 1 wt% Tween80 (TM3030Plus).

5.2.2.2 Microcapsule Surface Properties

During the microencapsulation process, the formulating parameters were varied to observe its effect microencapsulation. The core-shell ratio does not affect the surface properties; hence those samples are not tested inside the BET for SA measurements. However, the stirring speed affects the size and morphology, thus samples formulated with different mechanical stirrers and homogenisers are tested. Similarly, emulsifiers influence the surface characteristics, i.e. roughness of microcapsule surface, hence the need to examine samples formulated with different emulsifiers. Additionally, samples formulated with different core materials were also tested in the BET as those samples will be required and tested inside the continuous reactor for CO_2 loading capacity. Surface area (SA) and pore size are both important physical properties that impact the absorption capacity of the microcapsules. The difference in the porosity and SA of particles with otherwise same physical dimension greatly influences the sample characteristics.

Overall, the pores of the encapsulated samples can be classified as mesoporous in size (20-500 Å) (54).

Effect of stirring speed. During the formulation, different stirring speeds are used to produce microcapsules, where each speed produces different sized particle and hence gives each sample a different surface area. Higher stirring speed produces microcapsules with a smaller surface area but with larger pore size. A larger SA is more beneficial due to it providing better contact for gas to diffuse into, thus enhancing the absorption properties. A good understanding of SA and particle size can assist in the formulation process but also have an impact on the quality and the utilization of the solid phase (100).

Even though all three samples have mesopores (20-500 Å) (54), the samples differ in their specific surface area (SA), where 400 rpm sample had the highest particle SA with 92 m^2/g, whereas 100 rpm sample had the lowest with 29 m^2/g. The SA of a sample is depended on the pore size as well as pore volume. Particles with smaller pores tend to have larger SA but also tend to have a higher number of pores, e.g. 400 rpm sample showed the highest SA (92 m^2/g) and highest pore volume (0.097 cm^2/g) with the lowest average pore size (43 Å) (Table 5-1). It must be kept in mind that during the BET adsorption the material surface is assumed to be homogeneous while the adsorption is equal across the entire surface. However, the samples formulated contained agglomeration, suggesting that both inter and intra pore volume cannot be differentiated from each other. In this case, the agglomeration seems to decrease the surface area of a sample due to particles most likely covering the pores on the capsule surface and thus, decreasing the pore volume (54). This is the case with 600 rpm sample as it showed a lower SA than 400 rpm sample with 34 m^2/g due to higher

agglomeration presence even with a smaller average particle size of 20 μm compared to 105 μm (54).

Table 5-1 Microcapsule surface properties of sample formulated with 0.5 wt% PGPR, 6:4 core-shell ratio and varying mechanical stirring speeds (100 rpm - 600 rpm). The values in the table are the average of three testing's and the pore Ssze values are the BJH adsorption average pore size diameter.

Sample	BET Surface Area [m²/g]	Pore Volume [cm³/g]	Pore Size [Å]
100 rpm	29 ± 3	0.051 ± 0.005	71 ± 5
400 rpm	92 ± 7	0.097 ± 0.01	43 ± 3
600 rpm	34 ± 4	0.061 ± 0.009	72 ± 6

Effect of emulsifier. A change in the emulsifier, gave a slight change in the surface roughness of the microcapsules as can be observed from the SEM images (4.2.2.1). This change in surface property is reflected by the different SA, pore size and pore volume of the formulated samples. By changing the emulsifier from PGPR to Span85, the SA of the microcapsule decreased to 45 m²/g (Table 5-2), whereas when Tween80 is used the obtained SA is the smallest with 20 m²/g. Similarly, the pore volume and pore size also declined with 1 wt% Tween80 showing the smallest pore size (14 Å) and 1 wt% Span85 gave the smallest pore volume (0.07 m²/g). This is related to their microcapsule size. On average smaller microcapsules were produced with 0.5 wt% PGPR (~100 μm) compared to the other two emulsifiers. Larger capsules with smaller pore size and pore volume tend to have a smaller SA (54).

Table 5-2 Microcapsule surface properties of sample formulated with 6:4 core-shell ratio, 400 rpm mechanical stirrer speed and varying emulsifiers (PGPR, Span85, Tween80). The values in the table are the average of three testing's and the pore size values are the BJH adsorption average pore size diameter.

Sample	BET Surface Area [m²/g]	Pore Volume [cm³/g]	Pore Size [Å]
0.5 wt% PGPR	92 ± 7	0.097 ± 0.01	43 ± 3
1 wt% Span85	45 ± 5	0.07 ± 0.008	19 ± 3
1 wt% Tween80	20 ± 4	0.019 ± 0.012	14 ± 2

Effect of the homogeniser. An increase in mechanical stirrer speed from 400 rpm to 800 rpm lead to an increase in the SA and gave larger pores (66 m^2/g and 85 Å). However, a decrease in homogeniser speeds led to a decrease in both SA and pore size (40 m^2/g and 65 Å) but an increase in homogeniser speed from 600 rpm to 12000 rpm led to an increase in the SA and pore size (52 m^2/g and 93 Å). This differences in SA and pore size occurred due to the change in stirring speeds. Generally a higher stirring speed whether mechanical or homogeniser leads to higher collision of both the core material and hydrolysed TEOS which gives a rougher surface with larger pores (54).

Table 5-3 Microcapsule surface properties of sample formulated with 1 wt% Span85 and 6:4 core-shell ratio and varying homogeniser and mechanical stirrer speeds (* mechanical stirrer speed; ** homogeniser speed). The values in the table are the average of three testing's and the pore size values are the BJH adsorption average pore size diameter.

Sample	BET Surface Area [m^2/g]	Pore Volume [cm^3/g]	Pore Size [Å]
1 wt% Span85 800 rpm*	66 ± 6	0.078 ± 0.01	85 ± 3
1 wt% Span85 400 rpm* 600 rpm**	40 ± 8	0.032 ± 0.013	65 ± 7
1 wt% Span85 400 rpm* 2000 rpm**	52 ± 5	0.116 ± 0.05	93 ± 5

Effect of the core material. A change in core material not only changes the morphology of the microcapsules but also changes the surface properties. As already seen from the SEM images (4.2.2), encapsulated MEA resulted in a rougher surface finish which is reflected by a high SA, however the pore size and pore volume are smaller than that of pure AMP encapsulated with 0.07 m^2/g and 19 Å. This suggests that most of the pores are situated at the surface of the particles, whereas fewer pores are found inside the particle itself. In contrast, 30% TEA encapsulated sample presented the lowest SA and pore size with 20 m^2/g and 9 Å respectively (Table 5-4)

due to the very high density of the core material obstructing the formulation process. The heavier and viscous (914 mPa.s) the core material the less likely it is going to be encapsulated and will more likely descend to the bottom of the system (81).

In comparison to the encapsulated sample, silica particle had a smaller particle SA (40 m^2/g) than both AMP and MEA encapsulated sample, though the pore size, in contrast, is very low (10 Å). Without a core material the size of the silica particles is lowered, hence a higher particles SA. Moreover, without a core material, the hydrolysed silica particles are more likely to collide with each other, leading to more polymerisation, thus smaller pore size (67).

Table 5-4 Microcapsule surface properties of sample formulated with 1 wt% Span85 and 6:4 core-shell ratio and varying core materials, as well as silica particles. The values in the table are the average of three testing's and the pore size values are the BJH adsorption average pore size diameter.

Sample	BET Surface Area [m^2/g]	Pore Volume [cm^3/g]	Pore Size [Å]
100% AMP encapsulated	92 ± 7	0.097 ± 0.01	43 ± 3
100% MEA encapsulated	81 ± 8	0.07 ± 0.009	19 ± 6
30% TEA encapsulated	20 ± 5	0.019 ± 0.007	9 ± 3
Silica Particles	40 ± 10	0.006 ± 0.001	10 ± 2

5.2.2.3 Payload

To further understand the encapsulation process and to estimate the amount of core material inside the sample, the payload is obtained with the help of TG analysis.

Effect of size. Figure 5-24 shows the payload of the individual samples. It can be seen from the figure that all samples exhibited similar payload (70-78%). The sample produced with 400 rpm – 1200 rpm showed a payload of 74% even though the sample had a less polydispersed size distribution compared to the other samples.

However, bigger particles are expected to have higher amounts of core material encapsulated though 100 rpm sample being the largest sized capsules (140 μm) did

have the highest payload (78%) even if it is not that much higher than that of the other samples.

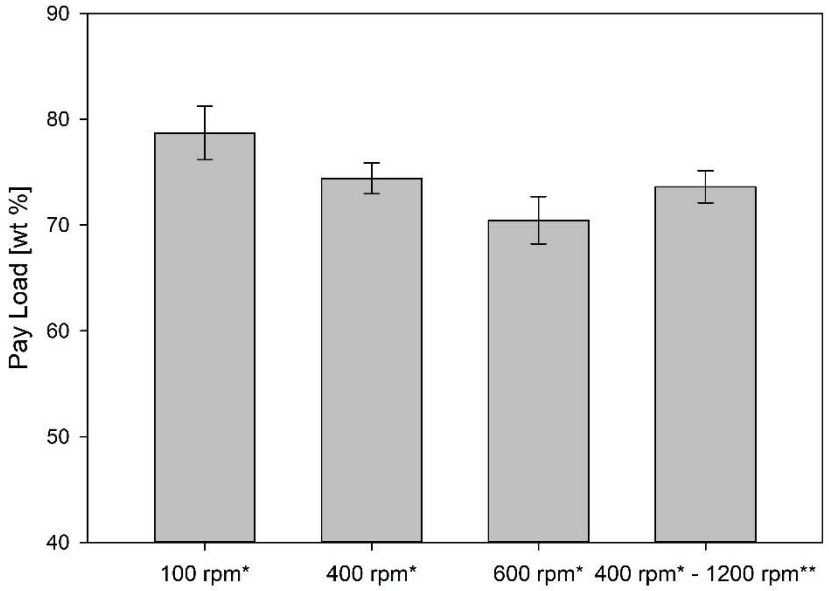

Figure 5-24 Payload of samples produced with varying stirring speeds (0.5 wt% PGPR, AMP core and 6:4 core-shell ratio). * mechanical stirrer speed; ** homogeniser speed

Samples 2000 – 400, 600 – 600 and 600 showed a very similar payload of ~69%, whereas the sample 1200 – 400 showed the highest payload with 79% (Figure 5-25). Thus, a change in mechanical stirrer or homogeniser speed does not have a high impact on the payload. This is due to the similar size distribution of the formulated samples. All showed an average size of 400 μm and a size range of 100 μm – 1000 μm which means all the samples were able to capture the same amount of core material.

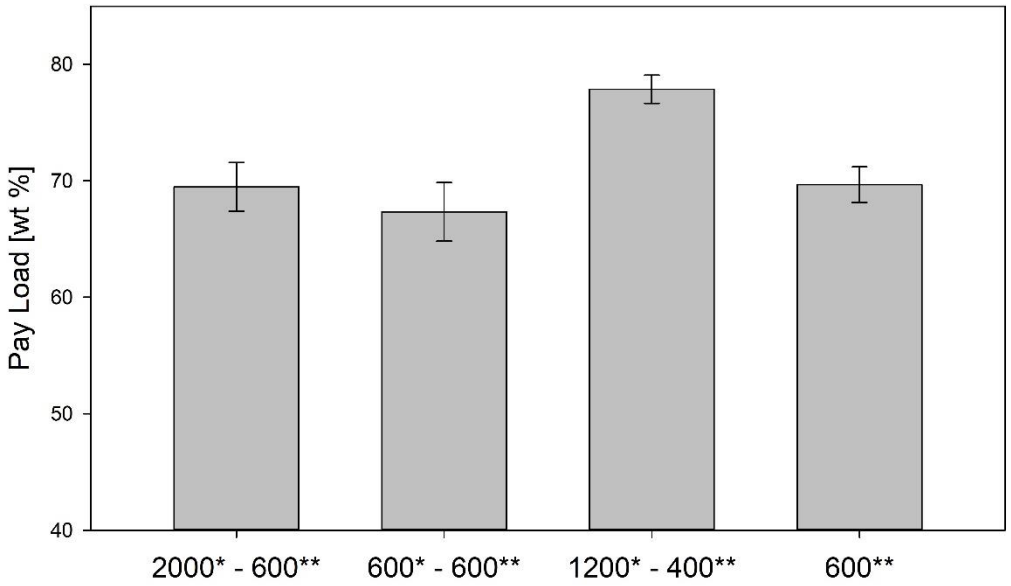

Figure 5-25 Payload of sample produced with varying stirring speeds (1 wt% Span85, AMP core and 6:4 core-shell ratio). * mechanical stirrer speed; ** homogeniser speed

Effect of emulsifier concentration. As can be seen from Figure 5-26 to Figure 5-29, a change in emulsifier concentration does not affect the payload of the samples even though the different samples had varying size distribution. A sample with a larger size is suspected to have a higher payload which would normally be the case for a typical core-shell type of microcapsules. However, from the SEM images it was concluded that the formulated microcapsules have a matrix structure, i.e. the particles contain multiple smaller core droplets. Hence, the payload is dependent on the amount of the core droplets inside the capsules. Moreover, the agglomeration of the sample needs to be considered. The agglomeration inside the sample is caused by the core material that was not able to be encapsulated and polymeric silica species that were not removed during the washing process. Hence, the payload just gives an indication of the core material inside the sample and should not be confused with an encapsulation efficiency (EE) since EE gives the core amount encapsulated inside the capsules (36).

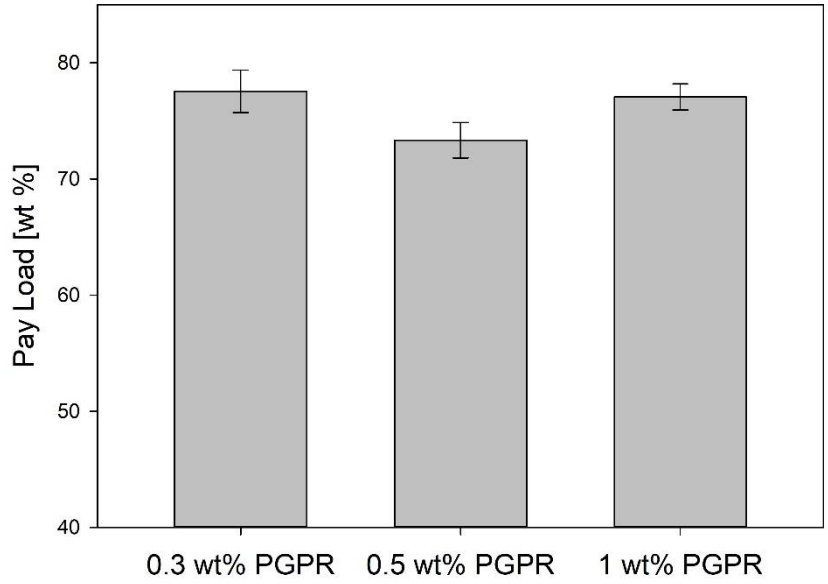

Figure 5-26 Payload of sample produced with varying PGPR concentrations (AMP core, 6:4 core-shell ratio, 400 rpm mechanical stirrer speed and 1200 rpm homogeniser speed).

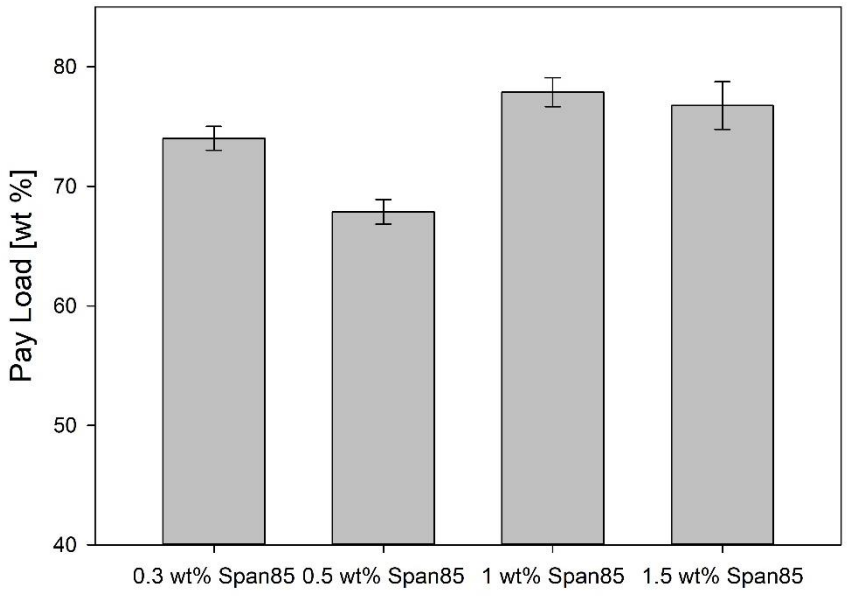

Figure 5-27 Payload of sample produced with varying Span85 concentrations (AMP core, 6:4 core-shell ratio, 400 rpm mechanical stirrer speed and 1200 rpm homogeniser speed).

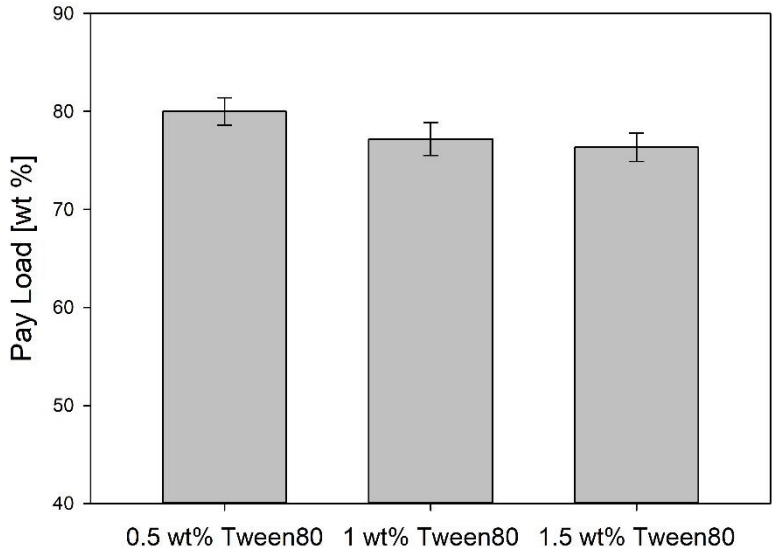

Figure 5-28 Payload of sample produced with varying Tween80 concentrations (AMP core, 6:4 core-shell ratio, 400 rpm mechanical stirrer speed and 1200 rpm homogeniser speed).

From Figure 5-29 it can be concluded that the same amount of core is found inside all the samples with varying emulsifier concentrations. Since all samples show similar payload, the microcapsules are compared in terms of their quality, hence 0.5 wt% PGPR, 1 wt% Span85 and 1 wt% Tween80 are chosen for the CO_2 absorption testing (Chapter 6).

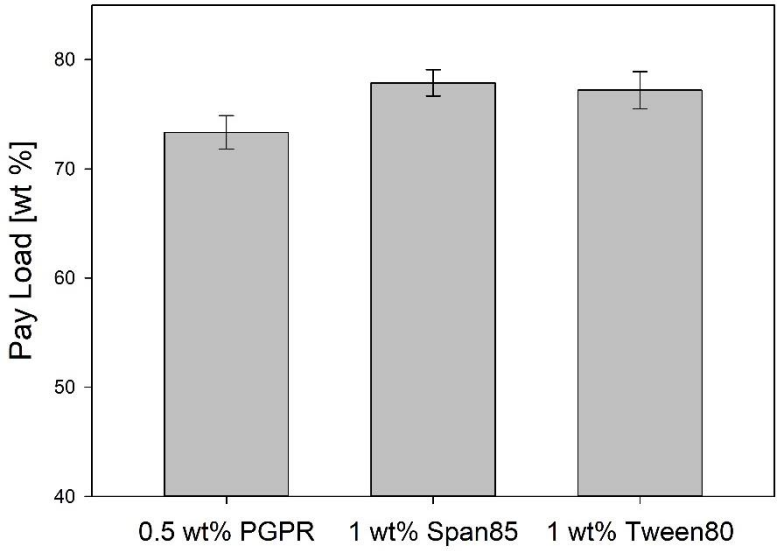

Figure 5-29 Payload of good quality samples from each emulsifier (AMP core, 6:4 core-shell ratio, 400 rpm mechanical stirrer speed and 1200 rpm homogeniser speed).

Effect of core-shell ratio. By increasing the core-shell ratio from 5:5 to 8:2, the core material concentration inside the emulsion phase is increased, thus more core is found inside the formulated sample, hence a higher payload. Even though samples with a 6:4 core-shell ratio produced larger microcapsules, their payload is lower than that of 8:2 ratio with 79% and 95% respectively which is due to the agglomeration and washing process explained earlier. Theoretically, a higher payload is preferred as it provides more core material, hence higher absorption capacity (Figure 5-30) (101). However, the quality of the 8:2 microcapsules are inferior to the 6:4 ratio microcapsules, thus 6:4 ratio samples are chosen for the CO_2 absorption testing in the continuous reactor (chapter 7).

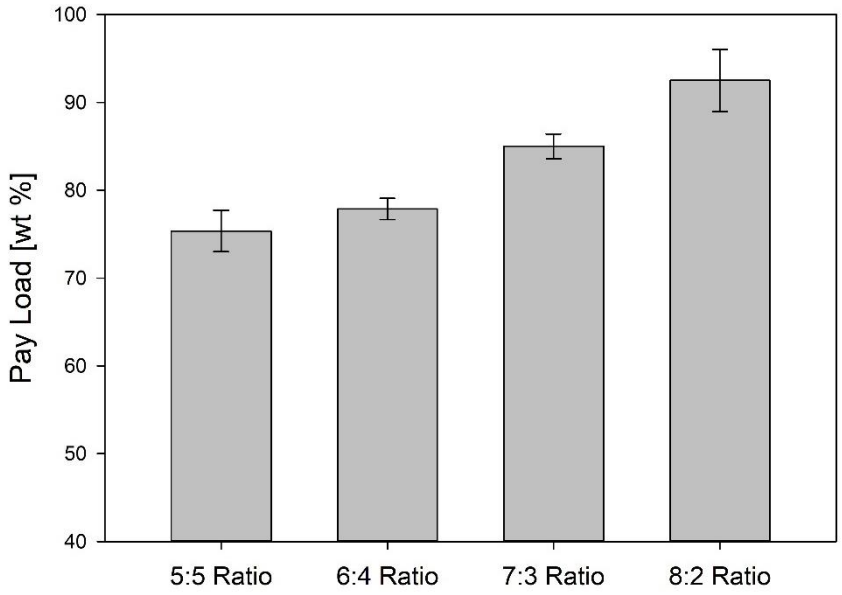

Figure 5-30 Payload of sample produced with 1 wt% Span85 and varying core-shell ratios (AMP core, 400 rpm mechanical stirrer speed and 1200 rpm homogeniser speed).

Effect of reaction time. A longer reaction time gave a higher payload (from 63% to 79%) allowing the reaction to formulate more microcapsules at the end of the process. The silica formation through hydrolysed TEOS followed by polycondensation is a slow process due to the low formulation temperature (64). This suggests that after 6 h, not all the core material was encapsulated, thus samples are formulated over a time span of 24 hrs showed a higher payload (Figure 5-31).

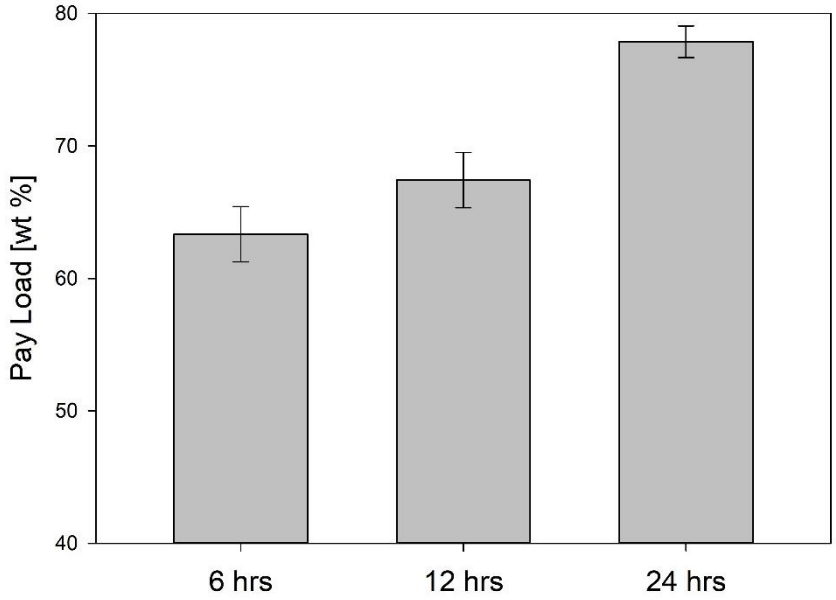

Figure 5-31 Payload of sample produced with varying reaction times (1 wt% Span85, AMP core, 6:4 core-shell ratio, 400 rpm mechanical stirrer speed and 1200 rpm homogeniser speed).

Comparison of the different core material. Changing the core material from AMP to MEA or TEA decreased the payload of the sample. AMP encapsulated sample showed a payload of 79%, while MEA encapsulated sample had a payload of 63% and encapsulated TEA had a payload of 55%. This is due to their differences in densities. As mentioned previously MEA has a lower density than AMP, whereas TEA has a very high density. In both cases the difference in their densities compared to the mineral oil hinders the formulation process, leading to less core material being found inside sample at the end of the formulation process (102).

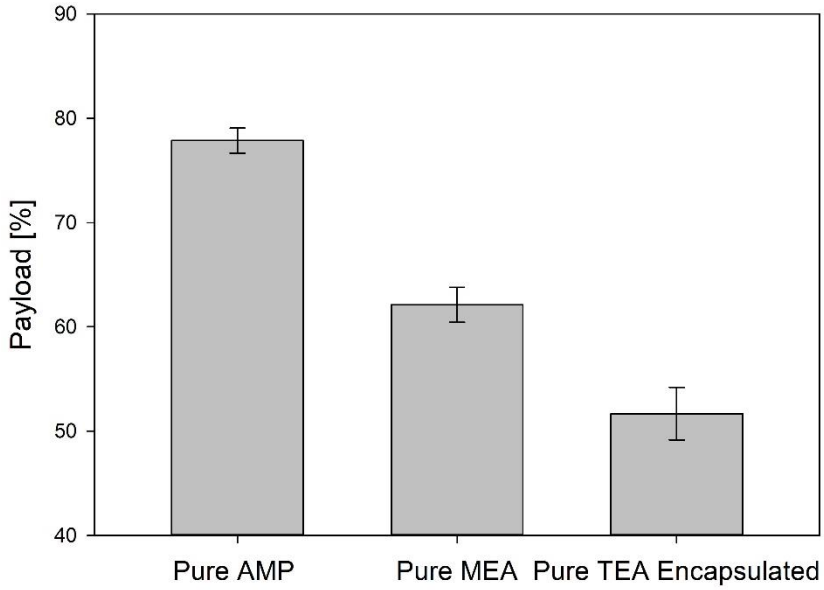

Figure 5-32 Payload of sample produced with varying core material (1 wt% Span85, 6:4 core-shell ratio, 400 rpm mechanical stirrer speed and 1200 rpm homogeniser speed).

5.2.3 Initial Absorption Capacity testing

5.2.3.1 CO_2 absorption capability

To prove that the formulated sample can absorb carbon dioxide, a TG was connected to a carbon dioxide cylinder. Figure 5-33 shows the CO_2 absorption test result.

From the graph, it can be concluded that the sample is able to capture CO_2 as the mass of the sample increased when it was exposed to CO_2. Additionally, the samples were exposed to nitrogen as well to confirm that the capsules only capture carbon dioxide and no other gas as the weight of the sample did not change when the samples were exposed to nitrogen gas.

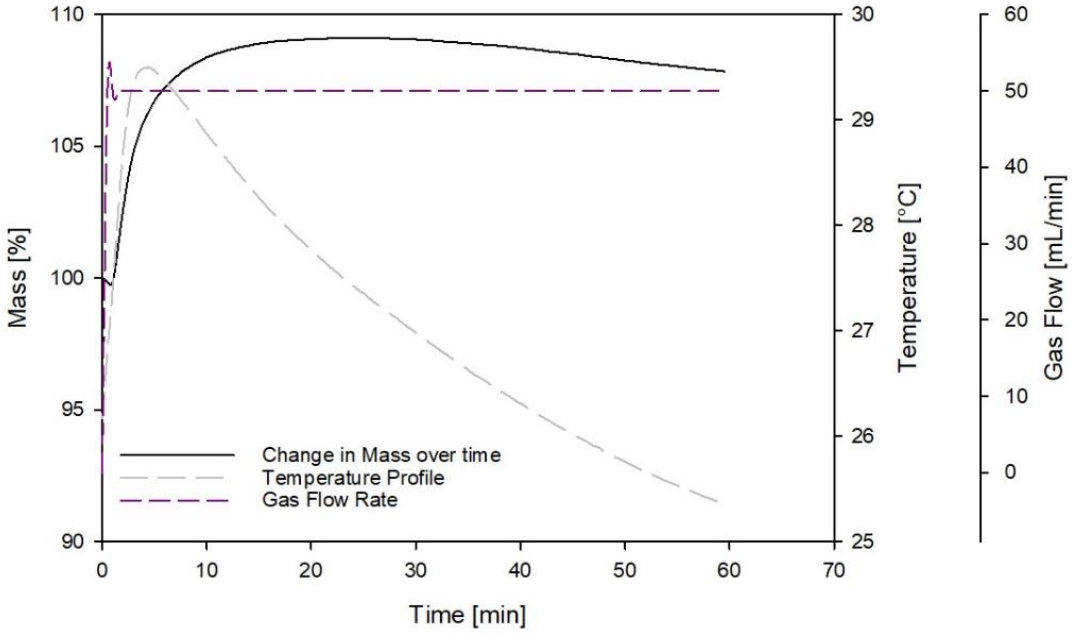

Figure 5-33 Mass change of sample while exposed to 20 °C and a flow of 50 mL/min CO_2.

Moreover, samples exposed to CO_2 undergo a colour change from blue to yellow which is shown in Figure 5-34. This colour change suggests carbamate formation (32,103) and thus provides evidence of successful CO_2 absorption by the samples. The change in colour occurs due to the presence of Thymol Blue inside the microcapsules. This method of visual CO_2 absorption has also been used by Vericella et al. (104) where sample colour changed when up to ~90% of maximum carbon uptake reached. This visible colour enables qualitative evaluation of the CO_2 absorption and desorption capacity of microcapsules. The pH of the sample before testing is >10 due to the high alkalinity of AMP but drops to <6 after the absorption as carbamate ions are formed while hydrogen ions are released (103). This chemical absorption process is a widely known method and is under consideration for an industrial-scale CO_2 capture system (105).

However, this TG set-up is not temperature sensitive enough to test the effect of temperature on the absorption capacity of the samples. The system is not completely

closed off and the temperature control is abysmal especially for low temperature hence making it unsuitable for CO_2 capture testing not only at room temperature but also at low temperatures like -60°C. To this end, a pressure rig and a continuous reactor were set-up to identify the effect of size (SA), core material and emulsifiers on the absorption capacity of the formulated samples. In the following chapters the theoretical CO_2 uptake will be considered as the benchmark which will be estimated from the payload, i.e. the core material mass inside the sample, and the literature value for the individual amine materials.

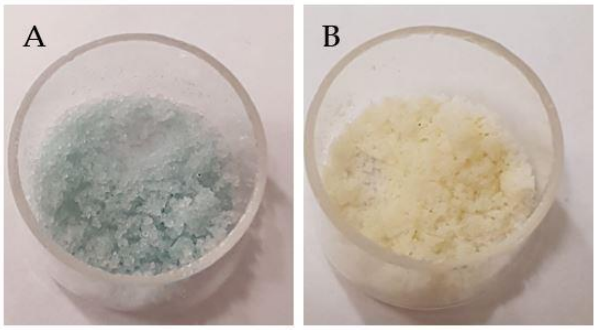

Figure 5-34 Colour change from blue (A) to yellow (B) after CO_2 exposure.

5.3 Conclusions

The formulated microcapsules showed no phase change in the temperature range of 20 °C to -60 °C despite the pure core materials displaying melting and freezing indicating that these microcapsules are stable over the tested temperature range. A phase change is disadvantageous as it may lead to a decrease in the CO_2 sorption capability. These microcapsule were also exposed to thermal cycling which showed that microcapsules formulated with mechanical stirring speeds higher and lower than 400 rpm had weaker shells and hence more susceptible to thermal damage (88).

The different size range occurred due to the created force by the impeller not being even across the emulsion system. A higher stirring speed results in more collisions of the core droplet which leads to high agglomeration to be seen in the final product, hence highest agglomeration was seen with sample formulated with 600 rpm (91). Therefore, homogenisers were used to control the size distribution by trying to reduce the droplet size in a liquid-liquid dispersion by disrupting the core droplet formation inside the emulsion (92). Thus, a less polydispersed particle size distribution was seen with sample formulated with a homogeniser.

The stirring and homogenisation speeds not only affected the size distribution but also the SA where higher stirring speeds gave microcapsules smaller SA with larger pore size which is advantageous as it provides a better contact for gas to diffuse into, thus enhancing the absorption properties (100). However, by changing the emulsifier from PGPR to Span85, the SA of the microcapsule decreased to 45 m^2/g, whereas when Tween80 is used the obtained SA is the smallest with 20 m^2/g. In contrast, a higher core material concentration, i.e. 8:2 core-shell ratio led to rougher surface finish which is reflected by a high SA, however the pore size and pore volume are smaller than that of pure AMP encapsulated with 0.07 m^2/g and 19 Å.

For the payload results, it can be concluded that a similar amount of core is found inside all the samples with varying emulsifier concentrations as all samples showed similar payload values (70 - 80%). By changing the core material from AMP to either MEA or TEA, the payload decreased from 70% to 63% and 55% respectively as the higher densities of the two material hindered the formulation process (102).

It can be concluded that the relationship between the different formulation parameters is not straight forward and it is not easy to predict how the different parameters will

affect the microcapsule properties as the encapsulation process is very delicate but from the work presented some guidelines can be given which are found in Table 5-5.

Table 5-5 Brief summary of the effect of formulation parameters on the microcapsule properties.

Formulation Parameter	Effect on Microcapsules
Mechanical stirrer speed ↑	Particle size ↑
homogenisation speed ↑/↓	No effect of particle size
Emulsifier concentration ↑	Particle size slight ↓
Core concentration ↑ with 0.5 wt% PGPR	Particle size ↑
Emulsifier concentration ↑	Very small change in payload
Core concentration ↑	Payload ↑
Reaction time ↑	Payload ↑
AMP core change to TEA core	Payload ↓

Chapter 6 CO_2 Absorption Analysis using Manometric Method

6.1 Introduction

As mentioned in the previous chapter, the formulated samples exposed to CO_2 undergo a colour change from blue to yellow. This colour change suggests carbamate formation (32,103) and provides evidence of successful CO_2 absorption by the samples (Figure 6-1). The change in colour occurs due to the presence of Thymol Blue inside the microcapsules. This method of visual CO_2 absorption has also been used by Vericella et al. (104) where sample colour changed when up to ~90% of maximum carbon uptake reached. This visible colour enables qualitative evaluation of the CO_2 absorption and desorption capacity of microcapsules. The pH of the sample before testing is > 10 due to high alkalinity of AMP but drops to < 6 after the absorption as carbamate ions are formed while hydrogen ions are released (103). This chemical absorption process is a widely known method and is under consideration for an industrial-scale CO_2 capture system (105). Moreover, this carbamate reaction is reversible with heat. This thermal regeneration heat requirement is dependent on the energy required to break the bonds that were created during the CO_2 absorption - the lower the required energy, the lower the energy-intensive CO_2 release process (30,105). In our case when the microcapsules are heated up to 40 °C slightly higher than the melting point, the colour changes back to light blue, suggesting the release of CO_2. In comparison, aqueous amine scrubbing (120 °C) (106), a mature CO_2 absorption process, is known to be by far more energy-intensive where it can take up ≥ 80% of the energy cost. A CO_2 release at a lower temperature would require less energy for the CO_2 release, thus reduce the energy cost of the CO_2 absorption process (104).

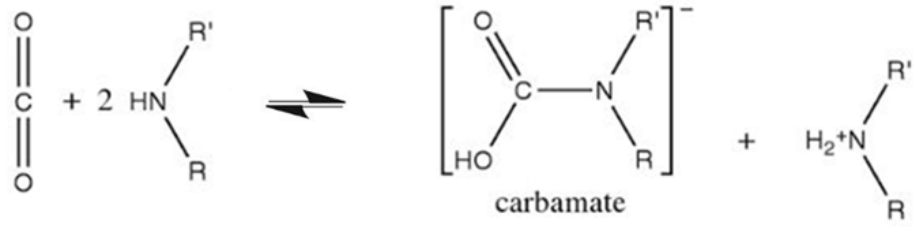

Figure 6-1 Simplified chemical reaction of amine-based adsorbent with carbon dioxide to form carbamate ions (26).

In the previous two chapters, the formulation and characterisation of microcapsule with various process parameters were described. In this chapter, the absorption capacities of the formulated microcapsules were studied to relate the microcapsule properties to their loading capacity. To this end, a pressure rig based on the manometric method is a set-up for CO_2 absorption testing.

From the wide range formulated samples, certain parameters were selected to be tested inside the pressure rig: 1) size; 2) encapsulated core compared to pure, liquid core 2) different emulsifier; 3) core-shell ratio; 4) different core materials; 5) effect of temperature. The individual absorption capacities of each sample are tested by exposing the microcapsules to 10 barA of CO_2.

6.2 Result and Discussion

6.2.1 CO_2 Absorption

To analyse the type of reaction happening during CO_2 absorption, the temperature curve of both sample and control is studied while the rig is pressurised with 10 bar. The control in this case refers to the chamber being pressurised without any sample to observe the drop in pressure over time in the empty chamber to get a baseline. In Figure 6-2 an increase in temperature is observed for both sample and control during the absorption tests after rig chamber is pressurised. A second smaller temperature

increase of 0.5 °C is observed only with the sample after the initial temperature drop. For both (sample and control), the temperature and pressure stabilised over time, indicating that the CO_2 absorption and thus the carbamate formation is of exothermic nature.

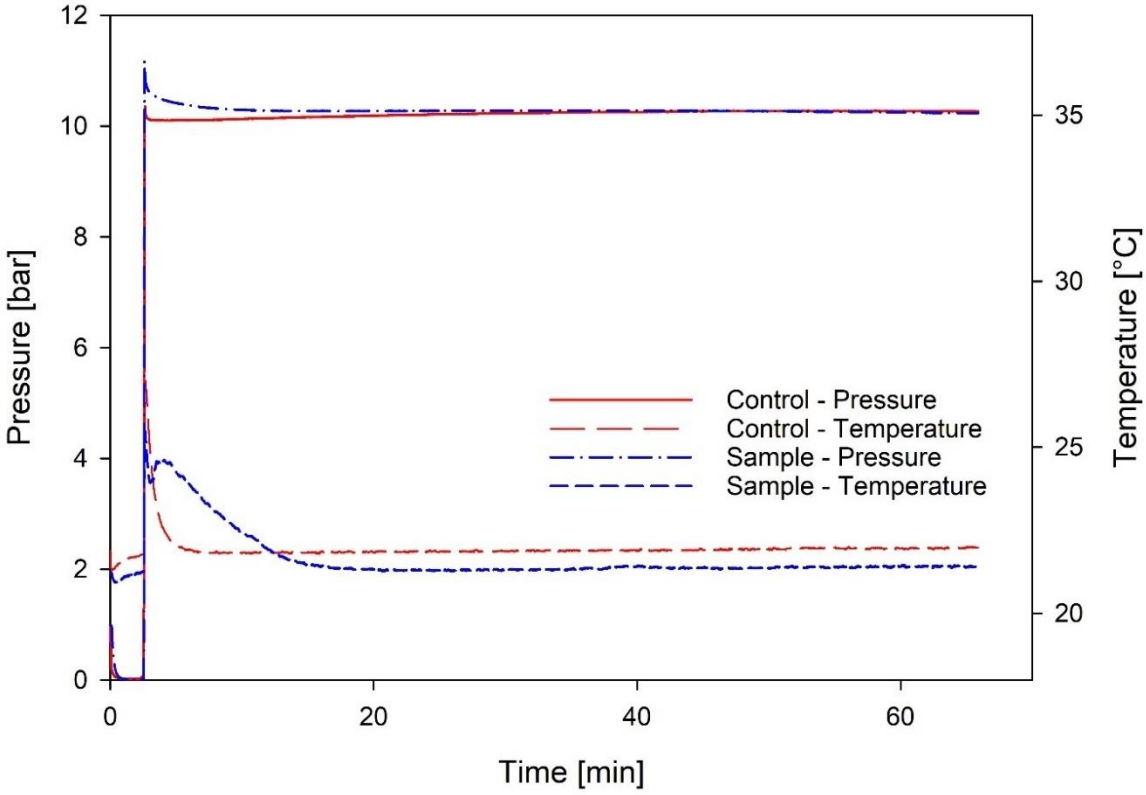

Figure 6-2 Pressure behaviour comparison of control and 400 rpm sample exposed to CO_2. For sample the pressure stabilises after 2h, whereas the pressure stabilised for control in 20 min.

As soon the chamber is pressurised the sample starts to absorb the CO_2. This fact, however, is negligible for the pressure to CO_2 absorption conversion as it only takes 1-2 minutes for the pressure to settle down. Furthermore, this method relies on the pressure stabilisation after initial pressure introduction into the chamber for the absorption conversion which is related to the temperature. Temperature increased because the vessel become pressurised as both influences each other. A temperature

increase can lead to an increase in pressure and vice versa. This necessitates the wait for temperature stabilisation before absorption can be measured.

To validate the calculated CO_2 absorption capacity of the samples at the end of an experiment, each sample is weighed before and after CO_2 absorption and the two values are compared. Only if the calculation values are within 5% error margin of the physical weight measure is the calculation accepted and used for comparison. The absorbed CO_2 by the sample is measured by converting the pressure drop into the density of CO_2 at the tested temperature with the reduced state of PREoS, thus allowing the calculation of the absorbed CO_2 mass by the sample. This weight gain is attributed to the CO_2 absorption by the sample due to the pressure drop over time. As the system is completely sealed off and no leakage is occurring, the sample absorbs CO_2 and hence leads to a drop in the pressure. This absorption capacity is calculated with ambient pressure and 20 °C to -60 °C and its reduced form (see 3.5.1). An example for the CO_2 absorption calculation is provided below for easier understanding of the calculation at 20°C.

1) Density of CO_2 is obtained from the Chemical Engineering's guide excel spreadsheet which uses the reduced state of PREoS:

CO_2 density at start of experiment (10 bar) = 19.2 kg/m^3

CO_2 density at end of experiment (9.7 bar) = 18.18 kg/m^3

2) Conversion of CO_2 densities to CO_2 mass:

$$Volume\ of\ vessel\ is\ 61\ mL\ =\ 6.1\ x\ 10^{-5}\ m^3$$

$$mass\ of\ CO_2\ =\ density\ of\ CO_2\ x\ volume\ of\ gas\ (=\ volume\ of\ vessel)$$

$$CO_2\ mass\ at\ start = 19.2\ x\ \ 6.1\ x\ 10^{-5} = 0.00117\ kg = 1.17g$$

$$CO_2\ mass\ at\ start = 18.18\ x\ \ 6.1\ x\ 10^{-5} = 0.00115\ kg = 1.109g$$

3) Absorbed CO_2 mass:

$$CO_2\ mass\ at\ start - \ CO_2\ mass\ at\ end = \ CO_2\ absorption$$

$$1.17g - \ 1.15 = \ 0.061\ g\ CO_2\ per\ 0.5\ g\ Sample \rightarrow 0.122\ g\ CO_2\ per\ g\ Sample$$

6.2.2 Effect of Size on CO_2 Absorption

Comparing formulated samples with different mechanical stirring speeds regarding CO_2 absorption at room temperature, the sample made with 400 rpm stirring speed showed the highest CO_2 loading capacity of 0.187 g/g compared to the sample made with the higher stirring speed of 600 rpm (0.157 g/g) and lower stirring speed (0.173 g/g) (Figure 6-3). Regardless of the absorption capacity of the samples, all three samples showed a similar sorption behaviour with an initial rapid sample weight increase which is then followed by a continuous, slow CO_2 uptake, though the absorption time to achieve maximum absorption capacity for each time differed (similarly to the absorption curve of sample seen in Figure 6-2) (3).

Accessibility to the interfacial area, i.e. the available surface area (SA), is important and favourable for CO_2 diffusion and absorption, thus the differences in the absorption capacity despite their similar payload (69-79%) is seen due to the different particle size and their surface properties. 400 rpm sample had the largest SA (92 m^2/g) with higher pore volume (0.097 m^2/g) compared to the other two samples. Particles with larger surface area are more intimate in contact with the gas and thus increase the absorption efficiency which is the case for the 400 rpm sample (65). Additionally, the agglomeration present inside the sample affects the CO_2 absorption of dry sample due to the smaller particles, i.e. agglomerates, occupying the mesopores which would lead

to a decrease in SA, pore volume and absorption. The formulated samples displayed a matrix structure that contains interconnected channel which is important for fast CO_2 ingress within the matrix structure for effective sorption. However, the pores do not seem to be affected by the agglomeration as the absorption capacity of 100 rpm sample is higher than that of the 600 rpm sample even though it showed higher agglomerates in comparison. Nevertheless, this suggests that the actual surface area of the tested samples might be different than the measurement obtained from the BET as the SA testing relies on a vacuuming process that removes a lot of the smaller particles and the thymol blue as well since the sample after vacuuming loses one-third of their mass. Hence, the tested samples inside the Pressure Rig most likely have a smaller SA, pore volume and pore size due to blocked pores (107). Furthermore, the absorption capacity can be increased by decreasing the size of particles, however, in this case the smaller sized particles do not show higher absorption (600 rpm sample) due to lower surface area related to the smaller pore size and pore volume (108). A larger pore volume provides a larger gas/core interfacial area which gives better CO_2 diffusion, thus the sorption behaviour coincides with the pore volume and SA of the formulated sample (107). Sample formulated with 400 rpm mechanical stirrer had the largest particle SA (92 m^2/g) along with the highest absorption capacity (0.187 g/ g) compared to the other samples.

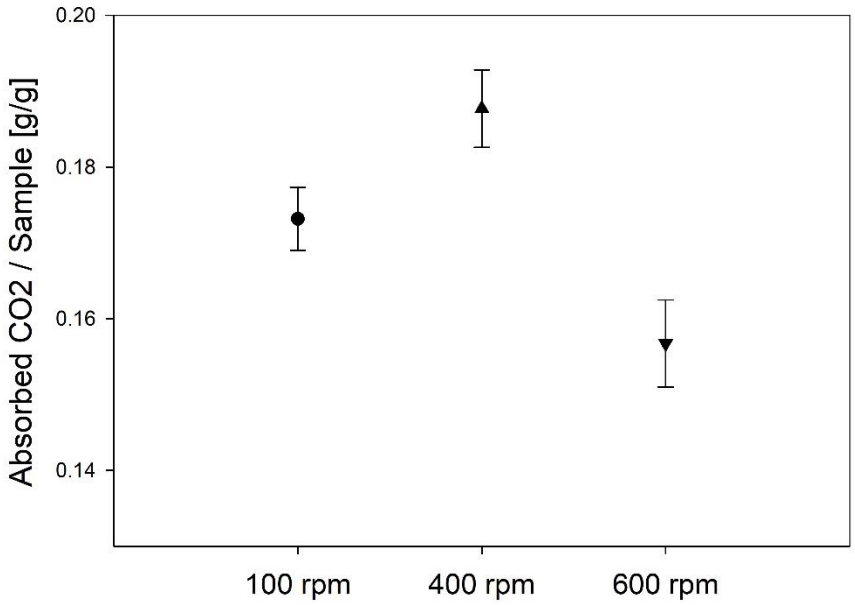

Figure 6-3 Effect of size on the CO_2 absorption capacity of 0.5 wt% PGPR formulated sample (pure AMP core, 6:4 core-shell ratio, 400 rpm mechanical stirrer speed and 1200 rpm homogeniser speed).

This experiment concluded that samples formulated with 400 rpm (AMP core, 0.5 wt% PGPR, 6:4 core-shell ratio, 400 rpm mechanical stirrer and 12000 rpm homogeniser speed) display the best balance between the absorption and its surface properties as well as payload capacity.

6.2.2.1 Comparison of Encapsulated Sample vs pure, liquid Core Material

Figure 6-4 shows the CO_2 absorption capacity comparison between encapsulated AMP, pure, liquid AMP and the theoretical, literature value for AMP. The encapsulated AMP (400 rpm sample) captured 0.187 g/g which is one-third less of the liquid AMP (measured value: 0.3 g/g). In contrast, the absorption capacity of liquid AMP is reported to be 1 mol of CO_2/ 1 mol of AMP which converted gives a theoretical absorption of 0.49 g of CO_2/ 1 g AMP.

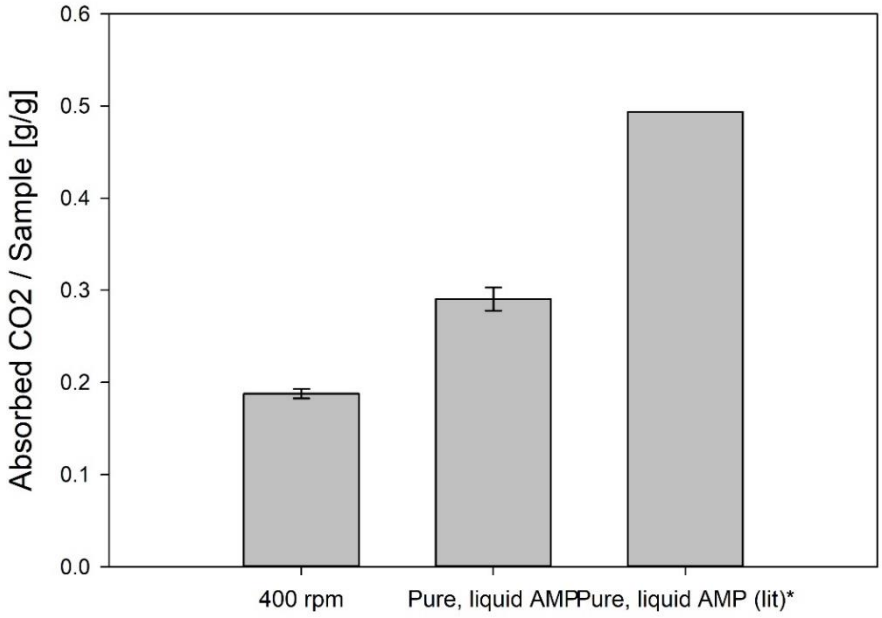

Figure 6-4 Comparison of CO_2 absorption capacity between encapsulated AMP (0.5 wt% PGPR, 6:4 core-shell ratio, 400 rpm mechanical stirrer speed and 1200 rpm homogeniser speed) and pure, liquid AMP and literature value for liquid AMP. * is the theoretical absorption capacity from literature.

Lower absorption capacity is seen with the encapsulated sample as its content of AMP is lower than in pure, liquid form which is supported by the previous FTIR result due to lower N-H bond shown in the IR spectra. Additionally, containing the core material inside an inert material also reduces the absorption due to the sample being compact in a small space. This hinders the CO_2 from getting to the amine for absorption. However, at this point it cannot be concluded how large the effect of the inert material or the stacking of a sample are on the absorption. Further in-depth testing of the inert material and sample volume itself are required to make more accurate statement in regard to it. Similarly, lower absorption capacity is obtained for liquid AMP compared to the literature value. This is due to the difference in the testing conditions (literature value obtained from absorption at higher temperatures (> 40°C) and large pressures (50bar)) and the use of small sample holder during absorption testing. The small sample holder limits the contact of the gas with the liquid. Also the material inside the

pressure rig is non-static, whereas amine scrubbing process or pressure-swing set-ups use continuous batch process to which allows new amine to be fed into the chamber for absorption while the ones with CO_2 capture is removed. A continuous process allows better contact of gas with the material (27,106,109). The pressure rig contains a 61mL chamber which limits the size of the sample holder. It can be observed from Figure 6-5 that the liquid AMP exposed to CO_2, absorbs carbon leading to a phase change from liquid to (soft) solid This phase change occurs due to the chemical reaction taking place between CO_2 and AMP (107):

$$2RNH_2 + CO_2 \rightarrow RNHCOO^- + RNH_3^+ \quad \textbf{Equation 6-1}$$

$$RNHCOO^- + H_2O \rightarrow RNH_2 + HCO_3^- \quad \textbf{Equation 6-2}$$

$$RNH_2 + CO_2\,H_2O \rightarrow RNH_2 + HCO_3^-\ (overall) \quad \textbf{Equation 6-3}$$

The above reactions (Equation 6-1 to 6-3) are observed when AMP encounters CO_2 in an aqueous solution where the amine acts as a base. A sterically, hindered amine like 2-Amino-2-methyl-1-propanol exposed to CO_2, leads to an unstable AMP-carbamate (Equation 6-2) formation due to the two methyl groups attached to one of the carbon atoms of AMP slowing down the reaction. This AMP-carbamate is easily hydrolysed into bicarbonate due to the amines being more unstable which facilitates CO_2 capture (85).

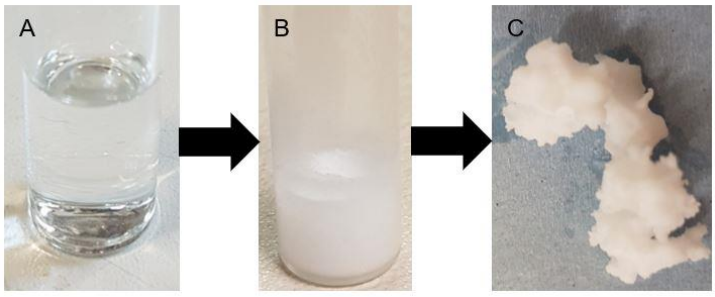

Figure 6-5 Pure, liquid AMP before (A) and after (B, C) CO_2 exposure. After AMP absorbs CO_2, the material undergoes a phase change leading to the formation of a soft solid (C).

6.2.3 Effect of Emulsifier on CO_2 Absorption

The absorption capacity of the formulated microcapsules is lowered when the emulsifier is changed from 0.5 wt% PGPR to either 1 wt% Span85 and 1 wt% Tween80 where 1 wt% Tween80 had the lowest absorption with 0.156 g of CO_2 (Figure 6-6) The absorption capacity again can be related to its surface properties since the payload of the three samples is similar (75% - 78%). Microcapsules formulated with 1 wt% Tween80 had the lowest SA with 20 m^2/g compared to 0.5 wt% PGPR (92 m^2/g) and 1 wt% Span85 (45 m^2/g). This lower SA not only slows down the absorption but also gives the gas molecules far less surface to be absorbed into. Additionally, 1 wt% Tween80 also contains higher amounts of agglomeration which further hinders the absorption of CO_2 into the microcapsule as the smaller particles at surface potentially block the pores that lead to a decrease in the gas and microcapsule interfacial area (110).

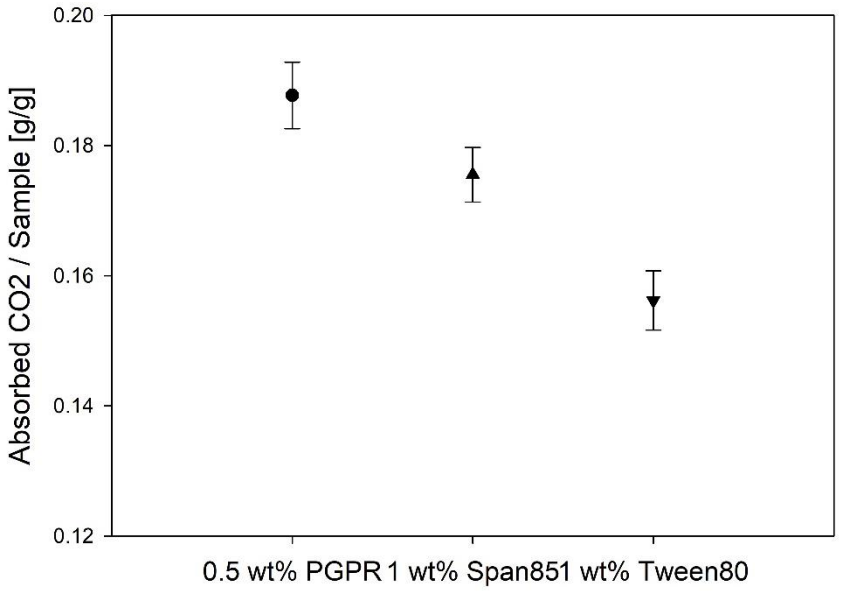

Figure 6-6 Effect of different emulsifiers on the CO_2 absorption capacity of the formulated samples (pure AMP core, 6:4 core-shell ratio, 400 rpm mechanical stirrer speed and 1200 rpm homogeniser speed).

6.2.4 Effect of Core-shell Ratio on CO_2 Absorption

By increasing the core concentration from 5:5 core-shell ratio to a 6:4 ratio, the absorption capacity of the formulated sample (0.5 wt% PGPR) increased drastically from 0.11 g/g to 0.187 g/g. Any further increase in the core concentration does not have a drastic effect on the absorption capacity, however, a 7:3 core-shell ratio sample showed the highest absorption with 0.195 g/g (Figure 6-7).

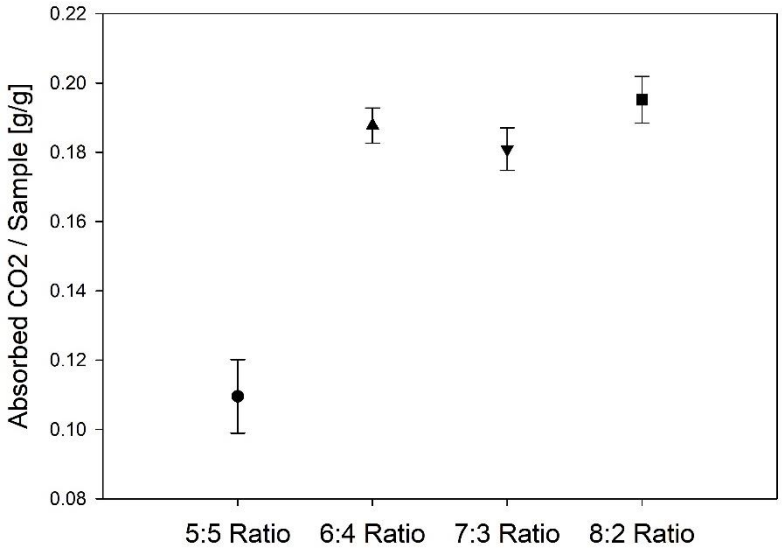

Figure 6-7 Effect of core-shell ratio on the CO_2 absorption capacity of samples formulated with 0.5 wt% PGPR, pure AMP core, 6:4 core-shell ratio, 400 rpm mechanical stirrer speed and 1200 rpm homogeniser speed.

In comparison, a steady increase in absorption capacity is seen with an increase in the core-shell ratio for samples formulated with 1 wt% Span85 except for the 8:2 ratio. The absorption capacity increases from 0.135 g to 0.204 g CO_2 absorbed/ g sample for 5:5 and 7:3 ratio respectively. However, the absorption capacity drops afterwards to 0.161 g/g for an 8:2 core-shell ratio. Samples formulated with 0.5 wt% Tween80 show a similar trend (Figure 6-8).

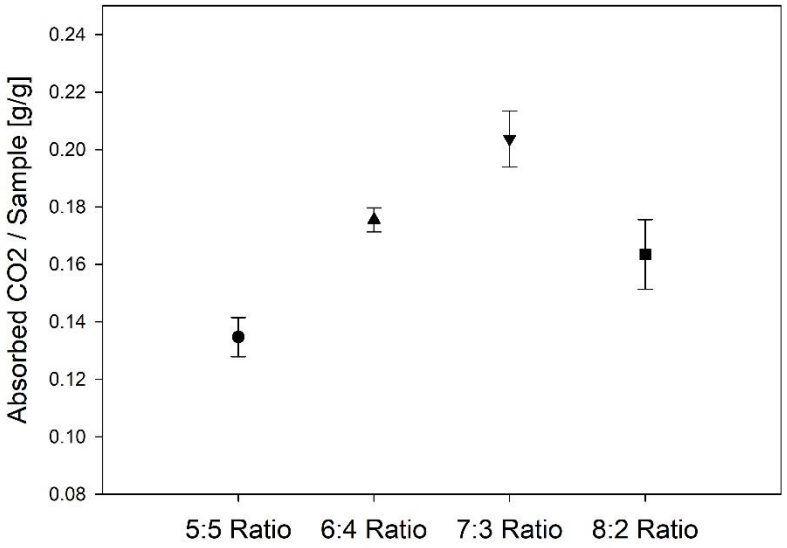

Figure 6-8 Effect of core-shell ratio on the CO_2 absorption capacity of samples formulated with 1 wt% Span85, pure AMP core, 6:4 core-shell ratio, 400 rpm mechanical stirrer speed and 1200 rpm homogeniser speed.

The formulated samples with different core-shell ratio displayed a similar payload where the payload increases with the core-shell ratio. It has been reported in literature that the absorption capacity increases with an increase in amine content until a point is reached where a further increase in the core material has a disadvantageous effect on the absorption of the material. The samples formulated with 7:3 core-shell ratio had on average a higher payload and a slightly larger particle size compared to lower ratios, hence why an increase in CO_2 absorption is seen. However, any further increase than a core-shell ratio of 7:3 for 1 wt% Span85/Tween80 led to the disappearance of the gas interfacial area due to higher agglomeration present with higher amine content, thus, decreasing the gas contact with the microcapsule and thus, making it harder for the CO_2 to diffuse into the pores as the gas needs to overcome the diffusion barrier, i.e. the agglomerates at the microcapsule surface to spread deeper into the pores. The samples formulated with an 8:2 core-shell ratio had the highest agglomeration, hence the lowest absorption capacity (110).

In contrast with a low core-shell ratio, less agglomeration is present (6:4 and 7:4), except for the 5:5 ratio (Figure 6-9). A 5:5 core-shell ratio produced microcapsule, irrespective of the emulsifiers used, that had the lowest average particle size (210 – 300 μm) and the lowest payload (~75%). This indicates that the amine content is lower than that of the other ratios, hence the lowest absorption capacity is seen (110).

However, the absorption capacity of samples formulated with 0.5 wt% PGPR does not decrease even with an 8:2 core-shell ratio. This indicates that even though this sample contained the highest agglomeration the agglomeration does not affect the absorption for this sample.

Comparing the samples regarding their absorption capacity and surface properties, these results suggest that a 6:4 core-shell ratio is the best regardless of the emulsifier used, making it a potential CO_2 sorption microcapsule for the low-temperature testing.

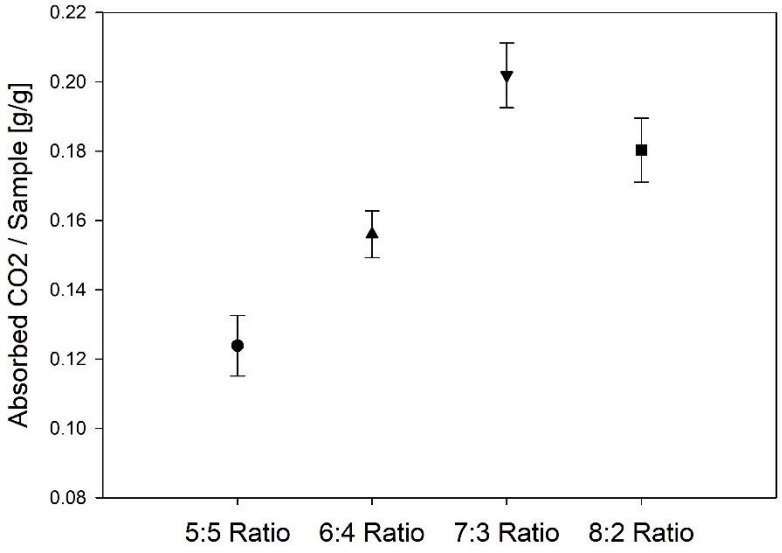

Figure 6-9 Effect of core-shell ratio on the CO_2 absorption capacity of samples formulated with 1 wt% Tween80, pure AMP core, 6:4 core-shell ratio, 400 rpm mechanical stirrer speed and 1200 rpm homogeniser speed.

6.2.5 Effect of Core Material

Figure 6-10 shows the comparison of the absorption capacity of the formulated samples with different core materials. Samples that contained pure AMP as a core showed the highest absorption capacity with 0.186 g/g, whereas samples formulated with 30% TEA showed the lowest absorption capacity with 0.06 g/g. In comparison, sample with an MEA core had a loading capacity of 0.163 g/g (Figure 6-10).

The differences in the absorption capacity occur due to the difference in their payload, SA as well as the chemical structure of the amines. As mentioned already, a higher payload is advantageous for CO_2 absorption. A higher payload presents more amine for the chemical absorption of CO_2, hence the highest absorption is seen with AMP core as that sample had the highest payload with 75%. In comparison, encapsulated pure MEA had a lower payload, hence a lower absorption capacity is seen, whereas 30% TEA encapsulated sample showed the lowest absorption due to their very low payload (52%).

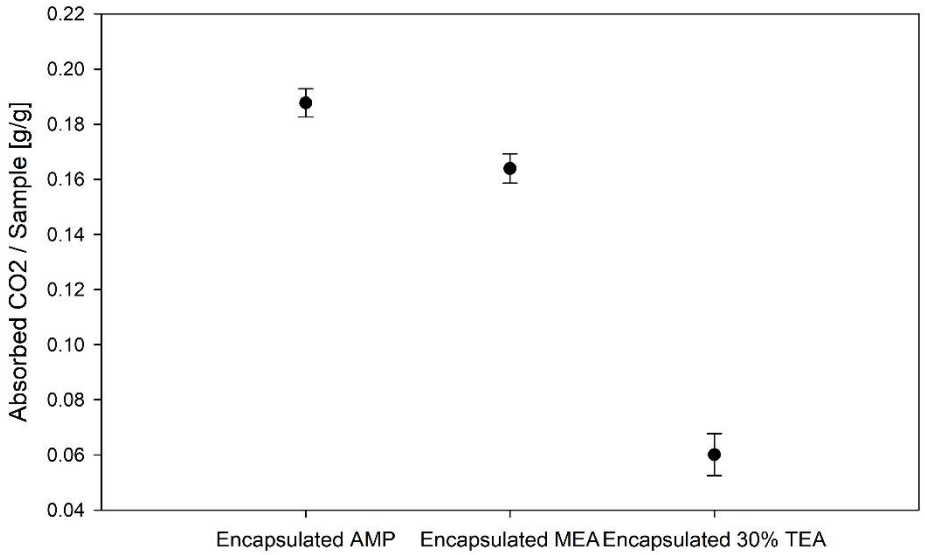

Figure 6-10 Comparison of samples formulated with different core material on CO_2 absorption capacity (1 wt% Span85, 6:4 core-shell ratio, 400 rpm mechanical stirrer speed and 1200 rpm homogeniser speed).

These difference in the absorption not only occur due to the difference in the microcapsules' properties but also due to the different amine cores. Due to the different structure of AMP, MEA and TEA they can be categorised as primary and tertiary amine depending on the number of carbon atoms attached to the nitrogen atom. These differences in chemical structures give the amines different CO_2 capacities with 1 mol, 0.5 mol and 1 mol of CO_2 absorption per 1 mol of amine (theoretical values) for AMP, MEA and TEA respectively (35,111). AMP and MEA are primary amines as both are attached to one carbon, whereas TEA is a tertiary amine due to the amine being attached to three carbon atoms. AMP and MEA can further be distinguished from each other by their difference in functional groups. AMP has more functionally groups and is therefore, a sterically hindered amine as the functional groups prevent the AMP structure from rotating, whereas MEA is an unhindered amine as the molecular structure can easily be rotated (35).

Previous studies have elucidated how primary, secondary and tertiary amine capture carbon dioxide in an aqueous media which involves the formation of carbamates, carbonates and bicarbonates. The carbon atom of CO_2 has an electrophilic nature and hence is susceptible to nucleophilic attacks by N-donors like that of amines. Primary like MEA and AMP can act a nucleophile and directly attack the carbon dioxide molecule to form a zwitterion that rapidly rearranges itself to a carbamic acid through an intermolecular proton transfer. In the instance of another free amine, the carbamic acid is converted into a carbamate through a second intermolecular proton transfer. Additionally, these amines can be transformed into bicarbonate salts by carbamate hydrolysis or the deprotonation of carbonic acid (111).

According to literature, MEA, a primary amine acts as a strong base during the early reaction stage to form carbamate at a fast rate. After the theoretical maximum of carbamate is reached, i.e. CO_2/N = 0.5 and the pH of the solution is reduced significantly, the less nucleophilic liquid (water) hydrolyses the carbamate product into bicarbonate that creates a carbamate-bicarbonate equilibrium (Figure 6-11) (111).

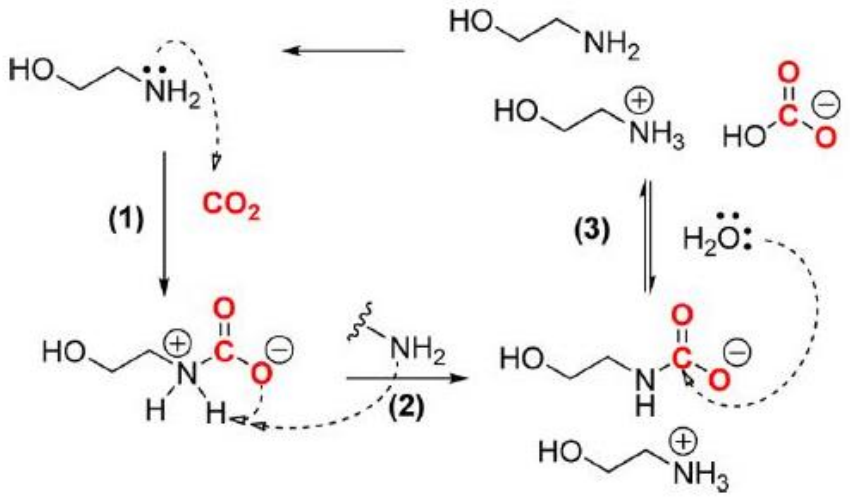

Figure 6-11 Reaction mechanism of a primary amine in presence of CO_2 in aqueous solution (111). The N-atom of amine attacks (nucleophilic) the free CO_2 to form a zwitterion/ carbamic acid (step 1) which is then followed by the deprotonation by another amine that leads to the formation of a carbamate (step 2). Then the carbamate undergoes partial or complete hydrolysis forming bicarbonate (step 3).

During the carbamate hydrolysis, an amine becomes free which can again react with a new CO_2 molecule to form another carbamate again which either decomposes into bicarbonate or forms a bicarbonate salt through an aqueous carbonic acid at a low pH. This carbamate-bicarbonate equilibrium is dependent on the alkalinity, nucleophilicity and concentration of amine, temperature of solution as well as carbon dioxide pressure (111).

In contrast to primary amines, tertiary amines are weak bases that can act as proton acceptors to form two different types of stable products in presence of CO_2: bicarbonate and/or carbonate. It has been reported that tertiary amines reaction with

CO_2 results in carbonate and bicarbonate formation in the early reaction stage (Figure 6-12) where bicarbonate is formed in all the reaction stages, even at high pH. The higher the protonation of the tertiary amine, the more amine is used hence a pH drop is seen which then favours the bicarbonate formation from the carbonic acid. Initially, the carbonate concentration is high with a high pH but as the pH decreases the carbonate concentration declines as well. The other route for bicarbonate formation happens at low pH after the amine protonation where carbonate ions deprotonate a carbonic acid molecule to form two bicarbonate ions (111).

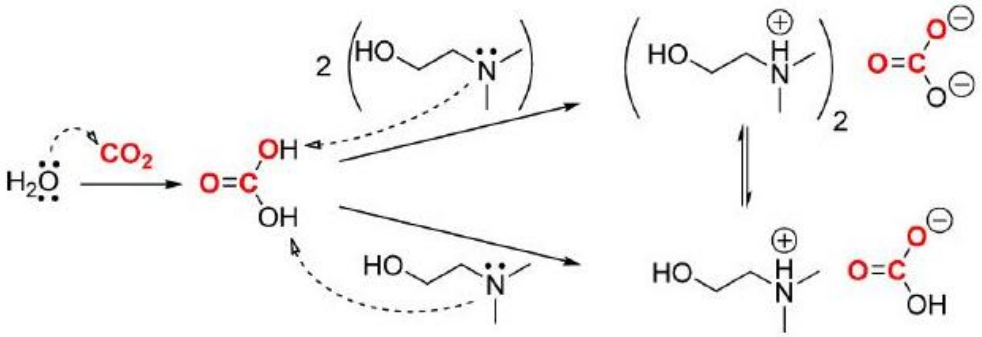

Figure 6-12 Reaction mechanism of a tertiary amine in presence of CO_2 in aqueous solution (14). Carbonic acid is formed when CO_2 encounters H_2O which is then followed by the deprotonation by a tertiary amine that leads to the formation of carbonate (at high pH) or bicarbonate (low pH). These reactions exist in equilibrium.

However, considering that the amines (AMP, MEA, TEA) are encapsulated and not used as an aqueous solution, the water concentration inside the formulated sample is only 7% (maximum) due to the use of thymol blue (1g). The thymol blue is dissolved in water before mixing it with the amine for the formulation. But technically no water is required for the primary amine absorption, hence the absorption mechanism of encapsulated AMP and MEA does not differ much from the aqueous amine, however for the tertiary amine (TEA) a high water content is required, hence, the carbon dioxide

absorption is hindered due to the low water content which in turn gave a significant lower CO_2 absorption for 30 wt% TEA (111).

6.2.6 Effect of Temperature on CO_2 Absorption

For the CO_2 absorption tests, the effect of temperature was also observed for samples formulated with 100 rpm, 400 rpm and 600 rpm. It can be seen from Figure 6-13 that the absorption capacity for pure core material (AMP) decreased from 0.3 g to 0.28 corresponding to the temperature drop from 20 °C to 0 °C. The encapsulated sample, in contrast, show an increase in absorption capacity as temperature decreased, e.g. absorption capacity of 400 rpm sample increased from 0.186 g at 20 °C to 0.28 g for -40 °C (Figure 6-13). This occurred due to both physical and chemical absorption. At lower temperature chemical absorption slows down due to a decrease in kinetic energy, hence slower diffusion which is the case with the pure core material. CO_2 absorption is reliant on the kinetic diffusion and thermodynamic sorption where at low temperature the kinetic resistance for CO_2 needs to be overcome (it's a prerequisite for effective CO_2 absorption). Thus, high gas-sorbent interfacial area with large pores and high core concentration gave highest sorption capacity at -20 °C. Additionally, the lower kinetic energy of the CO_2 molecules allows the gas to have more contact with the porous structure which increases in the particle surface interaction with the CO_2, hence allowing more particles to be trapped inside the porous structure. In comparison, 20 °C facilitates CO_2 diffusion, where a higher concentration supplies more amine sites to boost the carbon dioxide capacity, hence the highest absorption capacity is seen for pure, aqueous amine at room temperature where the chemical absorption is larger than the physical adsorption (110).

As the temperature decreased, the absorption capacity of the material increased. However, for physical adsorption, the surface area is more important and hence why a higher absorption is seen at a lower temperature. Though, the absorption capacity only increased up to -20 °C, suggesting the maximum absorption capacity is reached for all samples (Figure 6-13). CO_2 absorption is reliant on the kinetic diffusion and thermodynamic sorption where at low temperature the kinetic resistance for CO_2 needs to be overcome (it's a prerequisite for effective CO2 absorption). Thus, high gas-sorbent interfacial area with large pores and high core concentration give highest sorption capacity at -20 °C. In comparison, 20 °C facilitates CO_2 diffusion, where a higher concentration supplies more amine sites to boost the carbon dioxide capacity, hence the highest absorption capacity is seen for pure, aqueous amine at room temperature. Comparing the absorption capacity of 100 rpm and 600 rpm sample with each other, 600 rpm sample initially had the lowest absorption capacity at room temperature with 0.157 g but steadily increased to 0.23 g as the temperature decreased due to the higher surface area to volume ratio and higher pore volume and due to them being the smallest sized sample (20 μm), giving the sample higher physical adsorption on the surface. In contrast, 400 rpm sample showed the highest CO_2 adsorption capacity, suggesting the best balance between the core material and surface area to volume ratio. This result proves that lowering the temperature has a positive effect on the absorption capacity of the microencapsulated AMP (112,113).

Overall, the experimental CO_2 capacity of the microcapsules with AMP core showed a lower absorption capacity compared to the literature value. However, the CO_2 absorption capacity of the AMP microcapsules is equivalent to the pure MEA solvents, showing a promising future for the AMP microcapsules (114).

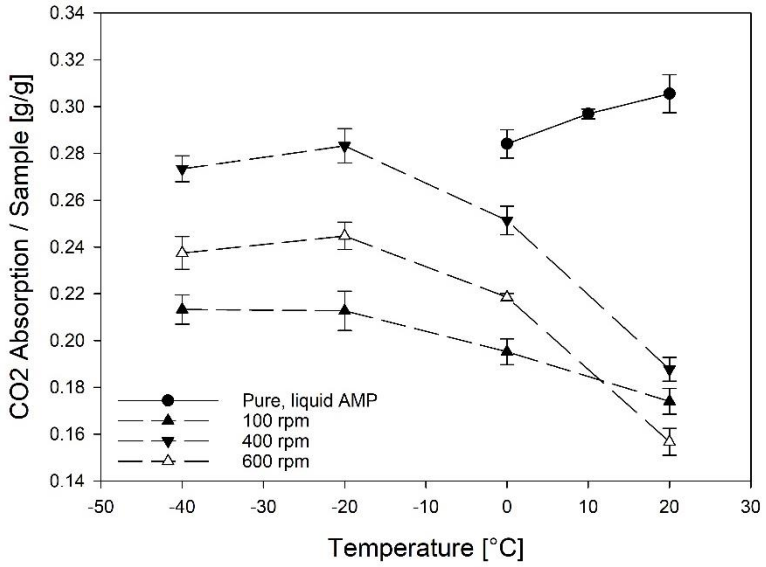

Figure 6-13 Effect of temperature on CO2 absorption capacity. The absorption capacity of pure, liquid AMP is compared with encapsulated sample formulated with 100 rpm - 600 rpm (0.5 wt% PGPR and 6:4 core-shell ratio).

6.3 Design Analysis

The pressure rig was set-up as a pressure decay method. A pressure decay method is a standard experimental technique for the characterisation of a material in terms of sorption capacity (115). Generally, this method has high sensitivity as the principle of this method is based on the amount of gas or molecules absorbed through measuring the pressure decay, i.e. the pressure drops over time, in a chamber with a known volume where the sample is placed. The amount of CO_2 absorbed is then determined by the difference at the start and end pressure of the experiment where the end pressure is the equilibrium pressure (115). The accuracy of this method is dependent on the vessel as well as the pressure transducers. In our set-up 20 barA pressure transducers were used when the maximum pressure used during the experiment was 10 barA. This did allow the extraction of absorption data for individual samples, however, due to the high oscillation of pressure data, no good absorption kinetic data were able to be obtained. Another limitation of this experimental set-up is the need of

exposing the sample to air/ CO_2 before testing starts. The sample is inserted into the chamber before it is pressurised, thus the corresponding results have to be taken with caution.

Additionally, the small volume of the pressure rig chamber (61 mL) restricted the amount of sample that could be used during the absorption testing. A smaller sample size, e.g. 0.5 g, is more susceptible to smaller changes in absorption observed as larger in comparison. Technically, a larger sample mass is preferable as the absorption mass increase will be more obvious.

Moreover, the pressure rig that was used is an old instrument, hence most of the fittings were old and worn out. This necessitated the need to replace most of the fitting like valves and piping that required leakage testing. These leakage testing tend to take up a lot of time as each individual connection needs to be tested individually.

As the pressure rig is made up of steel, it was not possible to reach temperatures below -40 °C with the Huber (CC-902) chiller. The hoses of the chiller and bottom part of the pressure rig where even insulated to minimise the heat loss, however, due to the design of the pressure rig, the top part could not be insulated as that would prevent the rig from being open. The top part of the pressure rig (valves and pressure transducer) where clamped unto the bottom part, i.e. the chamber. The clamp needed to be tightened with bolts. Hence making the insulation of the top part not possible. This lead to the clamp and bots freezing at below 0 °C (Figure 6-14). After testing finished at low temperature, the pressure rig needed to be heated up before it could be opened and in order to remove the samples. Additionally, due to the many connections of the pressure rig and large clamps, cooling down the rig to desired temperatures like -40 °C took considerable effort and time due to large heat losses. The chiller had to be set

to -70 ºC to reach a -40 ºC temperature after approximately 4 hours. Moreover, the sample needed to be inserted into the rig before the temperature was lowered as the rig needs to be opened to insert the sample. This meant that the sample was already exposed to low temperatures before CO_2 was introduced which might have affected the absorption of the microcapsules. To this end, a continuous reactor is set-up to obtain more accurate CO_2 absorption capacities and absorption kinetics. Furthermore, the continuous reactor allowed the samples to be tested in a slurry rather than as dry microcapsules.

However, if CO_2 absorption testing is required for static or dry samples and potentially at high temperatures, the use of magnetic suspension balance is proposed (Figure 6-15). These suspension balances allow a change in mass and force which can be acted on the samples under controlled environment (wide temperature, pressure, corrosive gases and fluids are able to be used) can be very highly accurately measured and can be used in a wide temperature and pressure range under aggressive media.

Figure 6-14 Pressure rig set-up used for CO2 absorption testing where the lid is frozen due to the low temperature used while the hoses are insulated with foam.

This allows the sorption, diffusion, surface tension, density, chemical compositions (decomposition, corrosion) and product process (drying, polymerisation) of materials to be determined (116,117).

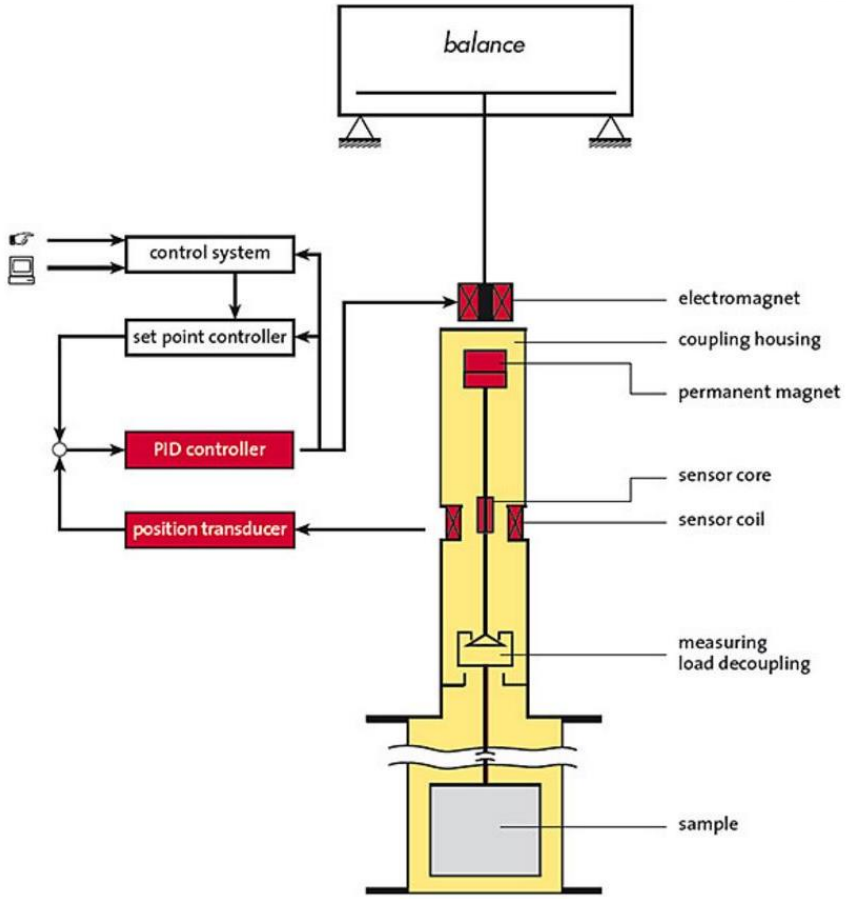

Figure 6-15 Illustration of a magnetic suspension balance from Rubotherm. A controlled suspension state is achieved through a direct control circle, i.e. PID controller and transducer. The control system allows the suspension balance to be held constantly in a vertical position (116).

6.4 Conclusions

The accessibility to the interfacial area, i.e. the available SA, is important and favourable for CO_2 diffusion and absorption, thus the differences in the absorption capacity despite their similar payload (69-79%) is seen due to the different particle size and their surface properties. Hence samples formulated with 400 rpm (AMP core, 0.5 wt% PGPR, 6:4 core-shell ratio, 400 rpm mechanical stirrer and 12000 rpm

homogeniser speed) displayed the best balance between the absorption (0.187 g/g) and its surface properties (92 cm^2/g) as well as payload capacity (75%). In comparison, pure, aqueous amine showed a higher absorption capacity (0.29 g) and underwent a phase change from liquid to solid (soft) once it was exposed to CO_2 due to the formation of carbamate and bicarbonates (**Error! Reference source not found.**) (107).

Microcapsules with a lower SA and higher agglomeration gave a lower absorption capacity due to less surface being available for the gas molecules to diffuse into as well as the agglomerates blocking the pores, hence 1 wt% Tween80 showed the lowest absorption with 0.156 g/g compared to the other two emulsifiers (110).

Overall, the differences in the absorption capacity occurred due to the difference in the samples' payload, SA as well as the chemical structure of the amines. A higher payload and SA are advantageous for CO_2 absorption. A higher SA with a higher PV gives the gas a larger interfacial area and thus facilitates easier diffusion. Additionally, a higher payload presents more amine for the chemical absorption of CO_2, hence the highest absorption is seen with AMP core as that sample had the highest SA with 92 cm^2/g with a 75% payload. In comparison, 30% TEA encapsulated sample showed the lowest absorption due to their very low SA (20 cm^2/g) and low payload (52%) due to the absorption being hindered because of the low water content in the sample as water is required for the carbamate/bicarbonate formation, hence a significant less CO_2 absorption is seen with 30% TEA (111).

In terms of the temperature effect on absorption, the experimental CO_2 capacity of the microencapsulated sample showed an increase in the absorption as the temperature is lowered with 400 rpm sample showed the highest absorption at -20 °C with 0.28 g

absorbed CO_2/ g sample. In contrast, the CO_2 absorption capacity of the pure, aqueous amine decreased with a decrease in temperature

Due to many disadvantages of the pressure-rig like poor heat transfer, a continuous reactor is a set-up to allow more accurate CO_2 absorption capacities and absorption kinetics to be obtained. Additionally, the continuous reactor allowed the samples to be tested in a slurry rather than as dry microcapsules.

Chapter 7 Effect of Low Temperature on CO_2 Absorption (Continuous Reactor)

7.1 Introduction

The manometric method is only used to test sorption capacity at 10 bar pressure but in practice the formulated microcapsules are potential for post-combustion CO_2 capture which runs at ambient pressure, hence why a continuous reactor is set-up. The solubility of a gas into a liquid can be increased by decreasing the temperature according to Henry's Law. The attractive intermolecular interactions are usually zero in the gas phase for most materials. A gas molecule dissolves into a liquid by interacting with the solvent molecules that leads to heat release due to the new attractive interactions, hence gas dissolving in a liquid is most cases is an exothermic process. Conversely, by increasing the temperature heat is added to the solution which leads to higher thermal energy being present in the liquid that overcomes the forces between the gas and liquid molecule, therefore, decreasing the solubility of a gas. Henceforth, lower temperatures are used for CO_2 absorption testing inside the reactor not only to increase the gas solubility into the carrier fluid but to also initiate a possible freezing of microcapsule after CO_2 capture (118).

The absorption properties of the microencapsulated samples were obtained with the pressure rig set-up, however, that method is very time consuming and temperature sensitive at low temperatures. Hence, a second method for CO_2 capture is set-up to observe the absorption capacity of the microcapsules as a slurry and to study the absorption kinetics below 20°C. By dispersing microcapsules into a liquid, the disadvantage of the agglomeration was overcome and allowed easier diffusion of CO_2 into/unto the microcapsule surface due to easier access. Inside the pressure rig, the samples were contained into a small space, hence making it harder for the gas to

encounter the sample, whereas in the continuous reactor the gas is diffused into the liquid which allows more contact of the gas with the sample.

7.2 Result and Discussion

The following samples were tested in the continuous reactor to observe the effect of temperature on the absorption capacity and kinetics:

- **Size:** 100 – 600 rpm sample (0.5 wt% PGPR, AMP core and 6:4 core-shell ratio)
- **Emulsifier:** 0.5 wt% PGPR, 1wt % Span85, 1 wt% Tween80 (AMP core, 6:4 core-shell ratio, 400 rpm mechanical stirrer and 1200 rpm homogeniser speed)
- **Core material:** 100% AMP, 100% MEA, 30% TEA-70% AMP core (6:4 core-shell ratio, 400 rpm mechanical stirrer and 1200 rpm homogeniser speed)

7.2.1 Effect of Size

It can be observed from Figure 7-1, that the absorption capacity increased with a decrease in temperature from 20 °C to -60 °C independently of size which is similar to the trend seen by the pressure rig (PR) results though the absorption capacity seemed to slightly decrease after -20 °C (PR). The PR result indicated that the highest absorption is reached at that specific temperature for 10 barA pressure. In contrast, samples exposed to CO_2 in the continuous reactor showed the highest absorption at -60 °C and -40 °C with 0.0684 g, 0.0993 g and 0.0719 g of CO_2 absorbed per g sample for 100 rpm, 400 rpm and 600 rpm sample respectively. The absorption capacity of the continuous reactor was lower than that of the pressure rig results due to the lower pressure used. A higher pressure means a higher number of gas molecules hence a higher driving force of the gas to react with the amines thus higher absorption.

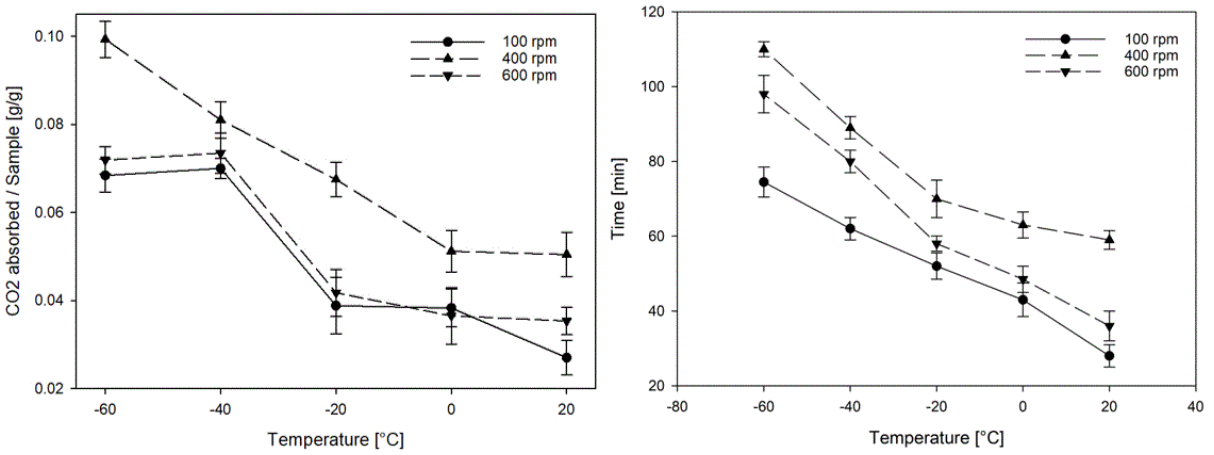

Figure 7-1 Effect of temperature on absorption capacity and absorption time of samples with different size (0.5 wt% PGPR, AMP core, 6:4 core-shell ratio, 100, 400 and 600 rpm mechanical stirrer speed).

However, 400 rpm sample showed not only the highest absorption capacity at room temperature but also at lower temperatures with the sample showing the highest absorption capacity of 0.0993 g/g sample at -60°C. In comparison 100 rpm and 600 rpm samples showed an interesting absorption trend where both had similar loading capacity to each other and showed the highest absorption at -40°C, but 600 rpm had a slightly higher capacity (with the exception at -20°C). The unexpected result at -20°C could be due to the sample preparation or inaccuracy of the system. The used samples might have been exposed to air (which contains CO_2) for too long during sample preparation prior to testing. In contrast the absorption capacity result of the pressure rig showed that 100 rpm sample had a higher absorption capacity at room temperature with 0.173 g/g. The higher absorption with the pressure rig is seen due to better physio-absorption of CO_2 into the porous particle structure as well as higher intermolecular forces. This phenomenon is described by Le Chatelier's principle that states if stress, i.e. pressure change, is applied to a system which is in equilibrium then the equilibrium shifts to counteract the constraint's effect. Hence, an increase in pressure leads to the system shifting to counteract the strain by favouring the reaction where the gas

molecules are forced into the microcapsule through the pores as well as immobilise the molecules on the porous surface of the capsules (119).

In terms of absorption time, the absorption time is closely related to the absorption capacity. A higher absorption requires more time due to higher interaction between the gas and the microcapsules (Figure 7-2), however, 600 rpm sample is expected to show lower absorption time compared to 100 rpm sample due to its higher SA to volume ratio. The sample produced with 600 rpm were on average smaller (160 μm) than the 100 rpm sample (250 μm). Similarly, the 600 rpm sample showed a higher SA (34 m^2/g) and pore volume (0.061 cm^3/g) than 100 rpm (29 m^2/g and 0.051 cm^2/g), hence faster absorption would have been expected for that specific sample which was not the case. Additionally, 100 rpm sample had a higher loading capacity with 79% compared to sample 600 rpm (69%), suggesting that the smaller SA allowed the microcapsules to absorb CO_2 faster (120).

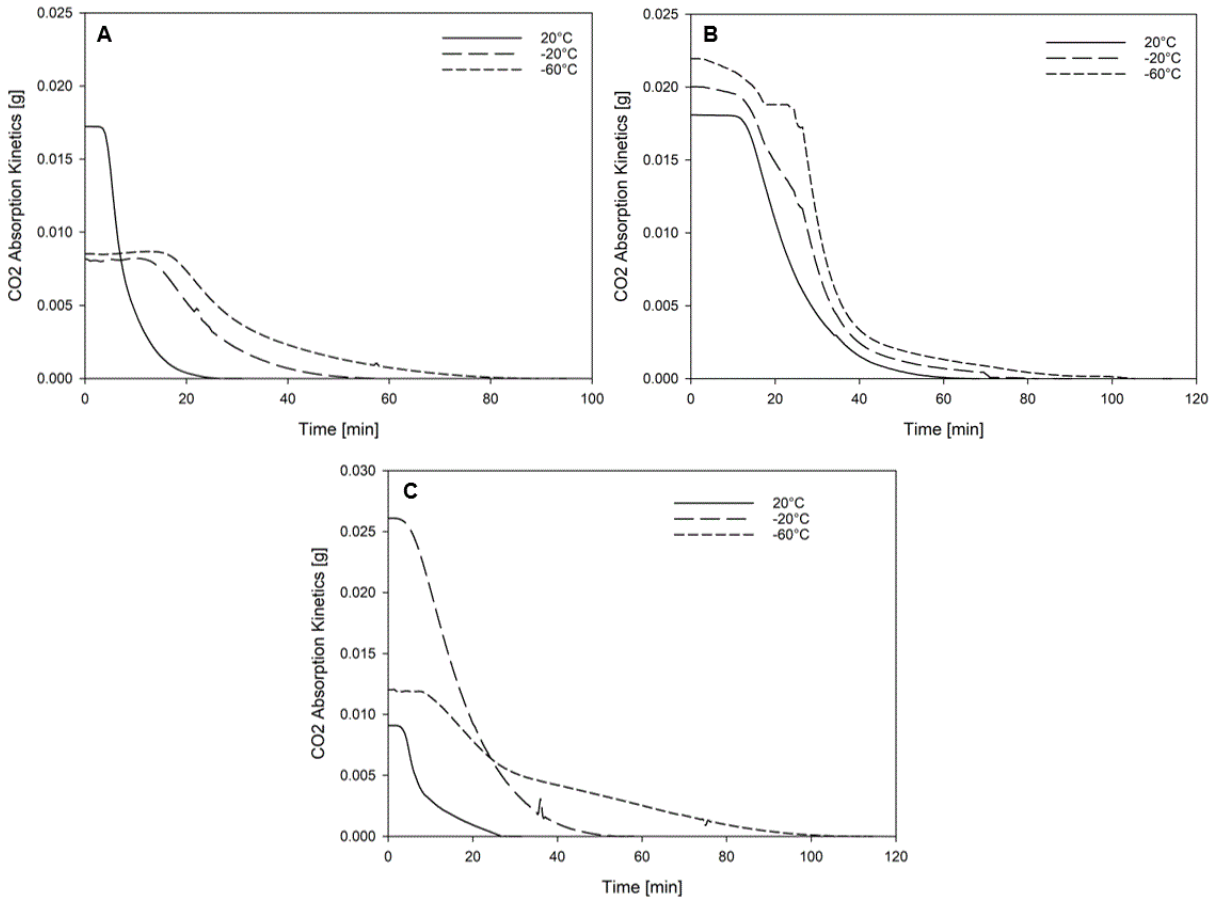

Figure 7-2 CO_2 absorption kinetics of formulated sample at 20 °C, -20 °C and -60 °C: A) 100 rpm sample; B) 400 rpm sample; C) 600 rpm sample (0.5 wt% PGPR, AMP core and 6-4 core-shell ratio).

Comparing the absorption kinetics of 400 rpm sample at different temperatures, it can be observed that at any given temperature a high absorption is seen in the first 20 minutes which is then followed by a drop in absorption (Figure 7-2). The decrease in absorption, i.e. slowing down of CO_2 uptake, is smaller with lower temperature, e.g. at -60 °C more than 90 minutes were required to reach the maximum absorption capacity, where the absorption rapidly decreased as it neared its absorption limit. This is due to the gas molecules travelling at a slower speed compared to higher temperatures because of lower kinetic energy. A lower kinetic energy results in slower chemical absorption which is important for the CO_2 absorption compared to the physical adsorption due to the higher payload (average payload of microcapsules 70-80 %)

(121). A similar effect of temperature is seen with 100 rpm and 600 rpm sample. It has been reported that CO_2 absorption is reliant on the kinetic diffusion where at low temperature the kinetic resistance for CO_2 needs to be overcome (it's a prerequisite for good/effective CO_2 absorption) (107). Thus, a high gas-sorbent interfacial area with large pores and high core concentration can give a high sorption capacity for sample 400 rpm as it had the highest SA (92 cm^3) though its pore size was smaller than that of 100 rpm and 600 rpm sample (71 and 72 Å respectively). In comparison, high working temperatures like 70 °C facilitates CO_2 desorption, where more concentration supplies more amine sites to boost the carbon dioxide capacity. Further increasing the temperature leads to the desorption to dominate the absorption process which degrades the sorption performance (Figure 7-3) (107).

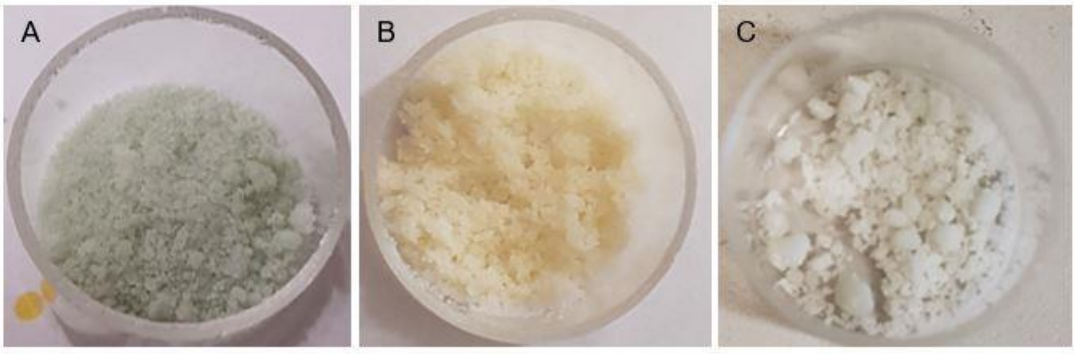

Figure 7-3 Colour change during the absorption and desorption process of AMP encapsulated sample.

7.2.1.1 Comparison of an encapsulated sample against pure, liquid AMP

Comparing the absorption capacity of the encapsulated sample against the pure core, encapsulated AMP showed a lower absorption capacity (0.0505 g) compared to the pure, liquid AMP (0.069 g) at room temperature, however, at -60 ºC the encapsulated sample showed a higher absorption with 0.0993 g compared to 0.0889 g of CO_2 absorbed per g sample (Figure 7-4). The theoretical absorption capacity of CO_2 for liquid AMP is 0.49 g, however, these differences in the absorption values occurred due

to the different conditions and amine concentrations used. In the continuous Reactor only a 20 wt% amine solution is exposed to CO_2, whereas the theoretical absorption values refer to pure, liquid amine without any dilutions. Additionally, amine is used at higher temperatures than 20°C for CO_2 capture (>40°C) and larger pressures (>50 bar) (106).

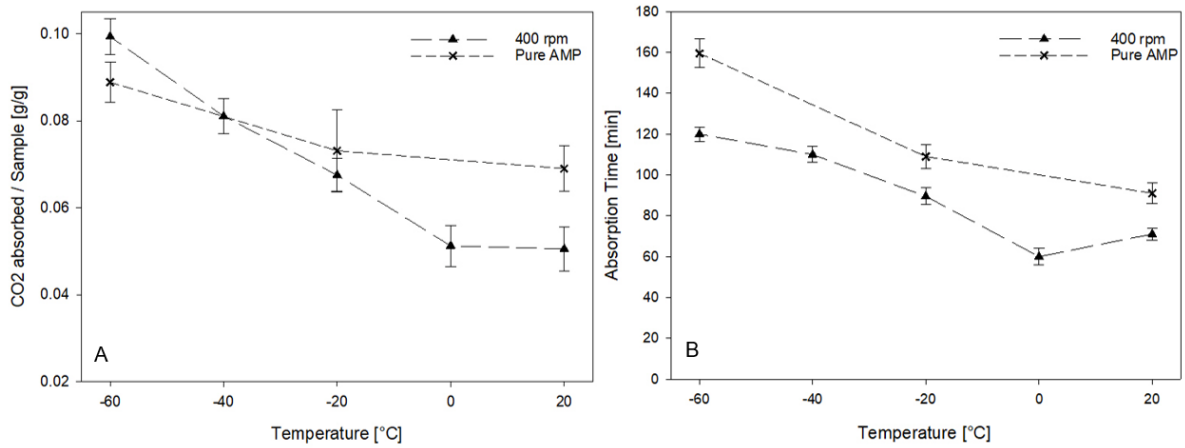

Figure 7-4 Comparison of CO_2 absorption kinetics and absorption time of pure, liquid AMP and formulated sample at 20°C, -20 °C and -60 °C (0.5 wt% PGPR, 400 rpm mechanical stirrer speed, AMP core and 6-4 core-shell ratio).

In contrast, pure AMP required more time for the absorption compared to the encapsulated core material throughout the whole testing temperature range. This is because pure, liquid AMP is reliant on chemical absorption which slows down at low temperatures. At low temperature the gas molecules possess less kinetic energy and hence will be absorbed more slowly into the aq AMP. This is supported by the absorption kinetics of pure, liquid AMP. Initially a high absorption is seen for all temperatures which is then followed by a slower absorption, however, at -60 °C there is a large drop in absorption seen after the first 20 min (Figure 7-5). This is due to the gas initially having more kinetic energy but as time passes more and more CO_2 is dissolved into the cold liquid, hence the gas loses their kinetic energy more which led

to slow CO_2 uptake (122). Furthermore, once the liquid AMP slurry is transferred from the reactor to a glass bottle, the slurry is seen to be bubbling (Figure 7-6).

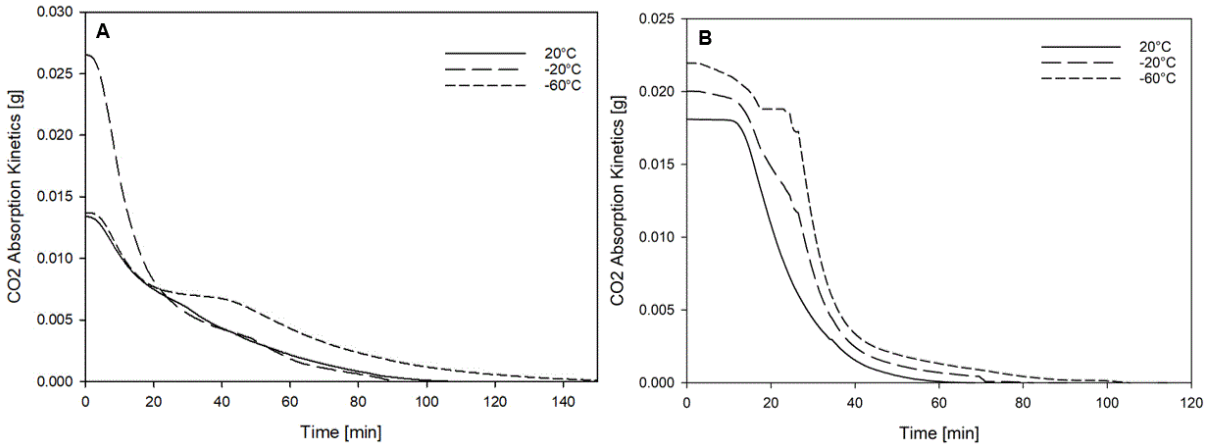

Figure 7-5 Comparison of CO2 absorption kinetics of A) pure, liquid AMP and B) formulated sample at 20 °C, -20 °C and -60 °C (0.5 wt% PGPR, 400 rpm mechanical stirrer speed, AMP core and 6-4 core-shell ratio).

The reactions of AMP with CO_2 in an aqueous solution are reversible and are known to be reliant on temperature difference (51). The CO_2 was released from the slurry, despite the desorption of AMP being thought to be at 80 °C under certain conditions. Thus, it can be concluded that CO_2 desorption occurred due to the 80 °C temperature difference between the bottle (20 °C) and the slurry (-60 °C). This phenomenon was not observed by the encapsulated sample (123)., hence making the sample more stable at -60 °C than aq AMP.

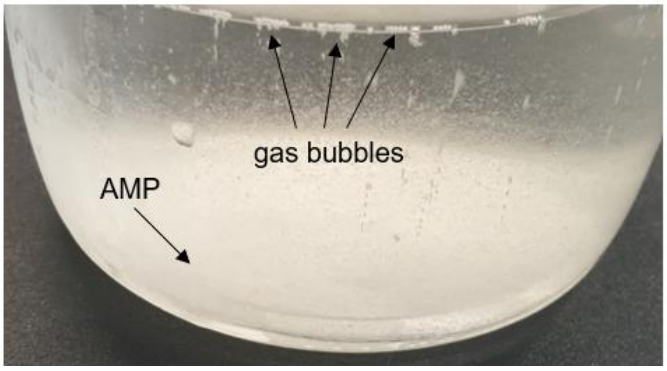

Figure 7-6 Gas bubbles observed after AMP-EtOH slurry is transferred from Reactor to glass bottle where AMP is found at bottom due to it being heavier then EtOH.

7.2.2 Effect of Emulsifiers

The use of different emulsifiers gave different absorption capacities due to the different surface properties produced. The absorption capacity of the formulated microcapsules is lowered when the emulsifier is changed from 0.5 wt% PGPR to either 1 wt% Span85 or 1 wt% Tween80 where 1 wt% Tween80 had the lowest absorption irrespective of the temperature. In comparison 0.5 wt% PGPR showed the highest absorption capacity throughout 20 °C to -60 °C. This trend is also seen in the pressure rig results at room temperature (section 6.2.3). The highest absorption was seen at -60 °C for all three samples with 0.0993 g, 0.0793 and 0.0719 g of CO_2 absorbed per g sample for 0.5 wt% PGPR, 1 wt% Span85 and 1 wt% Tween80 respectively (Figure 7-7). Correspondingly, 400 rpm sample also required more time for the absorption compared to the other two samples with 1 wt% Tween80 showing the lowest absorption time, except at -60 °C where 1 wt% Span85 showed the lowest absorption time with 78 min. This is due to the differences in microcapsule's physicochemical structure. All three samples showed a similar payload of 75-78% indicating that the absorption difference occurred due to the difference in the surface properties. Microcapsules formulated with 1 wt% Tween80 had the lowest SA with 20 m^2/g compared to 0.5 wt% PGPR (92 m^2/g) and 1 wt% Span85 (45 m^2/g). This lower SA not only slows down the absorption but also gives the gas molecules far less surface to be absorbed onto. Hence a larger SA gives higher absorption due better accessibility of the interfacial area which is favourable for CO_2 diffusion and absorption. Additionally, 1 wt% Tween80 also contained higher amounts of agglomeration which further hindered the absorption of CO_2 into the microcapsule as the smaller particles at surface potentially block the pores that lead to a decrease in the gas and microcapsule

interfacial area (110). Thus, 0.5 wt% PGPR sample gave the highest loading capacity and 1 wt% Tween80 formulated sample were unfavourable for CO_2 absorption at low temperature.

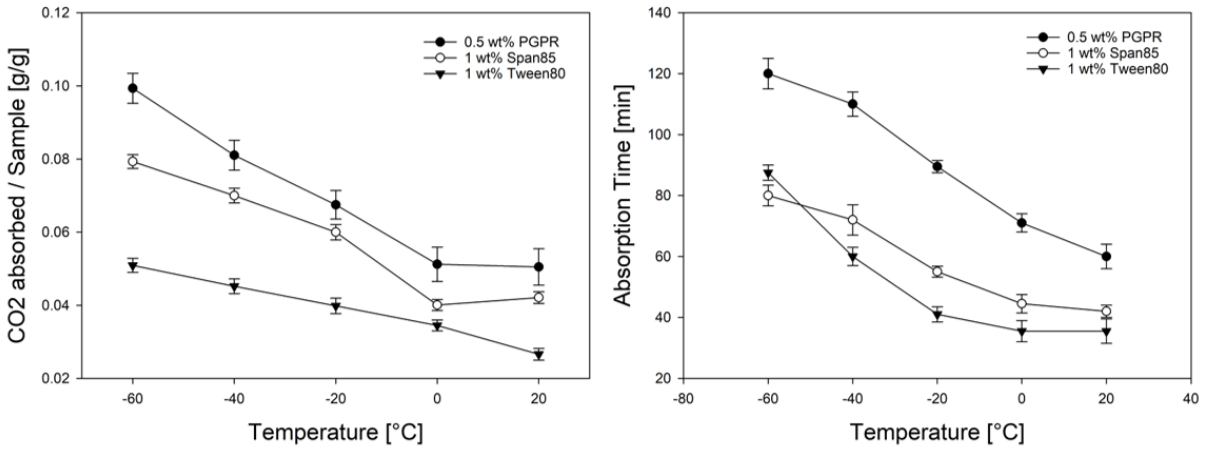

Figure 7-7 Effect of temperature on absorption capacity and absorption time of samples produced with 0.5 wt% PGPR, 1 wt% Span85 and 1 wt% Tween80 (AMP core, 6:4 core-shell ratio, 400 rpm mechanical stirrer speed and 1200 rpm homogeniser speed).

Figure 7-8 shows the absorption kinetics of the samples formulated with different emulsifiers. For 0.5 wt% PGPR sample, the highest overall absorption is seen at -60 °C with the lowest absorption kinetics seen at 20 °C (Figure 7-8A). An initial fast absorption is seen for the first 40 min which is then followed by a slower absorption where the absorption profile is similar at 20 °C and -20 °C (first 30 min) where the absorption is slower for samples exposed at 20 °C compared to -20°C. In contrast, a high and fast absorption is seen for 1 wt% Span85 sample (Figure 7-8B) during the first 10 min at 20 °C, whereas at -60 °C a steady slower CO_2 absorption over a longer time period is observed. In comparison 1 wt% Tween80 sample showed a steadily lower CO_2 loading over time at 20 °C, however, at -60 °C a fast and steady CO_2 is absorbed by sample for the first 30 minutes which is then followed by a rapid decrease in absorption and required double the amount of time to reach the equilibrium

compared to sample exposed at 20°C. At low temperature the gas solubility is increased (124) and the CO_2 absorption is a diffusion-limited process for microcapsule inside the pores, hence why a higher absorption is seen at -60 °C than room temperature, however due to less gas molecule movement, the absorption is compromised with requiring more time for absorption. Additionally, the pore size also affected the absorption kinetics. 0.5 wt% PGPR not only had the largest pore size with 43 Å compared to the other two samples but also higher pore volume (0.097 cm^3/g), hence providing for a large gas-core material interfacial area which gives higher CO_2 kinetic diffusion. This indicated that the sorption behaviour coincides with the pore volume and SA of the formulated sample (107).

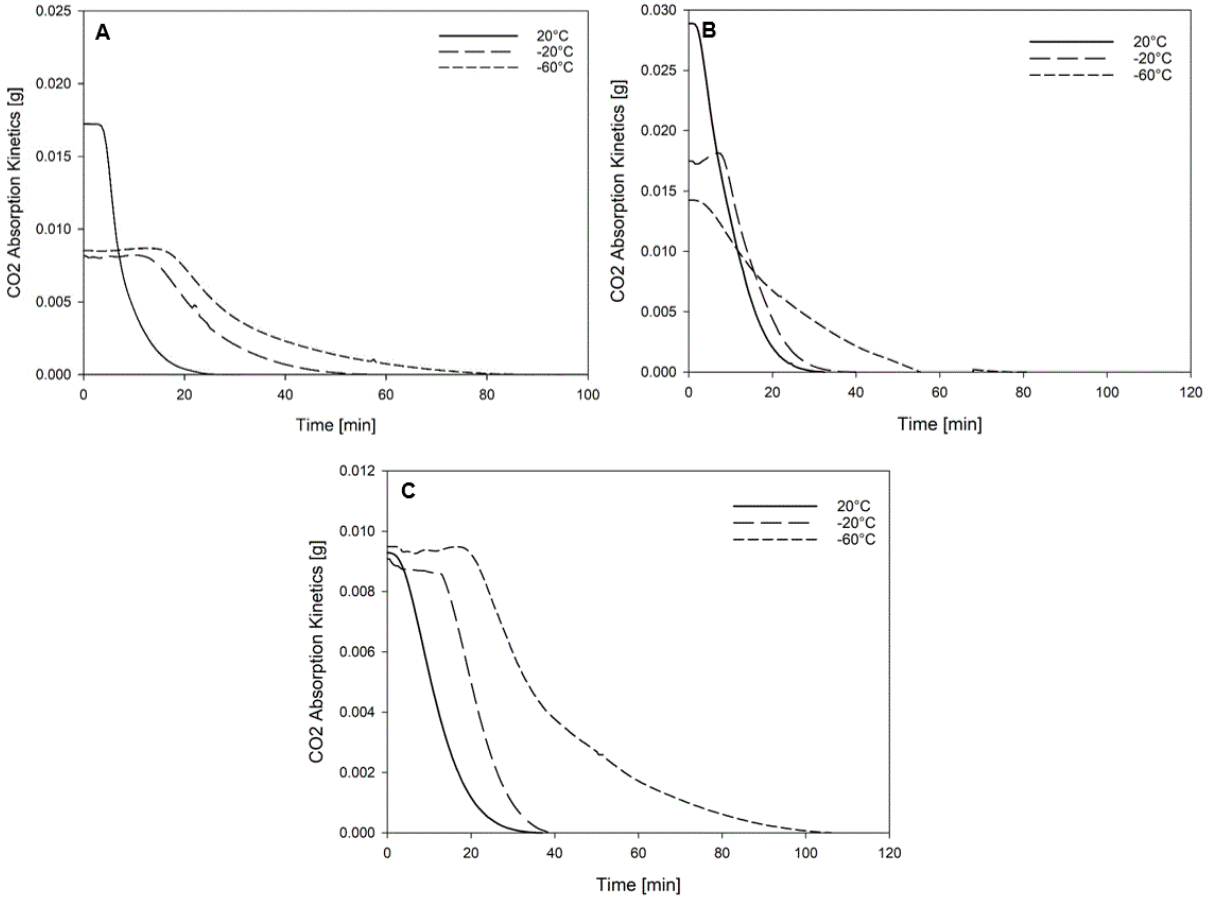

Figure 7-8 CO_2 absorption kinetics of formulated sample at 20 °C, -20 °C and -60 °C: A) 0.5 wt% PGPR; B) 1 wt% Span85; C) 1 wt% Tween80 (AMP core, 6:4 core-shell ratio, 400 rpm mechanical stirrer speed and 1200 rpm homogeniser speed).

7.2.3 Effect of Core Materials

The effect of different core materials on the absorption capacity and kinetics were also observed. Pure AMP encapsulated sample showed the largest absorption (exception at 0°C) along with the highest absorption time for all the tested temperatures. Microcapsules that contained MEA showed a steady increase in absorption over a decrease in temperature where highest absorption was seen at -60 °C with 0.0646 g (Figure 7-9). Similarly, the absorption time required to reach the equilibrium increased with an increase in absorption capacity, however the time required for MEA samples to reach the maximum capacity is nearly ½ than that of AMP encapsulated sample, e.g. MEA sample required 68 min to reach absorption limit whereas AMP sample required 120 min at -60°C. In contrast 30% TEA-70% AMP encapsulated sample showed the lowest absorption juxtapose to the other encapsulated core materials. Additionally, a very high absorption was seen at -60°C with 0.057 g (double) compared to 20 °C (0.021 g) (Figure 7-9).

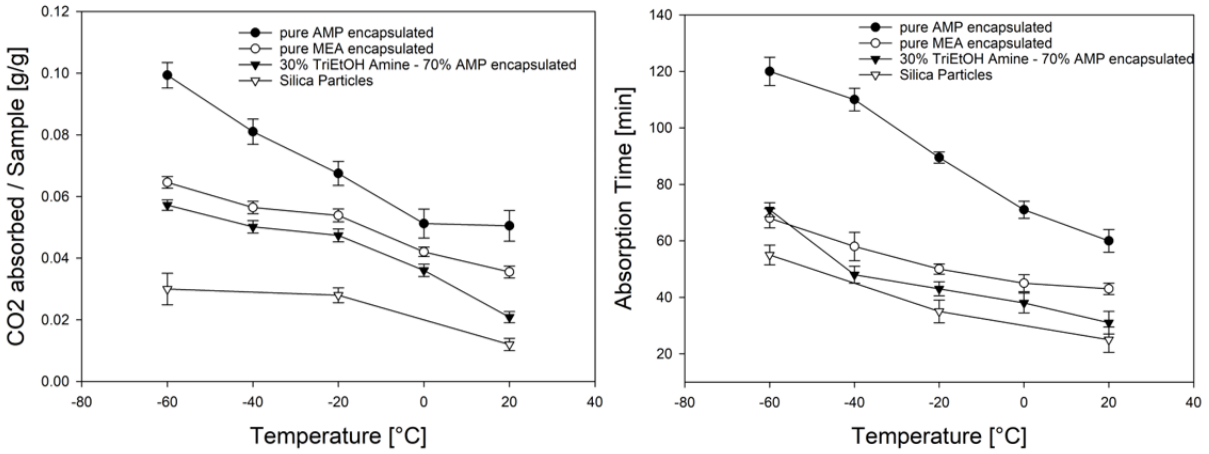

Figure 7-9 Absorption capacity of sample with different core materials A) pure AMP (100%); B) pure MEA (100%); C) 30% TEA and D) silica particles (no core) (1 wt% Span85, 6:4 core-shell ratio, 400 rpm mechanical stirrer speed and 1200 rpm homogeniser speed).

The differences in the absorption occurred due to the structural differences of the amine cores as well as the microcapsule's surface properties. MEA solution has shown to have a rapid CO_2 loading, whereas TEA and AMP are known to have slower CO_2 absorption, suggesting that the carbamate formation reactions occur rather quickly for primary amines like MEA, whereas for tertiary and sterically hindered amines the unstable carbamate formation and the following bicarbonate formation are slower in comparison. Hence why MEA containing microcapsules required less time for absorption (84). Additionally, the larger SA of these microcapsules (81 m^2/g) allowed better contact and accessibility (110). Though it would be expected for 30% TEA containing microcapsules to require more time for absorption, however, due to a lower core quantity (30%) less CO_2 capture was observed and hence less time required for the absorption (84). The experimental CO_2 absorption capacities are lower than that of literature values where AMP (aq) can capture up to 0.49 g CO_2 per g AMP and MEA (1 mol/ mol) (aq) can capture up to 0.036 g of CO_2 per g MEA (0.5 mol / mol) in a solution. The lower numbers were obtained due to the amines being encapsulated for CO_2 exposure rather than use aqueous amines. The exact CO_2 absorption values for TEA cannot be found in the literature but are known to have lower capacity than primary (MEA) and secondary (AMP) amines as they do not react directly with CO_2:

$$CO_2 + R_3N + H_2 \rightarrow HCO_3^- + R_3NH^+ \qquad \textbf{Equation 7-1}$$

TEA reacts with CO_2 by acting as a base catalyst to form bicarbonate and hydroxyl ions (Equation 7-1). During these reactions no bicarbonate ions are formed unlike with MEA and AMP, hence required less time for the loading at the cost of lower CO_2 absorption In case of MEA containing microcapsules, two molecules of amines are required to absorb one molecule of CO_2 due to the stable carbamate formation as a

consequence of its unhindered amine structure which has already been elucidated in section 6.2.5. In contrast, AMP is known to have the highest loading capacities from all the amines due to its restricted structural spin that form unstable carbamate (section 6.2.5). Hence AMP containing microcapsules exhibited the highest absorption capacity compared to the unhindered primary amine (MEA) and tertiary amine (TEA) containing microcapsules (84).

In terms of absorption kinetics, pure MEA encapsulated showed a very fast and high absorption for the first 20 min which is then followed by a steady slower CO_2 loading compared to the AMP encapsulated sample though the absorption at -60 °C is lower (Figure 7-10). But AMP containing microcapsules showed a slower absorption overall due to the absorption mechanism. This lower and slower absorption of MEA could be linked to the freezing point seen during the DSC experiment for pure, liquid MEA (5.2.1.1). The microcapsule might have already started freezing before the microcapsules had a chance to absorb CO_2. The freezing of MEA at -60 °C could potentially hinder the absorption as the MEA will be less likely to absorb CO_2. However, to be able to make more conclusive theories, MEA encapsulated sample should be observed under microscope at -60 °C to verify whether these microcapsules freeze similarly to pure, liquid MEA. 30% TEA-70% AMP encapsulated sample showed a similarly fast and high initial CO_2 absorption (20 min) which was then followed by a fast drop in absorption capacity where sample exposed to -60 °C showed the highest absorption overall. The zwitterion mechanism of AMP produces unstable products that lead to slower absorption compared to MEA/TEA containing microcapsules. TEA foregoes the need to form carbamate (slow reaction) for CO_2 capture, hence why there is a larger and longer absorption initially for the sample (84).

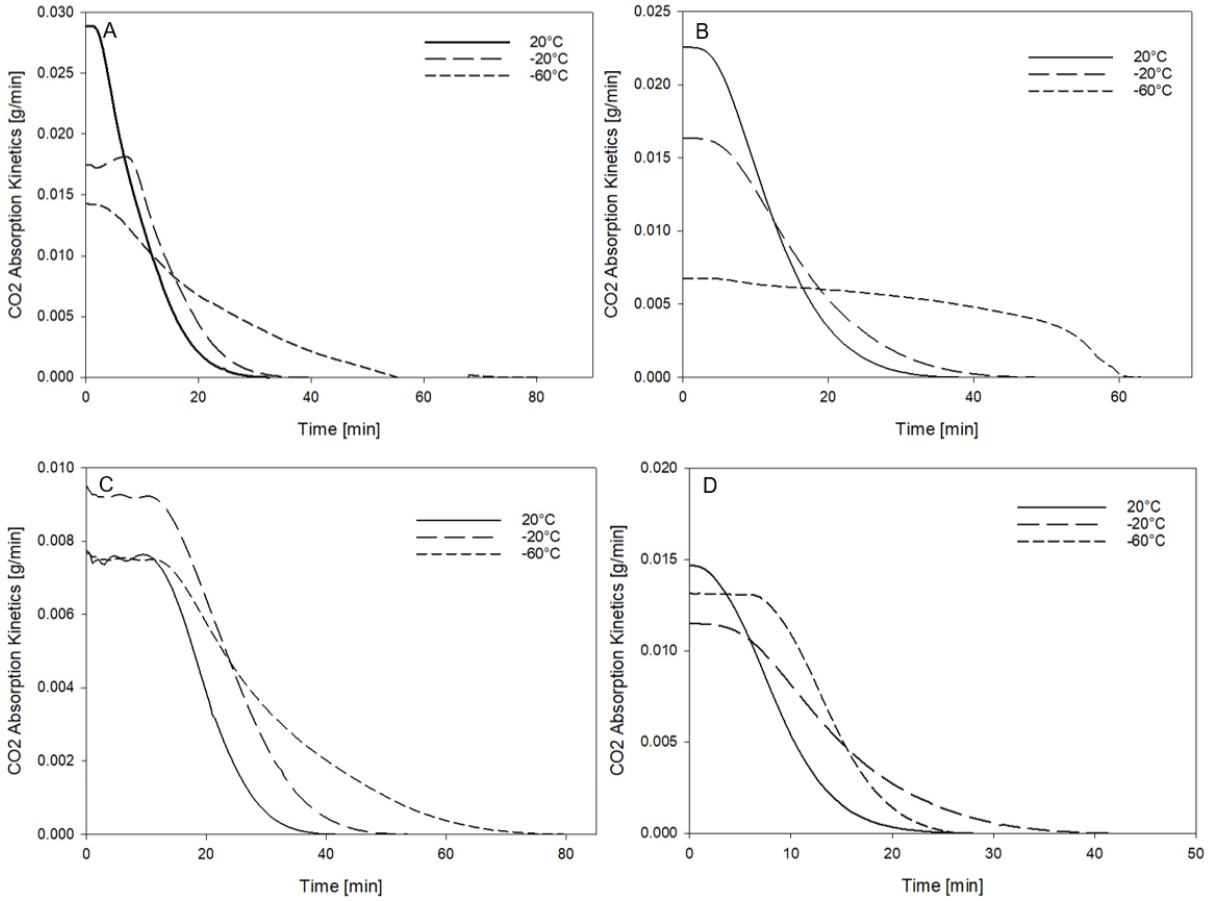

Figure 7-10 Absorption time of sample with different core materials A) pure AMP (100%); B) pure MEA (100%); C) 30% TEA and D) silica particles (no core) (1 wt% Span85, 6:4 core-shell ratio, 400 rpm mechanical stirrer speed and 1200 rpm homogeniser speed).

7.2.3.1 Silica particles

Porous materials have been considered to have CO_2 capturing potential due to their surface having an affinity for CO_2 gas molecules which determines the material's adsorption ability. It can be observed that silica particles displayed a very low absorption (0.012 – 0.03 g), whereas the silica particles exposed inside the pressure rig showed nearly no absorption. Even with a low adsorption capacity the particles required considerably high amount of time to reach their equilibrium, e.g. going from 25 min required at 20 °C to 55 min at -60 °C (Figure 7-9). Silica particles rely on the synergy effect of the pores for CO_2 adsorption, unlike the chemical absorption. Studies

have shown that generally activated carbons with a controlled pore size (> 1 nm) and pressure are able to capture CO_2 efficiently. A porous material that contains pore size larger than the kinetic diameter of a CO_2 molecule (0.33 nm) is able to adsorb CO_2, hence the silica particles with 10 Å (1 nm) pore size were able to show CO_2 loading. Additionally, the matrix structure of the particles was also able to help with the adsorption as it gave rise to internal pores. However, the pore volume of the silica particles was rather low with 0.006 cm^3/g and lower SA (40 m^2/g) than AMP or MEA containing microcapsules, giving it a low gas molecule and surface interaction hence why a very low absorption is seen with a high absorption time (125).

Additionally, these silica particles showed a faster absorption for the first 10 min compared to the microcapsules containing amine cores (Figure 7-10). Without the amine, the micropores of the particles are not blocked by the N-functional group of amines. Molecules that are amine-based and/or long-chained are able to hinder the CO_2 molecule from depositing onto the particle surface or getting access to the interparticle pores (107,125).

7.3 Design Analysis

The continuous Radley^{TM} reactor set-up allowed the obtaining of good results in terms of the effect of temperature on absorption capacity but also allowed the observation of the absorption kinetics. It is challenging to reach temperatures of -60 °C on a laboratory scale but the use of a Huber chiller (CC-902) permitted testing of below 20 °C to be possible. Additionally, very limited research has been undertaken at these temperatures. It is common knowledge that the solubility of a gas is increased with a decrease in temperature, however, whether it influences the absorption ability of

samples is not known yet. This allowed our group to contribute to this research field by giving a better understanding of the effect of low temperature on AMP, MEA and TEA containing microcapsules.

Though there are a few adjustments recommended for future or replication of the work. First, the use of an electrical flow meter would eliminate the inaccuracy of the flow meter as well as the need to manually transfer the recorded data to an excel file. Then, the Radley^{TM} reactor required that the reactor is opened after the desired temperate is reached to insert the sample-slurry. This lead to an increase in temperature inside the reactor which required 5-10 min to settle to its set temperature again. Ideally, the CO_2 absorption should start when the sample is introduced without the temperature changing from its set point.

7.4 Conclusions

Overall, a low temperature had a positive effect on the absorption capacity on the formulated sample though the effect varied with different microcapsule properties. Comparing the microcapsules formulated with different stirring speeds to give different sized microcapsules, 400 rpm sample showed the highest absorption capacity with 0.0993 g/g (-60 °C) but also faster absorption kinetics due to better surface properties like larger SA and pore volume that gave better gas-microcapsule interface. Additionally, the microencapsulated sample showed higher absorption than the pure, aq AMP (0.0889 g/g at -60 °C) which had very slow absorption kinetics in comparison. A change in emulsifier showed a similar effect of surface properties on the absorption capacity and kinetics. 0.5 wt% PGPR formulated sample had the highest capacity with

fast kinetics, whereas samples made with 1% Tween80 showed the lowest absorption with 0.0719 g CO_2/ g sample at -60 °C due to their smaller SA and pore volume.

In contrast, the change in core materials affected the absorption through the difference in the amine structures. Microcapsule containing AMP, a secondary, sterically hindered amine, showed the highest absorption capacity with 0.0793 g/g (-60 °C), whereas the absorption kinetics of the samples were slower due to the unstable carbamate formation followed by bicarbonate formation.

Taken all the factors affecting absorption in consideration, it can be concluded that 0.5 wt% PGPR with 400 rpm and AMP core gave not only the better surface properties but also the highest absorption capacities.

Chapter 8 Conclusions

The constant yearly increase in CO_2 emission due to the growing energy consumption has led to global warming that necessiates the need to address this problem (1). Hence why research has been conducted for CO_2 capture and thus various technologies and methods have been developed like CCS, CES, membranes, cryogenics and sorbents. However, most of these technologies are not mature enough to be implemented in power plants at the moment due to the high energy demand during the regeneration process (35), though the most common CO_2 absorption method is the use of MEA solvent for post-combustion process due to its high absorption capacity even though these solvents are prone to form corrosive side-products (10). This led to the need to develop new CO_2 capturing methods, hence leading to the proposal of MCES. Thus, this research focuse on the encapsulation of absorbent such as AMP, MEA and TEA for carbon capture offering the potential of combining chemical absorption of CO_2 with physical adsorption. Additionally, the effect of low temperature was studied as it is a newly discovered opportunity due to CCCS displaying its potential to give very pure flue gas stream after CO_2 capture (17), having lower cost and energy requirements for CO_2 capture (18).

8.1 Microcapsule Formulation and Characterisation

A wide range of formulaton parameters were investigated to identify the parameters that lead to successful encapsulation of CO_2 absorbents. To this end the following conditions were studied:

- Emulsifiers: PGPR (non-ionic); Span85 (mild non-ionic); Tween80 (mild non-ionic)
- Emulsifier concentrations: 0.1, 0.2, 0.3, 0.5, 1, 1.5 wt%

- Mechanical stirrer speeds: 100, 400, 600 and 800 rpm
- Homogenisation speeds: 600, 1200, 2000 rpm
- Core-shell ratios: 5:5, 6:4, 7:3, 8:2
- Core materials: AMP, MEA, TEA

For the formulation process, it was decided to use the emulsion method due to its easy set-up and as it is known to allow the size distrbution of the sample to be controlled to a certain degree. In contrast, the polymerisation can only be controlled to a small degree and introduces agglomeration inside the sample. To form the shell of the microcapsules, TEOS, silica precursors, were chosen that produced the silicon dioxiode shell of the microcapsules under basic conditions through alkaline catalysed hydrolysis and condensation which are caused by the hydroxyl ions (OH^-) of the sodium hydroxide. This polycondensation of TEOS with an amine core lead to the formation of spherical-shaped microcapsules due to the migration of the hydrolysed particles towards the core droplet interface because of the immiscibly of the materials inside the bulk phase.

Emulsifier concentrations of < 0.3 wt% led to unsuccessful encpasulation of AMP because of the unstable emulsion formation. Similarly, it was not possible to encapsulate pure, liquid TEA due to the large difference in densities between the continous and bulk phase. However, by lowering the TEA concentration through mixing it with AMP (7:3 ratio), microcapsules with 30% TEA core were formulated, indicating that the interfacial tension of the core was low enough for good encapsulation. By comparing the samples in terms of morphology and agglomeration, it was seen that a higher stirring speed during formulation led to higher agglomeration due to larger energy distribution which led to more core droplet collisions. Likewise, a higher core-

shell ratio resulted in higher agglomeration as the core concentration is too high, hence resulting in part of it not getting encapsulated. However, comparing the samples in terms of quality 1 wt% Span85 with a 6:4 core-shell ratio (400 rpm and mechanical stirrer 1200 rpm mechanical stirrer speed) showed the least amount of agglomeration with a smoother surface finish.

After formulating the microcapsules under different conditions, the effect of the formulation parameters on the microcapsules was investigated. The aim was to expose the microcpasules to low temperatures, hence the thermal properties of the encapsulated samples as well the liquid core materials were explored. The results from the DSC showed that the microcapsules did not undergo phase change while being exposed to 20 °C to -60 °C, thus indicating their stability at that temperature range. This is advantageous as a phase change might lead to a decrease in CO_2 sorption capability. For recycling of the microcapsules, the samples were exposed to 10 thermal cycles from 20 °C to -10 °C which showed that most microcapules were able to withstand the thermal damage except the occasional cracks and dents found. The use of an emulsion for encapsulation process required the use of homogeniser and mechanical stirrer. The mechanical stirrer created shear forces that were not even across the system which resulted in a wide sample size distribution. Additionally, higher stirring speed like 600 rpm led to higher collision of the core droplets inside the emulsion, hence giving the sample more agglomeration in the end. To this end, homogenisers were used to try to control the size distrbution by reducing the droplet size in the liquid dispersion which did result in a less polydispersed particle size distribution with the samples formulated with a homogeniser. The homogeniser and mechanical stirrer also affected the SA of the samples. A higher stirring speed gave a

smaller SA, e.g. samples formulated with 600 rpm had a SA of 34 m^2/g with a pore size of 72 Å compared to samples formulated with 400 rpm which had a SA of 92 m^2/g and pore size of 43 Å. Larger pore size is advantageous for gas absorption as it allows faster diffusion into the material. In contrast, a change in the emulsifier from PGPR to Span85 decreased the SA fom 92 m^2/g to 45 m^2/g which is not favourable as it decreases the contact surface for the gas to diffuse into. In comparison, the use of a high core material concentration (8:2 ratio) produced microcapsules with a rougher surface and high SA, however the PS and PV were smaller than that of the samples formulated with 6:4 core-shell ratio with 0.07 m^2/g and 19 Å. Another factor of importance to the absorption capacity is the payload. Most of the formulated samples irrespective of the formulation conditions showed a similar payload (70 – 80%) with the exception of MEA and TEA core where the payload decreased to 65% and 55% respectively due to the formulation process being hindered by the larger difference in the densities of the continuous and bulk phases (Figure 4-15).

All in all, it can be concluded that predicting the effect of formulation parameters on the microcapsules properties is challenging and in-depth chemistry knowledge is required for good encapsulation understanding.

8.2 CO_2 Absorption

To confirm that the microcapsules are able to capture CO_2, a TG was connected to a carbon dioxide cylinder. The initial CO_2 absorption tests showed an increase in sample weight during CO_2 exposure, thus proving that the formulated samples captured carbon. Another indicator suggesting towards successful CO_2 capture is the colour change from blue to yellow that occurred to the presence of thymol blue which occurs due a drop in pH (from pH > 11 to pH < 6). This is a method that was used by Vericella

et. al. for visual CO_2 absorption due to the reaction of CO_2 with amine that leads to carbamate formation (104). The colour change inside the sample occurred due to reaching 90% of the maximum carbon uptake through chemical absorption. This method was not able to give a quantitate enough method for identifying the loading capacity and absorption kinetics of the samples, hence a pressure rig and a continuous reactor were set-up to identify the effect of size (SA), core material and emulsifiers on the absorption capacity of the formulated samples.

The availability of the SA is important for CO_2 diffusion and absorption; thus, it controls the absorption capacity to a certain degree. Though at room temperature payload also plays an important role in the chemical absorption of CO_2. However, if the payloads of the formulated samples are similar to each other, then the SA has a greater effect on the absorption, thus, sample formulated with 400 rpm (AMP core, 0.5 wt% PGPR, 6:4 core-shell ratio, 400 rpm mechanical stirrer and 12000 rpm homogeniser speed) displayed the best balance between the absorption (0.187 g/g) and its surface properties (92 cm^2/g) as well as payload capacity (75%). The higher SA of these microcapsules gave the gas a larger interfacial area and thus facilitated easier diffusion which leads to better and higher CO_2 absorption. Though the absorption capacity of the encapsulated sample compared to the pure, liquid amine (0.29 g/g) was significantly lower due to the lower amine quantity inside the microcapsules. At room temperature the chemical absorption is predominant since the silica particles only showed very low absorption (< 0.05 g/g). Additionally, the liquid AMP underwent a phase change from a liquid to a solid due to the carbamate formation. The microcapsules exposed to CO_2 show a similar phase change by becoming hard from being a soft solid. In contrast, microcapsules with a lower SA and higher

agglomeration, gave a lower absorption capacity due to less surface being available for the gas molecules to diffuse into as well as the agglomerates blocking the pores, hence 1 wt% Tween80 showed the lowest absorption with 0.156 g/g compared to the other two emulsifiers. Furthermore, samples with a lower amine concentrations, i.e. payload, like the 30% TEA encapsulated sample showed the lowest absorption due to their very low SA (20 cm^2/g) and low payload (52%) due to the absorption being hindered because of the low water content in the sample as water is required for the carbamate/bicarbonate formation, hence a much lower CO_2 absorption is seen with 30% TEA.

An increase in temperature decreases the solubility of a gas, hence lower temperatures were used for absorption testing to not only increase the CO_2 solubility into the liquids but also to potentially increase physical adsorption of CO_2 onto the microcapsules surface. To this end, the continuous reactor was set-up. Furthermore, the post-combustion CO_2 capture uses ambient pressure, hence why this provides a more effective testing environment. Generally, a low temperature had a positive effect on the samples absorption capacity though the effect varied with different microcapsules due to their difference in properties. Instead of size having a large impact on the absorption, the SA again affected the absorption capacity. Microcapsules formulated with 400 rpm showed the highest absorption capacity with 0.0993 g/g at -60 °C but also faster absorption kinetics despite being smaller in size (average size 120 µm) compared to samples with 100 rpm and 600 rpm formulation speed due to better surface properties like larger SA and pore volume that gave better gas-microcapsule interface. Though the aqueous AMP in comparison showed a larger absorption capacity with 0.0889 g/g but with very slow absorption kinetics. A change

in emulsifier showed a similar effect of surface properties on the absorption capacity and kinetics. 0.5 wt% PGPR formulated sample had the highest capacity with fast kinetics, whereas samples made with 1% Tween80 showed the lowest absorption with 0.0719 g/g at -60 °C due to their smaller SA and pore volume. In contrast, the change in core materials affected the absorption through the difference in the amine structures. Microcapsule containing AMP, a secondary, sterically hindered amine, showed the highest absorption capacity with 0.0793 g/g (-60 °C), whereas the absorption kinetics of the samples were slower due to the unstable carbamate formation followed by bicarbonate formation. Thus, sample formulated with MEA showed faster absorption kinetics though with lower absorption capacity (0.0646 g/g). Overall, sample formulated with 0.5 wt% PGPR with 400 rpm and AMP core gave not only the better surface properties but also the highest absorption capacities.

8.3 Future Work

This research has contributed to the development of a novel microencapsulated carbon sorbent approach for potential post-combustion CO_2 absorption system. However, the proposed work still requires several improvements prior to the development of this technology and it being robust enough for future applications.

8.3.1 Formulation

The in-situ polymerisation selected for the formulation method allowed limited control over the size distribution, hence why a microfluidic device is proposed to produce accurate, one-sized microcapsules. This method is based on double emulsion which requires more solvent, oil, middle and inner fluids compatible with one another, hence

making the set-up more challenging. However, once a successful microfluidic device is set-up it would allow good control over shape, size and composition of the microcapsules (44).

It is also recommended to investigate the effect of pH during the formulation process due to previous research showing that pH controls the reactions during the polymerisation. Hence, it is recommended that future work includes monitoring of pH during the formulation and maintaining a constant pH throughout the whole process (48,86). Furthermore, to formulate core-shell type of microcapsules, it would be best to replace TEOS a shell material like NOA, Norton Optical Adhesives as they have shown to be able to encapsulate carbonates for CO_2 capture to form a core-shell type microcapsule by Vericella et. al. (26).

To ensure that single microcapsules are formulated instead of agglomerated sample it is recommended to improve the drying process to find a solvent that will only dissolve the polymeric species and will not affect the microcapsule at all to reduce the agglomeration of the formulated sample. This would allow the microcapsules to be characterised further and allow a better understanding of the relationship between the absorption properties and the microcapsules property.

8.3.2 Microcapsules Characterisation

Obtaining the shell thickness is important and could give further insight on the CO_2 diffusion into the microcapsules, hence why it is proposed to measure the shell thickness either with a CryoTEM or FIB-SEM (Focused Ion Beam SEM). Both would not only be able to obtain the average shell thickness but also the internal structure.

This could then be linked to the absorption properties to provide further information on the microcapsules structural properties effect on the CO_2 absorption.

Furthermore, more than 10 thermal cyclings are recommend for CO_2 absorption testing to replicate the environment of the materials in real applications. At least 100 thermal cycling should be conducted to get a better understanding of the materials recyclability.

It is also important to test the thermal properties of the used materials at the specific testing temperatures, e.g. if the material/ microcapsules are supposed to be used at -100°C then the material needs to be tested at that temperature to get a good understanding of the materials phase change if there is any.

8.3.3 CO_2 Absorption

The encapsulation of amine sorbents for CO_2 capture showed potential for industrial application both for post-combustion process and low temperature CO_2 capture combined with energy storage as described in Chapter 6 and Chapter 7. However, it would be recommended to use a gas mixture similar to the flue gas composition of a power plant to observe the absorption capability. This would give a better understanding of the microcapsule's interaction with the flue gas and potentially allow a better insight on the potential industrial applications.

Good results were obtained from the continuous Radley^{TM} reactor set-up regarding the absorption capacity and kinetics and allowed this research to contribute to this research field. Though it would be recommended to replace the conventional gas flow meters with digital mass flow meters for more accurate kinetic studies and to lower the error margin due to the ability of being able to calibrate a digital mass flow meter against the specific gas employed. Furthermore, it would be suggested to study the

effect of low temperature (< -60 °C) on the CO_2 absorption of carbon sorbents to provide further insight since this temperature range has not been explored previously. An alternative method for static or dry sample CO_2 absorption testing is the magnetic suspension balance. This method allows better control of temperature, pressure and weight change during the experimental testing, thus allowing the study of the sorption interaction, diffusion, surface tension, density, chemical compositions (decomposition, corrosion) and product process (drying, polymerisation) of materials (116,117).

The end aim of this research is to use the microcapsules in CCC system, hence why it is important to test the proposed materials for CO_2 capture at a minimum temperature of -100°C to reproduce the CCC conditions during testing which unfortunately were not achievable during this thesis. A lower testing temperature would provide better insight on how the microcapsules would behave during the real application. Additionally, to further support the laboratory results, it is suggested to do some simulations by exposing the microcapsules to different conditions that they would be exposed to inside the CCC system or in real life application. This would provide the theoretical explanation behind the phenomena happening at low temperatures.

Appendix A: Cubic Equation of State Supplementary data

The following excel data sheet was used to obtain the CO_2 densities at different temperatures to calculate the absorbed mass:

Solving Cubic Equation of State

CheGuide.com		*Date*	*9-Aug-2015*
Chemical Engineer's Guide		*By*	*CheGuide*

Chemical	CARBON DIOXIDE				
Properties					
Molecular Weight	44.01				
Critical Temperature	304.2	Deg K			
Critical Pressure	73.765	Bar			
Accentric Factor	0.2250				
Calculation at					
Pressure	30	Bar	Reduced Pressure	0.407	
Temperature	285	Deg K	Reduced Temp.	0.937	
Gas Constant, R	8.3145				

Soave Redlich Kwong (SRK) Equation of State				**Result**	
Equation is reduced to form	$Z^3 - Z^2 + CZ - D = 0$			Z	0.8002
α	1.0536	C	0.1697	ρ	69.63 Kg/m^3
A	0.2087	D	0.0078	V	0.6321 $m^3/kmol$
B	0.0376				

Peng Robinson (PR) Equation of State				**Result**	
Equation is reduced to form	$Z^3 - CZ^2 + DZ - E = 0$			Z	0.7845
α	1.0459	C	0.9662	ρ	71.03 Kg/m^3
A	0.2216	D	0.1506	V	0.6196 $m^3/kmol$
B	0.0338	E	0.0063		

References

1. Florin N, Fennell P. Carbon capture technology: future fossil fuel use and mitigating climate change. Grantham Inst Clim Chang Brief Pap. 2010;3(3):20.
2. Anderegg WRL, Prall JW, Harold J, Schneider SH. Expert credibility in climate change. Proc Natl Acad Sci U S A. 2010;107(27):12107–9.
3. Leung DYC, Caramanna G, Maroto-Valer MM. An overview of current status of carbon dioxide capture and storage technologies. Renew Sustain Energy Rev. 2014;39:426–43.
4. Zhang X, Zhang X, Dong H, Zhao Z, Zhang S, Huang Y. Carbon capture with ionic liquids: overview and progress. Energy Environ Sci. 2012;5:6668.
5. Leung DYC, Caramanna G, Maroto-Valer MM. An overview of current status of carbon dioxide capture and storage technologies. Renew Sustain Energy Rev. 2014;39:426–43.
6. Kargari A, Ravanchi MT. Carbon Dioxide: Capturing and Utilization.
7. Climate G, Project E. Global Climate & Energy Project An Assessment of Carbon Capture Technology and Research Opportunities. Assessment. 2005;1–20.
8. Kenarsari SD, Yang D, Jiang G, Zhang S, Wang J, Russell AG, et al. Review of recent advances in carbon dioxide separation and capture. RSC Adv. 2013;3(45).
9. International Energy Agency. CO2 Emissions From Fuel Combustion Highlights 2015. IEA Publications. Paris; 2015.
10. CO2 Capture Project. Three basic methods to separate gases. CO2 Capture Proj. 2008;1–2.
11. CCOHS (Canadian Centre for Occupational Health and Safety). Cryogenic Liquids - Hazards : OSH Answers [Internet]. 2015 [cited 2017 Mar 15]. Available from: http://www.ccohs.ca/oshanswers/chemicals/cryogenic/cryogen1.html
12. Haijun B, Ψ , Xu W, Li X, Yu Q. A Novel Process for Natural Gas Liquids Recovery from Oil Field Associated Gas with Liquefied Natural Gas Cryogenic Energy Utilization. Process Syst Eng Chinese J Chem Eng. 2011;19(3):452–61.
13. Fox T, Ceng TF, Cenv F. Storing Electricity Using Cryogenic Technology in a UK

Policy Context 2012 Energy Storage Symposium Storing Electricity Using Cryogenic Technology in a UK Policy Context.

14. Highview Enterprise Limited. Liquid Air Energy Storage (LAES): from Pilot Plant to Multi MW Demonstration Plant. 2014;
15. Gibson E. Liquid Air Energy Storage (LAES): from Pilot Plant to Multi MW Demonstration Plant. PowerGen Eur 2014 Conf. 2014;
16. Sustainable Energy Solutions. Cryogenic Carbon Capture. Sustain Energy Solut Bookl. 2009;
17. James DW. Failing Drop CO2 Deposition (Desublimation) Heat Exchanger for the Cryogenic Carbon Capture Process. Thesis. 2011;
18. De-ar AP, Case B. Cryogenic carbon capture. 2012;1–2.
19. Baxter L, Baxter A, Burt S. Cryogenic CO2 Capture as a Cost-Effective CO2 Capture Process. 2009.
20. Zou J, Ho WSW. CO2-selective polymeric membranes containing amines in crosslinked poly(vinyl alcohol). J Memb Sci. 2006;286(1–2):310–21.
21. Tuinier MJ, Hamers HP, Van Sint Annaland M. Techno-economic evaluation of cryogenic CO2 capture-A comparison with absorption and membrane technology. Int J Greenh Gas Control. 2011;5(6):1559–65.
22. Li P, Tezel FH. Equilibrium and kinetic analysis of CO2-N2 adsorption separation by concentration pulse chromatography. J Colloid Interface Sci. 2007;313(1):12–7.
23. Li M, Jiang X, He G. Application of membrane separation technology in postcombustion carbon dioxide capture process. Front Chem Sci Eng. 2014;8(2):233–9.
24. Desideri U. Advanced absorption processes and technology for carbon dioxide (CO2) capture in power plants. In: Developments and Innovation in Carbon Dioxide (CO2) Capture and Storage Technology. Elsevier; 2010. p. 155–82.
25. Dai Z, Noble RD, Gin DL, Zhang X, Deng L. Combination of ionic liquids with membrane technology: A new approach for CO2 separation. J Memb Sci. 2016;497:1–20.
26. Vericella JJ, Baker SE, Stolaroff JK, Duoss EB, Hardin JO, Lewicki J, et al. Encapsulated liquid sorbents for carbon dioxide capture. Nat Commun.

2015;6(November):6124.

27. Davidson RM. Post-combustion carbon capture- solid sorbents and membranes. IEA Clean Coal Cent Reports. 2009;(March):1–68.
28. Sunday Ume C, Alper EG. Reaction kinetics of carbon dioxide with 2-amino-2-hydroxymethyl-1,3-propanediol in aqueous solution obtained from the stopped flow method. Turk J Chem. 2012;36:427–35.
29. Rao AB, Rubin ES, Berkenpas MB. An Integrated Modeling Framework for Carbon Management Technologies. Tech Doc Amin CO 2 Capture Storage Syst Foss Fuel Power Plant. 1.
30. Fredriksen SB, Jens K-J. Oxidative degradation of aqueous amine solutions of MEA, AMP, MDEA, Pz: A review. Energy Procedia. 2013;37:1770–7.
31. Sartori G, Savage DW. Sterically hindered amines for carbon dioxide removal from gases. Ind Eng Chem Fundam. 1983 May;22(2):239–49.
32. Vericella JJ, Baker SE, Stolaroff JK, Duoss EB, Hardin JO, Lewicki J, et al. Encapsulated liquid sorbents for carbon dioxide capture. Nat Commun. 2015;6:6124.
33. Stolaroff JK, Bourcier WL. Thermodynamic assessment of microencapsulated sodium carbonate slurry for carbon capture. Energy Procedia. 2014;63:2331–5.
34. Samanta A, Zhao A, Shimizu GKH, Sarkar P, Gupta R. Post-combustion CO 2 capture using solid sorbents: A review. Ind Eng Chem Res. 2012;51(4):1438–63.
35. Gray ML, Champagne KJ, Fauth D, Baltrus JP, Pennline H. Performance of immobilized tertiary amine solid sorbents for the capture of carbon dioxide. Int J Green. 2008;2:3–8.
36. Stolaroff JK, Ye C, Oakdale JS, Baker SE, Smith WL, Nguyen DT, et al. Microencapsulation of advanced solvents for carbon capture. Faraday Discuss. 2016;192(0):271–81.
37. Vericella J. Microfluidic Encapsulation of Carbon Capture Materials. 2012;
38. Hasib-ur-Rahman M, Siaj M, Larachi F. Ionic liquids for CO2 capture-Development and progress. Chem Eng Process Process Intensif. 2010;49(4):313–22.
39. Fardad MA. Catalysts and the structure of SiO 2 sol-gel films. 3(52):1835–41.

40. Kobayashi Y, Inose H, Nakagawa T, Gonda K, Takeda M, Ohuchi N, et al. Control of shell thickness in silica-coating of Au nanoparticles and their X-ray imaging properties. J Colloid Interface Sci. 2011;358:329–33.
41. Microtek Laboratories I. Technical Overview: Microencapsulation. 2017.
42. House of Commons Energy and Climate Change Committee Carbon capture and storage. Carbon Capture and Storage. Ninth Rep Sess 2013–14. 2014;(London: The Stationery Office Limited).
43. Jyothi Sri S, Seethadevi A, Suria Prabha K, Muthuprasanna P, Pavitra P. Microencapsulation: A review. Int J Pharma Bio Sci. 2012;3(1):P509–31.
44. Shah RK, Shum HC, Rowat AC, Lee D, Agresti JJ, Utada AS, et al. Designer emulsions using microfluidics. Mater Today. 2008;11:18–27.
45. CHANG TM. Semipermeable Microcapsules. Science. 1964 Oct 23;146(3643):524–5.
46. Berkland C, Kim K, Pack DW. PLG microsphere size controls drug release rate through several competing factors. Pharm Res. 2003 Jul;20(7):1055–62.
47. Madhu Mn, Banji D. A Review on Microencapsulation. Int J Pharm Sci Rev Res. 5(2).
48. Jyothi NVN, Prasanna PM, Sakarkar SN, Prabha KS, Ramaiah PS, Srawan GY. Microencapsulation techniques, factors influencing encapsulation efficiency. J Microencapsul. 2010;27(3):187–97.
49. Bastida-Rodríguez J. The Food Additive Polyglycerol Polyricinoleate (E-476): Structure, Applications, and Production Methods. ISRN Chem Eng. 2013;2013:1–21.
50. Ben-Mansour R, Habib MA, Bamidele OE, Basha M, Qasem NAA, Peedikakkal A, et al. Carbon capture by physical adsorption: Materials, experimental investigations and numerical modeling and simulations - A review. Appl Energy. 2016;161:225–55.
51. Xu S, Wang YW, Otto FD, Mather AE. Kinetics of the reaction of carbon dioxide with 2-amino-2-methyl-1-propanol solutions. Chem Eng Sci. 1996;51(6):841–50.
52. Rama S, Zhang Y, Tchuenbou-Magaia F, Ding Y, Li Y. Encapsulation of 2-amino-2-methyl-1-propanol with tetraethyl orthosilicate for CO2 capture. Frontiers of Chemical Science and Engineering. Springer; 2019.

53. Laurén S. Surface and interfacial tension -What is it and how to measure it? White Pap. 2017;
54. Lowell S, Shields JE, Thomas MA, Thommes M. Surface Area Analysis from the Langmuir and BET Theories. In 2004. p. 58–81.
55. Micromeritics Instrument Corporation. TriStar II 3020 Analyzer - Service Manual. 2009;48.
56. Malvern Instruments. Mastersizer 2000 User Manual. 2000;
57. Nielsen CJ, Herrmann H, Weller C. Atmospheric chemistry and environmental impact of the use of amines in carbon capture and storage (CCS). Chem Soc Rev. 2012;41(19):6684.
58. 1-Propanol, 2-amino-2-methyl-. National Institute of Standards and Technology;
59. Ebert DD, Nobis S, Lehr D, Baumeister H, Riper H, Auerbach RP, et al. Differential Scanning Calorimetry Techniques: Applications in Biology and Nanoscience. Diabet Med. 2017;34(1):99–107.
60. Lopez-Echeverry JS, Reif-Acherman S, Araujo-Lopez E. Peng-Robinson equation of state: 40 years through cubics. Fluid Phase Equilib. 2017 Sep 15;447:39–71.
61. CheGuide. Excel Spreadsheet for Solving Cubic Equation of State [Internet]. 2019 [cited 2019 Oct 31]. Available from: https://cheguide.com/cubic_eos.html
62. Vogt M, Pasel C, Bathen D. Characterisation of CO2 absorption in various solvents for PCC applications by Raman spectroscopy. Energy Procedia. 2011;4:1520–5.
63. Shimekit B, Mukhtar H. Natural Gas Purification Technologies - Major Advances for CO2 Separation and Future Directions. In: Advances in Natural Gas Technology. InTech; 2012.
64. Innocenzi P. From the Precursor to a Sol. In: Measuring the Sol to Gel Transition. 2016. p. 7–24.
65. Al. SB et. Sodium hydroxide catalyzed monodispersed high surface area silica nanoparticles. Mater Res Express. 2015;14(11):871–82.
66. Brinker CJ. HYDROLYSIS AND CONDENSATION OF SILICATES: EFFECTS ON STRUCTURE. Vol. 100, Journal of Non-Crystalline Solids. 1988.
67. Rahman IA, Padavettan V. Synthesis of Silica Nanoparticles by Sol-Gel : Size-

Dependent Properties , Surface Modification , and Applications in Silica-Polymer Nanocomposites — A Review. 2012;2012.

68. Wang R, Li H, Liu W, He & X, He X. Surface Modification of Poly(urea-formaldehyde) Microcapsules and the Effect on the Epoxy Composites Performance. 2010;
69. Author C, Kuriokase B, Padma S, Padma Priya S. A Review on Microcapsules. Glob J Pharmacol. 2015;9(1):28–39.
70. Tarcha PJ. Polymers for controlled drug delivery. CRC Press; 1991. 286 p.
71. Chang C, Fogler HS. Controlled Formation of Silica Particles from Tetraethyl Orthosilicate in Nonionic Water-in-Oil Microemulsions. 1997;7463(12):3295–307.
72. Chang Q. Emulsion , Foam , and Gel. In: Colloid and Interface Chemistry for Water Quality Control. 2016. p. 227–30.
73. Span® 85 CAS 26266-58-0 | 840124 [Internet]. [cited 2019 Jul 22]. Available from: http://www.merckmillipore.com/GB/en/product/Span-85,MDA_CHEM-840124?ReferrerURL=https%3A%2F%2Fwww.google.com%2F
74. Croda Europe Ltd. Span and Tween HLBs. WwwCrodaCom/Europe. 2009;44(0):6–11.
75. 1,2,3-Propanetriol, homopolymer, (9Z,12R)-12-hydroxy-9-octadecenoate | - PubChem [Internet]. [cited 2019 Jul 22]. Available from: https://pubchem.ncbi.nlm.nih.gov/compound/6441835
76. 2-[2-[3,4-Bis(2-hydroxyethoxy)oxolan-2-yl]-2-(2-hydroxyethoxy)ethoxy]ethyl octadec-9-enoate | C32H60O10 - PubChem [Internet]. [cited 2019 Jul 22]. Available from: https://pubchem.ncbi.nlm.nih.gov/compound/443315
77. Span(R) 20 | - PubChem [Internet]. [cited 2019 Jul 22]. Available from: https://pubchem.ncbi.nlm.nih.gov/compound/Span_R_-20
78. Bennion EB, Bamford GST, Bennion EB, Bamford GST, Bent AJ. Emulsions and emulsifiers. Technol Cake Mak. 2013;112–20.
79. Welsh LM, Davis RA. Density and Viscosity of Aqueous Blends of N-Methyldiethanolamine and 2-Amino-2-methyl-l-propanol. Vol. 40, J. Chem. Eng. Data. 1995.
80. Amundsen TG, Øi LE, Eimer DA. Density and Viscosity of Monoethanolamine +

Water + Carbon Dioxide from (25 to 80) °C.

81. Li X-X, Fan G-C, Zhang Z-L, Wang Y-W, Lu Y-Q. Density and Viscosity for Binary Mixtures of Diethylene Glycol Monobutyl Ether with Monoethanolamine, Diethanolamine, and Triethanolamine from (293.15 to 333.15) K. 2013;
82. Juttulapa M, Piriyaprasarth S, Takeuchi H, Sriamornsak P. Effect of high-pressure homogenization on stability of emulsions containing zein and pectin. Asian J Pharm Sci. 2017;12(1):21–7.
83. Weiss, JochenNatsir Sandiah, Petrus Dominggus Sadsoeitoeboen MRA dan H. Principle of Emulsion Formation. Weiss, JochenNatsir Sandiah, Petrus Dominggus Sadsoeitoeboen, Muhamad Rizal Amin dan Herdis Emuls Work Novemb 13-14th, 2008, Amherst, MA 1 *Food Struct Funct Lab Dep Food Sci Biotechnol Univ Hoh. 2008;1–50.
84. Kim YE, Lim JA, Jeong SK, Yoon Y Il, Bae ST, Nam SC. Comparison of carbon dioxide absorption in aqueous MEA, DEA, TEA, and AMP solutions. Bull Korean Chem Soc. 2013;34(3):783–7.
85. Jo E, Jhon YH, Choi SB, Shim J-G, Kim J-H, Lee JH, et al. Crystal structure and electronic properties of 2-amino-2-methyl-1-propanol (AMP) carbamate. Chem Commun (Camb). 2010;46(48):9158–60.
86. Shima M, Kobayashi Y, Kimura Y, Adachi S, Matsuno R. Effect of the hydrophilic surfactants on the preparation and encapsulation efficiency in course and fine W/O/W type emulsions. Physicochem Eng Asp. 2004;238:83–90.
87. Ashworth EN, Abeles FB. Freezing behavior of water in small pores and the possible role in the freezing of plant tissues. Plant Physiol. 1984;76(1):201–4.
88. Agbadua SA, Mgbemena CO, Mgbemena CE, Chima LO. Thermal Cycling Effects on the Fatigue Behaviour of Low Carbon Steel. J Miner Mater Charact Eng. 2011;10(14):1345–57.
89. Vysloužil J, Doležel P, Kejdušová M, Mašková E, Mašek J, Lukáč R, et al. Influence of different formulations and process parameters during the preparation of drug-loaded PLGA microspheres evaluated by multivariate data analysis. Acta Pharm. 2014;64(4):403–17.
90. Tamilvanan S, Sa B. Effect of production variables on the physical characteristics of ibuprofen-loaded polystyrene microparticles. J Microencapsul.

1999;16(4):411–8.

91. Yow HN, Routh AF. Formation of liquid core-polymer shell microcapsules. Soft Matter. 2006;2(11):940.
92. Liu M. Understanding the Mechanical Strength of Microcapsules and Their Adhesion on Fabric Surfaces. Measurement. 2010;(April):281.
93. Kim MS, Seok SI, Ahn BY, Koo SM, Paik SU. Encapsulation of water-soluble dye in spherical sol-gel silica matrices. J Sol-Gel Sci Technol. 2003;27(3):355–61.
94. Su JF, Wang XY, Dong H. Micromechanical properties of melamine-formaldehyde microcapsules by nanoindentation: Effect of size and shell thickness. Mater Lett. 2012;89:1–4.
95. Liao LP, Zhang W, Xin Y, Wang HM, Zhao Y, Li WJ. Preparation and characterization of microcapsule containing epoxy resin and its self-healing performance of anticorrosion covering material. Chinese Sci Bull. 2011;56(4–5):439–43.
96. Majury TG. Amines and carboxylic acids as initiators of polymerization in caprolactam. J Polym Sci. 1958 Sep;31(123):383–97.
97. Wan Isahak WNR, Che Ramli ZA, Mohamed Hisham MW, Yarmo MA. The formation of a series of carbonates from carbon dioxide: Capturing and utilisation. Renew Sustain Energy Rev. 2015;47:93–106.
98. Paridah M., Moradbak A, Mohamed A., Owolabi F abdulwahab taiwo, Asniza M, Abdul Khalid SH. Advantages and Limitations of Using FTIR Spectroscopy for Assessing the Maturity of Sewage Sludge and Olive Oil Waste Co-composts. Intech. 2016;i(tourism):13.
99. Gray A, Egan S, Bakalis S, Zhang Z. Determination of microcapsule physicochemical, structural, and mechanical properties. Particuology. 2016;24:32–43.
100. Linsinger T, Roebben G, Gilliland D, Calzolai L, Rossi F, Gibson N, et al. Requirements on Measurements for the Implementation of the EC Definition of the Term Nanomaterial. Belgium; 2012.
101. Hui PC-L, Wang W-Y, Kan C-W, Zhou C-E, Ng FS-F, Wat E, et al. Preparation and characterisation of chitosan microcapsules loaded with Cortex Moutan. Int

J Biol Macromol. 2013 Apr;55:32–8.

102. Li ’ M-H, Lie Y-C. Densities and Viscosities of Solutions of Monoethanolamine + N-Methyldiethanolamine + Water and Monoethanolamine + 2-Amino-2-methyl-1 -propanol + Water. J Chem Eng Data. 1994;39:444–7.
103. Nair PS, Selvi PP. Absorption of Carbon dioxide in Packed Column. Int J Sci Res Publ. 2014;4(1):2250–3153.
104. Aines RD, Spaddaccini CM, Duoss EB, Stolaroff JK, Vericella J, Lewis JA, et al. Encapsulated solvents for carbon dioxide capture. Energy Procedia. 2013;37:219–24.
105. Stephens JC, Van Der Zwaan B, Kennedy JF. CO 2 Capture and Storage (CCS): Exploring the Research, Development, Demonstration, and Deployment Continuum. 2005;
106. Rochelle GT. Amine scrubbing for CO2 capture. Science. 2009;325(5948):1652–4.
107. Wang J, Wang M, Zhao B, Qiao W, Long D, Ling L. Mesoporous carbon-supported solid amine sorbents for low-temperature carbon dioxide capture. Ind Eng Chem Res. 2013;52(15):5437–44.
108. Farha OK, Yazaydın a Ö, Eryazici I, Malliakas CD, Hauser BG, Kanatzidis MG, et al. De novo synthesis of a metal-organic framework material featuring ultrahigh surface area and gas storage capacities. Nat Chem. 2010;2(November):944–8.
109. Folger P. Carbon capture and sequestration (CCS). Carbon Capture Greenh Gases. 2010;325(September 2009):1–28.
110. Wang J, Wang M, Zhao B, Qiao W, Long D, Ling L. Mesoporous carbon-supported solid amine sorbents for low-temperature carbon dioxide capture. Ind Eng Chem Res. 2013;52(15):5437–44.
111. Kortunov P V., Siskin M, Paccagnini M, Thomann H. CO2 Reaction Mechanisms with Hindered Alkanolamines: Control and Promotion of Reaction Pathways. Energy and Fuels. 2016;30(2):1223–36.
112. Nicholas BP, Lu Y. CO2 ABSORPTION INTO CONCENTRATED CARBONATE SOLUTIONS WITH PROMOTERS AT ELEVATED TEMPERATURES.
113. T Haslam BR, Hershey RL, Keen RH. INDUSTRIAL AND ENGINEERING

CHEMISTRY Effect of Gas Velocity and Tempera-ture on Rate of Absorption1. Vol. 18. UTC; 2018.

114. Wang T, Jens KJ. Oxidative Degradation of AMP/MEA Blends for Post-combustion CO2 Capture. Energy Procedia . 2013;37:306 – 313.
115. Volkov A. Pressure Decay Method. In: Drioli E, Giorno L, editors. Encyclopedia of Membranes. Berlin, Heidelberg: Springer Berlin Heidelberg; 2015. p. 1–2.
116. RUBOTHERM, GMBH P. Rubotherm-your specialist for gravimetric analysis.
117. LINSEIS GmbH. Magnetic Suspension Balance.
118. General Chemistry Principles and Modern ApplicationsHardcover. Pearson Prentice Hall; 2010.
119. Susanti RF, Kim J, Yoo K pung. Supercritical Water Gasification for Hydrogen Production: Current Status and Prospective of High-Temperature Operation. Supercritical Fluid Technology for Energy and Environmental Applications. Elsevier B.V.; 2014. 111–137 p.
120. Yu CH, Huang CH, Tan CS. A review of CO2 capture by absorption and adsorption. Aerosol Air Qual Res. 2012;12(5):745–69.
121. Jayaraman G. Introduction to transport phenomena. In: Modelling and Monitoring of Coastal Marine Processes. Springer Netherlands; 2008. p. 11–21.
122. Verma SL, DeLancey GB. Thermal effects in gas absorption. AIChE J. 1975;21(1):96–102.
123. Nwaoha C, Saiwan C, Tontiwachwuthikul P, Supap T, Rongwong W, Idem R, et al. Carbon dioxide (CO2) capture: Absorption-desorption capabilities of 2-amino-2-methyl-1-propanol (AMP), piperazine (PZ) and monoethanolamine (MEA) tri-solvent blends. J Nat Gas Sci Eng. 2016;33:742–50.
124. Suloff EC. Permeability, Diffusivity, and Solubility of Gas and Solute Through Polymers. Sorption Behav an Aliphatic Ser Aldehydes Presence Poly(Ethylene Terephthalate) Blends Contain Aldehyde Scav Agents. 2002;(1):29–99.
125. Chiang YC, Yeh CY, Weng CH. Carbon dioxide adsorption on porous and functionalized activated carbon fibers. Appl Sci. 2019;9(10).